Modelling abrupt shifts of fish recruitment and growth

by

A Thesis submitted to the School of Graduate Studies in partial fulfillment of the requirements

for the degree of

Master of Science in Fisheries Science and Technology

Memorial University of Newfoundland

July 2021

St. John’s, Newfoundland and Labrador, Canada

Abstract

Regime shifts in marine ecosystems may result in abrupt changes in fish population dynamics, and not accounting for such shifts could have potentially large and far-reaching consequences for fisheries assessment and management decisions. In this work, I develop a methodology to model abrupt shifts in recruitment and somatic growth, which are two key processes in controlling fish population dynamics. In Chapter 1, I review the impacts of regime shifts on fish populations and find that abrupt shifts in productivity are very common among global fish species. In Chapter 2, I introduce the approach of modelling recruitment and regime shifts. The methodology includes a hidden Markov model for the unobserved environmental regimes, a stock-recruitment (SR) model for the regime-specific SR function, the maximum likelihood approach for evaluating the marginal likelihood, and the corrected Akaike information criterion (AICc) for the model selection. I conduct simulation tests to evaluate the performance of the method and results indicate that our method can objectively identify the unobserved environmental regimes and estimate regime-specific SR model parameters well. In Chapter 3, I extend the hidden Markov approach to model abrupt shifts in fish growth using a von Bertalanffy growth model (VBGM). Simulation results demonstrate that the method can accurately identify abrupt shifts in growth and estimate regime-specific growth parameters well. I apply both the hidden Markov stock-recruit model (HMSM) and the hidden Markov growth model (HMGM) to an Atlantic cod stock on the southern Grand Bank off Newfoundland, Canada. Results indicate that the cod stock has two distinct recruitment regimes and two distinct growth regimes, and our method identify one abrupt shift in recruitment and four abrupt shifts in somatic growth. I consider the methodology proposed in this thesis as a useful tool to model regime-like changes of fish population dynamics. In Chapter 4, I discuss the management implications of abrupt shifts in fish population dynamics and present the current challenges of managing fish stocks under marine ecosystem regime shifts. I consider the conditions under which our method might be useful to better assess and manage fish populations under changing environmental regimes.

Declaration of co-authorship / previous publication

I. Co-Authorship

I hereby declare that this thesis incorporates material that is result of joint research, as follows:

- *Chapters 2 and 4 of the thesis include unpublished material co-authored with* Nan Zheng, Rick M. Rideout, and Shijia Wang *under the supervision of professor* Fan Zhang. *In all cases, the primary contributions, simulation analysis, data analysis, interpretation, and writing were performed by myself; Nan Zheng contributed to the statistical model development;* Rick M. Rideout *contributed to the writing of management implications, Shijia Wang provided assistance in statistics analysis, and professor Fan Zhang provided the key ideas of setting up the paper structure, and contributed feedback on refinement of ideas and editing of the manuscript.*

I am aware of the Memorial University of Newfoundland Policy on Authorship and I certify that I have properly acknowledged the contribution of other researchers to my thesis, and have obtained written permission from each of the co-author(s) to include the above material(s) in my thesis.

I certify that, with the above qualification, this thesis, and the research to which it refers, is the product of my own work.

II. Previous Publication

This thesis includes one original paper that have been previously submitted to journals for publication, as follows:

Thesis Chapter	Publication title/full citation	Publication status*
Chapters [2] [4]	Identification of recruitment regime shifts with a hidden Markov stock-recruitment model	*accepted for publication*

I certify that I have obtained a written permission from the copyright owner(s) to include the above published material(s) in my thesis. I certify that the above material describes work completed during my registration as a graduate student at the Memorial University of Newfoundland.

III. General

I declare that, to the best of my knowledge, my thesis does not infringe upon anyone's copyright nor violate any proprietary rights and that any ideas, techniques, quotations, or any other material from the work of other people included in my thesis, published or otherwise, are fully acknowledged in accordance with the standard referencing practices. Furthermore, to the extent that I have included copyrighted material that surpasses the bounds of fair dealing within the meaning of the Canada Copyright Act, I certify that I have obtained a written permission from the copyright owner(s) to include such material(s) in my thesis.

I declare that this is a true copy of my thesis, including any final revisions, as approved by my thesis committee and the Graduate Studies office, and that this thesis has not been submitted for a higher degree to any other University.

Acknowledgments

I would like to thank the following people, without whom I would not have been able to complete this research, and without whom I would not have made it through my masters degree!

Thanks to Fisheries and Marine Institute of Memorial University of Newfoundland, Ocean Choice International, and Ocean Frontier Institute for providing funding for my research. I thank all the Fisheries and Oceans Canada sea-going staff involved in the collection and processing of the data used in the assessments of these stocks.

My thanks to my supervisor, Dr. Fan Zhang, for providing guidance and feedback throughout this project.

Our team member Dr. Nan Zheng, for providing guidance and support for the statistics part of our project.

And my thanks to my parents for their support and encouragement.

Contents

List of Tables

List of Figures

Chapter 1

Abrupt shift in fish population dynamics

1.1 Regime shift in marine ecosystems

It has been increasingly recognized that it is possible for marine ecosystems to exist in more than one environmental state (Folke *et al.*, 2004; Wooster and Zhang, 2004; Munch and Kottas, 2009). Different environmental states are characterized with different environmental conditions, such as sea surface temperature, salinity, and food availability (deYoung *et al.*, 2008). Sometimes dramatic changes might occur among these different environmental states (Munch and Kottas, 2009). I term the prolonged periods of time where the ecosystem stays in a relatively stable environmental state 'regimes', and the transition between one environmental state and another as a regime shift. Regime shifts are often sudden, dramatic and persistent changes that may occur over a short period of time and may not be detected for several years (Scheffer *et al.*, 2001; Peterson and Schwing, 2003; Jiao, 2009; Munch and Kottas, 2009).

Regime shifts in marine ecosystems are typically assumed to be caused by natural forcing, e.g. climate oscillations (Hare and Mantua, 2000), by human activities, e.g. overfishing (Myers *et al.*, 1997) or more commonly by some combination of the two (deYoung *et al.*, 2008). Climate-driven regime shifts have been extensively documented (Minobe, 2000; Overland *et al.*, 2008; Jiao, 2009; Levin and Möllmann, 2015; Möllmann *et al.*, 2015; Zhang *et al.*, 2018). Large scale atmospheric oscillations, including NAO (North Atlantic Oscillation), PDO (Pacific Decadal Oscillation) and El Niño Southern Oscillation (ENSO) can induce abiotic changes, such as changes in temperature, salinity, wind, ocean currents, and upwelling (Jiao, 2009), and biotic changes, such as internal foodweb dynamics and structural habitat changes (deYoung *et al.*, 2008) in marine ecosystems. Changes in biotic and abiotic variables contribute to oscillations in environmental conditions and thus shifts among environmental regimes. Intensive fishing is regarded as another key driver of regime shifts in marine ecosystems (Myers *et al.*, 1997; Reid, 2000; Jackson, 2001; Daskalov, 2002; Harvey *et al.*, 2003; Jiao, 2009). Overfishing can reduce the resilience of the current state of an ecosystem, making the marine ecosystem more vulnerable to changes in environmental conditions and easier to flip to an alternative environment state (deYoung *et al.*, 2008). Under the pressure of overfishing, subtle changes in key environmental variables such as temperature and food availability may also directly or indirectly cause a regime shift.

Regime shifts in marine ecosystems can result in substantial alterations to fish population dynamics (Mueter *et al.*, 2007; A'mar *et al.*, 2009). Regime-like changes of recruitment, somatic growth, and recruit-per-spawner have been observed in many fish stocks and are believed to be cause by marine ecosystem regime shifts (Munch and Kottas, 2009a; Echave *et al.*, 2012; Möllmann *et al.*, 2015; Perälä and Kuparinen, 2015; Stawitz *et al.*, 2015; Perälä *et al.*, 2017). Meta-analyses have suggested that regime shifts in stock productivity are very common among global fisheries species (Mueter *et al.*, 2007; A'mar *et al.*, 2009; Vert-pre *et al.*, 2013; Szuwalski and HolloId, 2016; Zhang *et al.*, 2020b). The rapid and alternate nature of regime shifts present formidable challenges for fisheries assessment and management (Steele, 1996; deYoung *et al.*, 2008; Crépin *et al.*, 2012; Klaer *et al.*, 2015; Rocha *et al.*, 2015), because fish stocks tend to be overestimated (or underestimated) at the beginning of a low-productivity (or high-productivity) period when regime shifts are not included in fisheries assessment and management. Hence, a method that can detect and account for abrupt shifts in fish population dynamics under changing environmental regimes could be of great use in providing scientific advice to fisheries management and setting regime-based management strategies.

1.2 Abrupt shift in stock-recruitment dynamics

The stock–recruitment relationship (SRR) describes recruitment as a function of spawning stock biomass (SSB). It is a fundamental concept in fisheries science. Classical forms of SRRs include Ricker and Beverton–Holt models and their numerous extensions. These parametric SRRs involve the idea that the annual number of recruits to a fish stock is positively related to the parental spawning stock biomass at low SSB (Gilbert, 1997), but the rate of recruitment decreases as SSB increases. SRRs are critical to predict future stock dynamics (Britten *et al.*, 2016), and the ability to accurately model recruitment is essential to determine appropriate management strategies (Plagányi *et al.*, 2019). In particular, SRRs are crucial to identify various biological reference points, e.g. B_0 (unfished biomass), SSB_0 (unfished SSB), B_{MSY} (biomass leading to maximum sustainable yield) and F_{MSY} (the rate of fishing mortality leading to maximum sustainable yield) (Mangel *et al.*, 2013; Zhang *et al.*, 2020b). SRRs are often assumed to be time-invariant, but it has been recently demonstrated that SRRs may show abrupt shifts over time (e.g., Britten et al., 2016; Szuwalski et al., 2019). Abrupt changes in the parameters of stock-recruitment models have been detected in Japanese sardine (*Sardinops melanostictus*) in the Pacific Ocean (Wada and Jacobson, 1998; Munch and Kottas, 2009). Both Wada and Jacobson (1998) and Munch and Kottas (2009) identified two recruitment regimes for the Japanese sardines. The recruitment of the Japanese sardines was detected in a high level from 1971 to 1987 and in a low level from 1988 to 1995. The similar regime-like recruitment patterns have also been detected in Atlantic cod, thorny skate, American plaice, and white hake in the Gulf of St. Lawrence (Perälä et al., 2017). For example, an exceptionally high recruitment regime was identified for the cod in the Gulf of St. Lawrence beginning in the mid-1970s and lasting throughout the 1980s, then the cod recruitment rates declined and returned to more normal levels in the 1990s and remained until 2013. These abrupt changes in SRRs are believed to be related to marine ecosystem regime shifts (Perälä and Kuparinen, 2015; Zhang *et al.*, 2018). When regime shifts occur in fish stocks, the egg production and early life stage survival may change, and further translate into shifts in SRRs (Perälä *et al.*, 2017). Consequently, the S-R models fitted to observations before such a shift may not describe the recruitment after the shift. As regime shifts in marine ecosystems are common (Vert-pre *et al.*, 2013; Möllmann *et al.*, 2015; Zhang, 2020), not including regime shifts in stock-recruitment dynamics will increase the uncertainty in stock assessment and management.

1.3 Abrupt shift in somatic growth

Somatic growth describes how body size changes with time. There is substantial evidence that growth is highly variable (Stawitz *et al.*, 2015). Variability in growth can have substantial consequences for survival, natural mortality, age at sexual maturity, and reproductive output (Deriso, 1987; Frater *et al.*, 2019). Temporal variation in fish growth has been extensively studied (Jiao *et al.*, 2010; Stawitz *et al.*, 2015; Thorson *et al.*, 2015; Thorson and Minte-Vera, 2016). However, abrupt, regime-like changes in fish growth caused by changing environmental regimes have received less attention. Much research has sought to model abrupt shifts in recruitment (Munch and Kottas, 2009; Britten *et al.*, 2016; Perälä *et al.*, 2017; Szuwalski *et al.*, 2019), but there is a lack of studies accounting for regime-like fish growth, although existing evidence suggests fish could experience dramatic and persistent changes of somatic growth. For example, the growth of Pacific halibut (*Hippoglossus stenolepis*) was slow in the 1920s and 1930s, then suddenly changed to fast growth in the middle years, and then slowed down again between the mid-1970s and the mid-1990s (Clark *et al.*, 1999). Moreover, the Alaskan sablefish *(Anoplopoma fimbria)* stocks in the northeast Pacific Ocean, the Pacific halibut (*Hippoglossus stenolepis)* in the Gulf of Alaska, and the Pacific hake (*Merluccius productus*) in the California Current also showed regime-like growth patterns (Echave *et al.*, 2012; Stawitz *et al.*, 2015). Somatic growth is one of the primary demographic mechanisms contributing to dynamics of populations. Changes in fish growth can affect a range of population and fishery metrics, such as recruitment success, maturation schedules, stock biomass, and fisheries yield (Morrongiello *et al.*, 2021), and hence is critical to fisheries stock assessment and management procedures (Shackell, 1997; Thorson and Minte-Vera, 2016; Frater *et al.*, 2019). A method that can account for abrupt shifts in fish growth is needed to provide reliable estimates for long-term growth trends and decide upon appropriate fisheries management strategies under changing environmental regimes (Dortel *et al.*, 2015; Mion *et al.*, 2020). However, we need to acknowledge that the variation in weight at age could reflect both variation in growth and variation in fish condition (i.e. health condition) but that only variation in growth was assumed in this work.

1.4 summary

Fluctuations in demographic processes such as recruitment, somatic growth, and mortality contribute to fish population dynamics. Understanding demographic variability in these processes and their corresponding effects on production can help us understand and forecast changes in marine fish populations (Stawitz *et al.*, 2015). There is substantial evidence that population dynamics such as recruitment and growth could experience regime-like changes due to changing environmental regimes (Clark *et al.*, 1999; Munch and Kottas, 2009; Echave *et al.*, 2012; Perälä and Kuparinen, 2015; Perälä *et al.*, 2017). While regime shifts in marine ecosystems are very common (Vert-pre *et al.*, 2013; Möllmann *et al.*, 2015; Zhang, 2020), not accounting for abrupt changes in fish population dynamics can have potentially large and far-reaching consequences for fisheries assessment and management decisions (Rice, 2011; Frater *et al.*, 2019). Therefore, a method that can detect abrupt shifts in fish population dynamics, infer year-specific environmental regime, and provide estimations of regime-specific population dynamic parameters could be of great value. In the following chapters, I introduce the hidden Markov stock-recruitment model (HMSM) for modeling abrupt shifts in stock-recruitment dynamics, and the hidden Markov Growth model (HMGM) for modeling abrupt shifts in somatic growth. I first conduct simulation tests to evaluate the performances of these two methods, such as the ability to specify the true number of regimes, and the reliability of the model estimation results. Next, I apply HMSM and HMGM to an Atlantic cod stock (*Gadus morhua*) on the southern Grand Bank off Newfoundland, Canada. Finally, in Chapter 4, I discuss potential causes of abrupt shifts in fish population dynamics and potential management implications.

Chapter 2

Hidden Markov stock-recruitment model (HMSM)

2.1 Introduction

Recent studies have shown that stock–recruitment relationships (SRRs) can show abrupt shifts (Perälä and Kuparinen, 2015; Britten *et al.*, 2016; Perälä *et al.*, 2017; Szuwalski *et al.*, 2019), and such abrupt changes in stock-recruitment dynamics will have great impacts on fisheries management (Rice, 2011; Frater *et al.*, 2019). There have been earlier attempts to account for regime-like changes of recruitment dynamics. For example, Peterman *et al.* (2003) used the Kalman filter which includes a time-varying Ricker α parameter (i.e. α evolves as a random walk process) to model potential long-term, persistent changes in productivity (recruits per spawner at a given spawner abundance) of eight Bristol Bay, Alaska, sockeye salmon (*Oncorhynchus nerka*) stocks. Their Kalman filter random-walk (KF-RW) model detected large temporal changes in productivity of the eight Bristol Bay sockeye salmon stocks. Similarly, Minto *et al.* (2014) proposed a multivariate stock–recruitment state-space model which assumes auto-correlated (i.e. AR(1)) state variables to estimate time-varying stock productivity across 21 North Atlantic cod (*Gadus morhua*) populations. They found clear productivity regimes across neighboring populations, especially in the Northeast Atlantic. The state-space models might be a good approach for quantifying the variables that are continuous. However, for discrete variables (i.e. recruitment regimes), the state-space models may not be able to model the sudden "shifts" in regimes very well. Munch and Kottas (2009) introduced a Bayesian modeling approach which incorporates a two-regime-based hidden Markov model for determining recruitment regime shifts based on a

Ricker SRR. They assume that there are two environmental regimes characterized by distinct productivities and use a hidden Markov model to describe the unobserved environmental regimes. Within each regime, they assume that recruitment follows a Ricker model with multiplicative lognormal errors. Munch and Kottas (2009) applied their method to recruitment data for Japanese sardine (*Sardinops melanostictus*) and successfully identified two distinct recruitment regimes for the Japanese sardine. In general, regime shift studies (e.g., Nisbet and Bence, 1989; Wada and Jacobson, 1998; Munch and Kottas, 2009) have typically assumed the existence of two environmental regimes, and a Bayesian approach is predominantly used to estimate model parameters (Munch & Kottas, 2009; Perälä et al., 2017).

In this chapter, I develop a Hidden Markov Stock-recruitment Model (HMSM) to model abrupt changes in stock-recruitment dynamics. In a vein similar to Munch and Kottas (2009), I combine a hidden Markov model for unobserved environmental regimes and a stock-recruitment model to describe the regime-specific recruitment. Unlike Munch and Kottas (2009), I choose a Beverton–Holt SRR instead of a Ricker model and assume that the number of regimes is unknown. We chose to use a Beverton-Holt model rather than a Ricker model because the latter can be written in a linear form and thus is, in general, easier to handle than the former. We adopted the Beverton-Holt model to demonstrate the flexibility of the proposed approach to the functional forms of the stock-recruitment models. A model selection method is used to determine the optimum number of regimes. Different from the previous endeavors with a Bayesian approach, I use the maximum likelihood (ML) method, which is more flexible to implement and amenable to simulation studies. In this regard I developed an efficient algorithm to calculate the marginal likelihood with Template Model Builder (TMB) (Kristensen *et al.*, 2020). In the following sections, I first describe the structure of the HMSM. I conduct simulation tests to evaluate whether the method is able to correctly identify the underlying regimes. Finally, I apply the HMSM to an Atlantic cod (*Gadus morhua*) stock on the southern Grand Bank off Newfoundland, Canada.

2.2 Model structure of HMSM

The HMSM incorporates a hidden Markov model (Scott, 2002) for the unobserved environmental regimes and a Beverton-Holt model for regime-specific SRR. Since the environmental regime in the ecosystems can hardly be directly observed, in the HMSM, I treat the unobserved regimes as latent random effects and assume that these environmental regimes evolve as a Markov chain. Based on the Markov property, the probability distribution of future regimes conditional on both past and present regimes depends only upon the present regime. It greatly facilitates the fast evaluation of the likelihood function, as explained later.

The number of regimes in the environment is unknown. Let K denote the total number of regimes. Let $t \in \{1,2,\dots,T\}$ denote the index of year, where T is the final year in which recruitment was observed. The regime in year t is denoted by $r_t \in \{1,2,..K\}$. The regime in year t depends on the regime in year *t-1* through q_{ij} which are the probabilities of transitions into regime j from regime i; that is,

$$q_{ij} = p(r_t = j \mid r_{t-1} = i)\ .$$

I assume that q_{ij} are stationary, i.e., they do not vary over time. The denotations of all the model variables are given in Table 2.1.

I applied a commonly used stock-recruitment model defining the relationship between spawning stock biomass (S) and recruitment (R): Beverton–Holt model

$$R = aS/(b + S) ,$$

where $a > 0$ and $b > 0$. In order to simplify subsequent inference procedures, I adopted a form of the Beverton–Holt model close to a linear model

$$y = \alpha - \log (1 + \beta S) , \tag{2.1}$$

where $y = \log (R/S)$, $\alpha = \log (a/b)$ and $\beta = 1/b$. The parameter a is the density-independent parameter that is proportional to fecundity, and the parameter b is the density-dependent parameter that is proportional to both fecundity and density-dependent mortality.

The regime-specific model of the SRR, conditional on regime $r_t = j$, is given by

$$y_t = \mathrm{F}(S_t, \theta_j) + \varepsilon_t,$$

where the error term ε_t is modeled as an independent normal random variable with mean 0 and standard deviation σ_j, $\theta_j = (\alpha_j, \beta_j)$, and $\mathrm{F}(S_t, \theta_j) = \alpha_j - \log (1 + \beta_j S_t)$. ε_t involves both process error and the measurement error in observing y_t. Here the subscript j indexes the regime. Let $\theta = (\theta_1, \theta_2, \dots, \theta_K)'$, $Q = (q_{11}, \dots, q_{KK})'$, and $\sigma = (\sigma_1, \dots, \sigma_K)'$. Θ is further defined as a vector of all the elements of θ, Q and σ.

The joint likelihood function of $y_{1:T}$ and hidden regimes $r_{1:T}$ for the HMSM is thus given by

$$p(y_{1:T}, r_{1:T} \mid \Theta) \ = \ \pi(r_1) \prod_{t=2}^{T} \ p(r_t \mid r_{t-1}) \prod_{t=1}^{T} \ p(y_t \mid r_t, \Theta), \tag{2.2}$$

where I abbreviate $\{y_1, y_2, \dots, y_T\}$ and $\{r_1, r_2, \dots, r_T\}$ respectively as $y_{1:T}$ and $r_{1:T}$. The marginal likelihood is evaluated by summing out all the latent random effects $r_{1:T}$; that is,

$$p(y_{1:T} \mid \Theta) \ \ = \sum_{r_{1:T}} \ \pi(r_1) \prod_{t=2}^{T} \ p(r_t \mid r_{t-1}) \prod_{t=1}^{T} \ p(y_t \mid r_t, \Theta), \tag{2.3}$$

A straightforward evaluation of (2.3) involves enumerating all the K^T routes from year 1 to year *T* and summing all the joint likelihoods (2.2) along these routes. The computational cost of this method increases exponentially with the sample size T, which is unfeasible even for moderate T. For ease of reference, I hereafter refer to this approach as the “brute-force method”. Instead of using the brute-force method, I applied an efficient algorithm with computational cost proportional to *T* based on the Markov property of the model. A major advantage of this algorithm is that any transition route between two regimes of two consecutive years is evaluated only once, while the brute-force method redundantly evaluates each of these transition routes K^{T-2} times. The use of the efficient algorithm greatly reduces the computational cost. The details of the efficient algorithm are provided in Appendix A For the purpose of comparison and validation, I also implemented the brute-force method with the flexible method of recursion (Graham *et al.*, 1990). Our numerical tests indicated that both methods give exactly the same marginal likelihood evaluations, but the efficient method takes much less time (see Appendix E).

Eq. (2.3) involves multiplications of many probably tiny probabilities, which can lead to computer overflow and loss of numerical accuracy. Chib (1996) and Scott (2002) also noticed that directly evaluating and maximizing the likelihood is unstable. To solve this problem, Scott (2002) proposed a solution to evaluate the log-likelihood by always working with the logarithms of the intermediate probabilities because log-transformation can effectively scale very large or small numbers into an amenable range. This solution requires the log-space summation, which can be easily done using the logspace_add function in TMB (Template Model Builder; Kristensen *et al.*, 2020). Although the Laplace approximation used in TMB for the integrations over continuous random effects cannot be applied to discrete latent variables (e.g., r_t) in this HMSM, the efficient algorithm for evaluating the marginal log-likelihood can be coded up in TMB. Then I am able to use TMB to calculate the marginal log-likelihood and the gradients. This can be combined with the R function nlminb (Gay, 1990) to find the MLEs and their standard errors. The gradient function of θ that TMB automatically provides can greatly improve estimation of θ using nlminb. As mentioned before, the modelling approach provides statistical inference for the unknown environmental regimes. The regime for each year is estimated by maximizing their conditional distributions given the data. That is

$$p\,(r_t = j \mid y_{1:T}, \Theta) = \frac{p(r_t = j,\ y_{1:T} \mid \Theta)}{p(y_{1:T} \mid \Theta)},$$

where

$$p(r_t = j,\ y_{1:T} \mid \Theta) = \sum_{r_{1:(t-1)}, r_{(t+1):T}} p\left(r_{1:(t-1)}, r_t = j, r_{(t+1):T}, y_{1:T} \,\middle|\, \Theta\right).$$

The fast evaluation of $p\,(r_t = j \mid y_{1:T}, \Theta)$ is presented in Appendix B.

Predicting the recruitment for year *t* has 2 steps: 1) predict the regime in year *t* by maximizing the conditional distribution of all regimes given the data; 2) calculate the recruitment using the regime-specific SRR model given the estimated regime. I use a “missing data” approach for future recruitment predictions.

In the case of missing data where recruitment in the past and/or future years are not available, the marginal likelihood can be rewritten as

$$p(\{y_t, t \in D_T\} \mid \Theta) = \sum_{r_{1:T}} \pi(r_1) \prod_{t=2}^{T} p(r_t \mid r_{t-1}) \prod_{t \in D_T} p(y_t \mid r_t, \Theta), \tag{2.4}$$

where D_T denotes all the years with recruitment data. The formula for the conditional distribution of the regimes can be similarly written as

$$p\,(r_t = j \mid \{y_t, t \in D_T\}, \Theta) = \frac{p(r_t = j, \{y_t, t \in D_T\} \mid \Theta)}{p(\{y_t, t \in D_T\} \mid \Theta)},$$

where

$$p(r_t = j, \{y_t, t \in D_T\} \mid \Theta) = \sum_{r_{1:(t-1)}, r_{(t+1):T}} p\left(r_{1:(t-1)}, r_t = j, r_{(t+1):T}, \{y_t, t \in D_T\} \,\middle|\, \Theta\right).$$

The procedures to evaluate the marginal likelihood (2.4) and the regime conditional probabilities are the same as for the complete data case.

2.3 Simulation

I validate the HMSM by first simulating data time series with known numbers of regimes, based on recruitment parameters derived from empirical data for real fish populations. I then test the ability of our method to 1) specify the correct number of regimes, 2) identify the exact regime for each year, and 3) precisely estimate the regime-specific parameters.

Theoretically, the maximum number of regimes does not have an upper bound. However, in most cases, the SRR time series are not long enough to support the existence of more than three regimes. The length of the recruitment time series of most fish stocks from the RAM legacy database is around 35 to 60 years, while the number of parameters for the two-regime HMSM, three-regime HMSM, and four-regime HMSM is nine, 17, and 27, respectively. Using 27 or even more parameters to estimate 60 data points could be overfitting. Thus, I conducted simulation tests under three scenarios, i.e. single regime, two regimes, and three regimes (Figure 2.1). Each scenario is repeated 1000 times, and each repetition generates 50 years of stock-recruitment data. In order to make the simulation tests more realistic, the recruitment parameters used for data generation under scenarios 2 and 3 were derived from the empirical data for the golden redfish from International Council for the Exploration of the Sea (ICES) subareas V, VI, XII, and XIV (Iceland and Faroes grounds, West of Scotland, North of Azores, East of Greenland) and the

Acadian redfish from the Gulf of Maine / Georges Bank, respectively. The SR data of these two real red fish stocks were obtained from the RAM legacy database (RAM Legacy Stock Assessment Database, 2018). I described how to analyze the SR data and use their recruitment parameter estimates for our simulation tests in Appendix C .

I generated y_t using the re-parametrized BH model

$$y_t = \alpha_t - \log(1 + \beta_t\, S_t) + \varepsilon_t,$$

where $t = 1, 2, \ldots, T$ is the index of year. ε_t are independent normal random variables with mean 0 and standard deviation σ_t.

Under scenario 1 with a single regime (i.e. no regime shift), the parameters α_t, β_t and σ_t are constant (Table 2.2). I let S_t follow a uniform distribution with the boundary (0,500).

Under scenario 2 with two regimes, the generated time series $\{y_1, y_2, \ldots y_t, \ldots y_T\}$ were characterized by two underlying regimes with parameters $\alpha_t \epsilon \{ \alpha_1, \alpha_2 \}$, $\beta_t \epsilon \{ \beta_1, \beta_2 \}$, and $\sigma_t \epsilon \{ \sigma_1, \sigma_2 \}$ depending on the regime in year *t* (Table 2.2). These regime-specific parameters $\{\alpha_1, \alpha_2\}$, $\{\beta_1, \beta_2\}$, and $\{\sigma_1, \sigma_2\}$ are the corresponding estimated parameters from fitting the 2-regime HMSM to the SRR data of the golden redfish stock from ICES (International Council for the Exploration of the Sea) subareas V, VI, XII, and XIV (Iceland and Faroes grounds, west of Scotland, North of Azores, East of Greenland) (RAM Legacy Stock Assessment Database, 2018). The time series of the latent random effects (i.e. the temporal variation of regimes), $\{r_1, r_2, \ldots, r_T\}$, are specified to follow a step-wise change among two regimes (Figure 2.1). I let S_t follow a uniform distribution with the same range as the SSB of the golden redfish, which is $(0{,}45)$.

Under scenario 3 with three regimes, the generated time series $\{y_1, y_2, \ldots y_t, \ldots y_T\}$ were characterized by three underlying regimes with parameters $\alpha_t \epsilon \{ \alpha_1, \alpha_2, \alpha_3 \}$, $\beta_t \epsilon \{ \beta_1, \beta_2, \beta_3\}$, and $\sigma_t \epsilon \{ \sigma_1, \sigma_2, \sigma_3 \}$ depending on the regime in year t (Table 2.2). Similar to scenario 2, the regime-specific parameters $\{\alpha_1, \alpha_2, \alpha_3\}$, $\{\beta_1, \beta_2, \beta_3\}$, and $\{\sigma_1, \sigma_2, \sigma_3\}$ were derived from the empirical data for Acadian redfish from the Gulf of Maine / Georges Bank (RAM Legacy Stock Assessment Database, 2018). The underlying regimes $\{r_1, r_2, \ldots, r_T\}$ follow step-wise changes among three regimes (Figure 2.1). S_t were randomly sampled from the SSB of the Acadian redfish.

I fitted three models to each of the generated data sets, i.e. single-regime model (BHM), two-regime HMSM (HMSM-2), and three-regime HMSM (HMSM-3). I then compared model performance using the Akaike information criterion with a correction for small sample sizes (AICc). The reason for using AICc instead of AIC is that the length of the recruitment time series is usually low when compared to the number of parameters for HMSM. Let *n* be the number of parameters in the model, and T be the sample size, namely, the total number of years observed. AICc is given by

$$AICc = 2n - 2\log\left(\hat{L}_\Theta\right) + (2n^2 + 2n)/(T - n - 1)$$

Finally, I evaluated the simulation performance of the parameter estimates of the selected model under each scenario by root-mean-squared error (RMSE), relative root-mean-squared error (RRMSE), and bias,

$$RMSE = \sqrt{\frac{\sum_{z=1}^{1000}\left(\hat{\theta}_z - \theta\right)^2}{1000}}$$

$$RRMSE = \frac{RMSE}{|\theta|}$$

$$bias = \frac{\sum_{z=1}^{1000}(\hat{\theta}_z - \theta)}{1000},$$

where θ denotes the true parameter values, and the hat denotes the parameter estimates.

2.4 Case study

After verifying the ability of our modeling approach to accurately identify regime shifts in simulated data, I applied the three models (BHM, HMSM-2 and HMSM-3) to identify potential regime shifts in stock-recruitment dynamics based on empirical data for the Atlantic cod stock on the southern Grand Bank (Northwest Atlantic Fisheries Organization (NAFO) Divisions 3NO) (Rideout *et al.*, 2018). The Grand Bank is a large offshore bank to the southeast of the island of Newfoundland. Catches of cod from this stock peaked during the late 1960s – early 1970s, with annual totals from 100 000 t to more than 200 000 t, but declined sharply thereafter. Estimates of spawning stock biomass declined from the mid-1960s to the mid-1970s due to high fishing mortality (Hutchings and Myers, 1994), and recruitment started to decline in the mid-1960s and reached very low levels in the 1990s. The cod stock collapsed in the early 1990s and was placed under a moratorium to all directed fishing in February 1994 (Brander, 2005). Despite more than 25 years under a fishing moratorium, the stock has shown little to no signs of recovery (Nogueira *et al.*, 2013).

The 3NO cod SR data (1962 to 2017) were taken from the most recent assessment of this stock (Rideout *et al.*, 2018) and the age of recruitment is considered to be 3 years old. Before fitting models to these data, I divided SSB by 10^4 to keep it in the same order of magnitude as y_t, and I denoted SSB/10^4 as S_t. I fit the BHM, HMSM-2, and HMSM-3 to the $S_t\ and\ y_{t+3}$ data. For the HMSM-2, the total number of regimes $K = 2$. The initial values for α's of the K regimes were set at the K points evenly spread across the range of y_t for small S_t values. I used 2/(range of S_t) as the initial values of β's. The $\sigma's$ were assigned the same initial value of 1. The initial 2 X 2 matrix of q_{ij} was assigned equal values summing to 1 for each row. The initial values of α's, β's, and $\sigma's$ for HMSM-3 were derived similar to those of HMSM-2, and the initial 3 X 3 matrix of q_{ij} of HMSM-3 was similarly given the same values with row-sums equal to 1. The starting values of parameters for BHM were fixed at $\alpha = 1.8$, $\beta = 0.02$, and $\sigma = 0.1$. The models were compared with AICc, and the selected model was used to identify the abrupt shifts of SRRs for 3NO cod. In order to demonstrate that the estimates for the HMSM are not very sensitive to starting values, some fitting examples of different initial values are provided in Appendix H .

2.5 Results

2.5.1 Simulation results

Our results confirmed that fitting multiple HMSM to recruitment data and comparing model performance via AICc is an effective and objective way of identifying regime shifts in fish populations. For single regime scenarios (i.e. scenario 1), the BHM outperformed HMSMs (HMSM-2 and HMSM-3) across all 1000 trials, and for 2-regime scenarios (i.e. scenario 2) the HMSM-2 outperformed BHM and HMSM-3 in all 1000 iterations (Table 2.3). For 3-regime scenarios (i.e. scenario 3), HMSM-3 specified the correct number of regimes in almost all the 1000 iterations (Table 2.3). The estimates of parameters α, β, and σ for the selected BHM and HMSMs were close to the true parameter values that were used to simulate the data (Figure 2.2). The precision of parameter estimates for each selected model across three scenarios was evaluated by root-mean-squared error (RMSE), relative root-mean-squared error (RRMSE), and bias (Table 2.4). The RMSEs, RRMSEs and bias of parameters for BHM were very close to zero, which indicated the high precision of parameter estimates. The parameters of HMSM-2 were also estimated very well given their low RMSEs, RRMSEs and bias. The bias in α_2 and β_2 was probably due to the uniform distribution of S_t. Compare to α_1 and β_1, α_2 and β_2 are relatively greater. In order to estimate β_2 well, more data points with smaller S_t are required. However, in scenario 2, S_t is uniformly distributed, and I cannot make sure that the data points in regime 2 have smaller S_t. The parameter estimates for HMSM-3 were mostly good with some exceptions (i.e. some RMSEs and RRMSEs > 1), but the precision was acceptable. For the multi-regime scenarios, both HMSM-2 and HMSM-3 were effective at correctly identifying the true regime for individual years. For the 2-regime scenario, 839 out of the 1000 trials accurately predicted the year-specific regime for all of the years in the time series (Figure 2.3). For the 3-regime scenario, the accurate regime was predicted for all years in 746 out of 1000 trials (Figure 2.3).

2.5.2 Simulation examples for HMSM-2 and HMSM-3

Under scenario 2, taking one of the 1000 trails as an example, the AICc values of HMSM-2, HMSM-3, and BHM were 56.553, 73.017, and 107.526 respectively. The predicted r_t's of HMSM-2 were the same as the true r_t's (Figure 2.4). The parameter estimates of HMSM-2 were close to true parameter values (Figure 2.5). HMSM-2 fits the data better than BHM: the true SR data points were relatively evenly distributed on the upper and lower sides of the stock-recruitment curves fitted by HMSM-2 (Figure 2.6). HMSM-2 can predict recruitment for each year much more reliably than BHM (Figure 2.6). The standardized residuals of HMSM-2 fitting were between -2 and 2 with the mean value zero, and there were no obvious temporal correlations (Figure 2.7). The standardized residuals for BHM fitting showed obvious temporal correlations, indicating the bad fitting of BHM (Figure 2.7).

Under scenario 3, taking one of the 1000 repetitions as an example, the AICc values of HMSM-2, HMSM-3 and BHM were 167.822, 0.064 and 350.203 respectively. The predicted $r_t's$

of HMSM-3 was the same as the true $r_t's$ (Figure 2.8). The parameter estimates of HMSM-3 were close to the true parameter values (Figure 2.5). The fit of BHM was obviously not as good as that of HMSM-3. The fitted stock-recruitment curves for HMSM-3 described the original data points substantially better than BHM, and HMSM-3 can provide much more reliable recruitment predictions for each year (Figure 2.6). There were no obvious temporal patterns in the standardized residuals for HMSM-3 fitting (Figure 2.9). In contrast, the standardized residuals of BHM fitting exhibited obvious temporal correlations within each of the three regimes (Figure 2.9).

2.5.3 Case study results

Fitting the three models to empirical SR data for cod in Divs. 3NO suggested the existence of two distinct regimes for this stock. The HMSM-2 outperformed the other two models with better fit to data (Figure 2.10a) and lower AICc (Table 2.5). A regime shift in 1986 was detected, which divided the time series into a favorable regime (regime 2) from 1962 to 1985 and an unfavorable regime (regime 1) from 1986 to 2017 (Figure 2.10b). Compared to the favorable regime, the unfavorable regime was characterized with lower reproduction rate α, greater impact of density-dependent parameter β, and greater standard deviation σ (Table 2.5). Furthermore, the estimated low transition probability (q_{12}) suggested that once the cod stock entered the unfavorable regime, it was very unlikely to return to the previous favorable regime (Table 2.5). The two regimes had substantially different SRRs, which led to drastically different levels of recruitment at the same level of SSB (Figure 2.10c).

2.6 Discussion

2.6.1 Model SRR using HMSM

Regime shifts have been observed in marine ecosystems around the globe (Hare and Mantua, 2000; Overland *et al.*, 2008; Vert-pre *et al.*, 2013; Möllmann *et al.*, 2015), and their impacts on the productivity of marine fish stocks present formidable challenges for the assessment and management of fisheries resources (Steele, 1996; Crépin *et al.*, 2012; Klaer *et al.*, 2015; Rocha *et al.*, 2015). The methodology I proposed here was able to correctly identify the number of regimes, predict the regime for each year with high precision, and provide precise parameter estimates for S-R models. It provides an objective and effective way to account for abrupt changes in SRRs under regime shifts and I believe that the ML approach has several advantages over Bayesian methods that have previously been used. The ML method may be more flexible than the Bayesian method in seeking suitable specifications for S-R models. To be specific, in Bayesian methodology, each time the S-R model is changed, the corresponding posterior distributions of the model parameters need to be derived, and when analytical posterior distributions of the model parameters are not available (e.g. Beverton–Holt model), the approximate and typically more complicated numerical methods need to be included (e.g., Perälä *et al.*, 2017). Unlike the Bayesian method, the ML approach can easily incorporate various S-R models without extensive programming changes and with no need for approximations. For example, before identifying equation (2.1) as the optimal form of the Beverton–Holt model, the flexibility of the ML approach allowed us to test various alternatives where the recruitment follows a lognormal or gamma distribution with mean given by the Beverton–Holt formula.

Another advantage of the ML method is that it allows for regime flexibility. Earlier studies pre-supposed the existence of two environmental regimes (e.g., Slatkin, 1978; Nisbet and Bence, 1989; Wada and Jacobson, 1998; Hare and Mantua, 2000). However, this may not always be the case. For example, the white hake (*Urophycis tenuis*) stock in the southern Gulf of St. Lawrence, has been characterized as having three distinct recruitment regimes (Perälä *et al.* 2017), shifting from a high to a low level in the 1970s, and then changing to a relatively high level in the mid-1990s (but not as high as pre-1970 conditions). Regime flexible models like HMSM should be better able to identify and model these complicated regime scenarios by not putting a priori restrictions on the number of regimes. Last but not least, the ML method allowed us to easily validate the proposed inference approaches by conducting simulation tests. The performance of the ML approach in the simulation studies gave us confidence that the HMSM could be applied to identify and characterize abrupt shifts in empirical recruitment data.

2.6.2 Abrupt shifts of stock-recruitment dynamics

The causes of abrupt shifts in fish populations are not always known, but are generally attributed to changing environmental and anthropogenic conditions, such as changes in atmospheric and ocean circulation, increasing water temperature, as well as changes in fishing pressure (deYoung *et al.*, 2008; Overland *et al.*, 2008; Bundy *et al.*, 2009; Möllmann *et al.*, 2015; Frank *et al.*, 2016; Karp *et al.*, 2019). I identified two distinct SRR regimes for 3NO cod, with a regime shift in 1986. The recruitment shift I identified for 3NO cod is a little earlier than the commonly assumed period for the climate-driven regime shift off Newfoundland and Labrador, which is in the early-1990s, characterized by the collapse of cod, capelin and other commercial and non-commercial finfish species (Dempsey *et al.*, 2017; Buren *et al.*, 2019). This may imply that the abrupt shift identified in recruitment for 3NO cod could be more attributable to anthropogenic factors such as overfishing than to climate oscillations. From 1962-1985, 3NO cod was in a high recruitment regime, and then in 1986 the cod stock shifted to, and has since remained in, a low recruitment regime. The 1986 recruitment shift of 3NO cod may be associated with overfishing of recruits and pre-recruits, particularly outside Canada's exclusive economic zone (EEZ) (Myers *et al.,* 1997). The overexploitation of these young fish may have directly led to the dramatic recruitment decline, and the transition from a high productivity regime to a low productivity regime. Furthermore, the low recruitment regime I identified beginning in the late 1980s coincided with depleted recruitment, increased fishing mortality, and extended period of cold surface water temperatures (Pedersen *et al.*, 2017). Ocean temperatures around Newfoundland and Labrador were below normal from the early-1980s to the mid-1990s, with a particularly cold period in the early-1990s (Lilly *et al.*, 2000). There is little reason to assume that the collapse of cod stock in the early 1990s would not correlate with the below-normal ocean temperatures (Buren *et al.*, 2019). It is also possible that fishing-induced changes in the size and age structure of the population increased the vulnerability of the stock to environmental changes (e.g., colder water temperature) that previously could be absorbed (Folke *et al.*, 2004; Lindegren *et al.*, 2010). Collectively, these anthropogenic and environmental factors may have caused the cod stock to shift to an unfavorable regime. The systematic changes of population traits and ecological conditions associated with regime shifts may prevent stocks from rapidly returning to a previous high productivity regime (Perälä and Kuparinen, 2015). In the case of 3NO cod, the stock remains in the poor recruitment regime to this day and has shown little to no evidence of stock recovery, despite being under a fishing moratorium since 1994, and fishing mortality (from by-catch in other fisheries) being very low.

2.7 Tables

Table 2.1 Variables included in HMSM model structure.

Variable	Denotation
t	The index of year, $t \in \{1, 2, \dots, T\}$
T	The final year in which recruitment was observed
K	The number of possible regimes
r_t	The regime state in year *t*, $r_t \in \{1, 2, \dots, K\}$
q_{ij}	The probabilities of transitions into regime *j* from regime *i*
S_t	The Spawning stock biomass in year *t*
R_t	The number of recruits in year *t*
y_t	$y_t = \log(R_t/S_t)$
α_j	α in regime j, *j*=1, 2, …*K*
β_j	β in regime j, *j*=1, 2, …*K*
ε_t	The process error and the measurement error of y_t
σ_j	The standard deviation of error term $\boldsymbol{\varepsilon_t}$ in regime j, *j*=1, 2, … *K*

Table 2.2 The true values of the parameters α_t, β_t, and σ_t used for data generation under the three scenarios.

	Scenario 1	Scenario 2		Scenario 3		
α_t	2	$\alpha_1 = 7.78$	$\alpha_2 = 10.20$	$\alpha_1 = 3.04$	$\alpha_2 = 6.35$	$\alpha_3 = 7.12$
β_t	0.025	$\beta_1 = 0.38$	$\beta_2 = 1.54$	$\beta_1 = 0.09$	$\beta_2 = 0.93$	$\beta_3 = 1.21$
σ_t	0.2	$\sigma_1 = 0.31$	$\sigma_2 = 0.40$	$\sigma_1 = 0.43$	$\sigma_2 = 0.04$	$\sigma_3 = 0.75$

Table 2.3 The counts of each model selected by AICc under three scenarios

scenario		HMSM-2	HMSM-3	BHM
1	#Best Model	0	0	1000
2	#Best Model	1000	0	0
3	#Best Model	88	912	0

Table 2.4 The bias, Root Mean Squared Error (RMSE) and Relative Root Mean Squared Error (RRMSE) of the parameter estimates for the selected model under three scenarios.

	Parameters	True value	RMSE	RRMSE	Bias
Scenario 1	α	2	0.14	0.07	0.008
BHM	β	0.025	0.01	0.19	0.001
	σ	0.2	0.02	0.1	-0.01
Scenario 2	α_1	7.78	0.38	0.05	0.02
HMSM-2	α_2	10.20	0.67	0.07	-0.41
	β_1	0.38	0.24	0.63	0.05
	β_2	1.54	0.69	0.45	-0.41
	σ_1	0.31	0.05	0.15	-0.02
	σ_2	0.40	0.06	0.16	-0.03
Scenario 3	α_1	3.04	0.16	0.05	0.03
HMSM-3	α_2	6.35	0.26	0.04	0.003
	α_3	7.12	0.69	0.1	0.23
	β_1	0.09	0.23	2.66	0.08
	β_2	0.93	0.41	0.44	0.05
	β_3	1.21	1.9	1.56	0.69
	σ_1	0.43	0.07	0.17	-0.03
	σ_2	0.04	0.08	1.87	0.03
	σ_3	0.75	0.27	0.35	-0.14

Table 2.5 The AICc values and parameter estimates of BHM, HMSM-2, and HMSM-3 for 3NO cod.

	BHM	HMSM-2		HMSM-3		
AICc	186.51	150.64		167.27		
α	$\alpha = -1.02$	$\alpha_1 = -1.44$	$\alpha_2 = 0.38$	$\alpha_1 = -1.01$	$\alpha_2 = -0.27$	$\alpha_3 = 0.40$
β	$\beta = 2.16 \times 10^{-10}$	$\beta_1 = 0.19$	$\beta_2 = 0.07$	$\beta_1 = 2.57$	$\beta_2 = 0.76$	$\beta_3 = 0.08$
σ	$\sigma = 1.21$	$\sigma_1 = 0.88$	$\sigma_2 = 0.55$	$\sigma_1 = 0.56$	$\sigma_2 = 0.48$	$\sigma_3 = 0.55$
q_{ij}	NA	$q_{11} = 1$	$q_{12} = 2.38 \times 10^{-10}$	$q_{11} = 0.83$	$q_{12} = 0.17$	$q_{13} = 2.17 \times 10^{-10}$
		$q_{21} = 0.04$	$q_{22} = 0.96$	$q_{21} = 0.17$	$q_{22} = 0.83$	$q_{23} = 2.23 \times 10^{-12}$
				$q_{31} = 1.37 \times 10^{-10}$	$q_{32} = 0.04$	$q_{33} = 0.96$

2.8 Figures

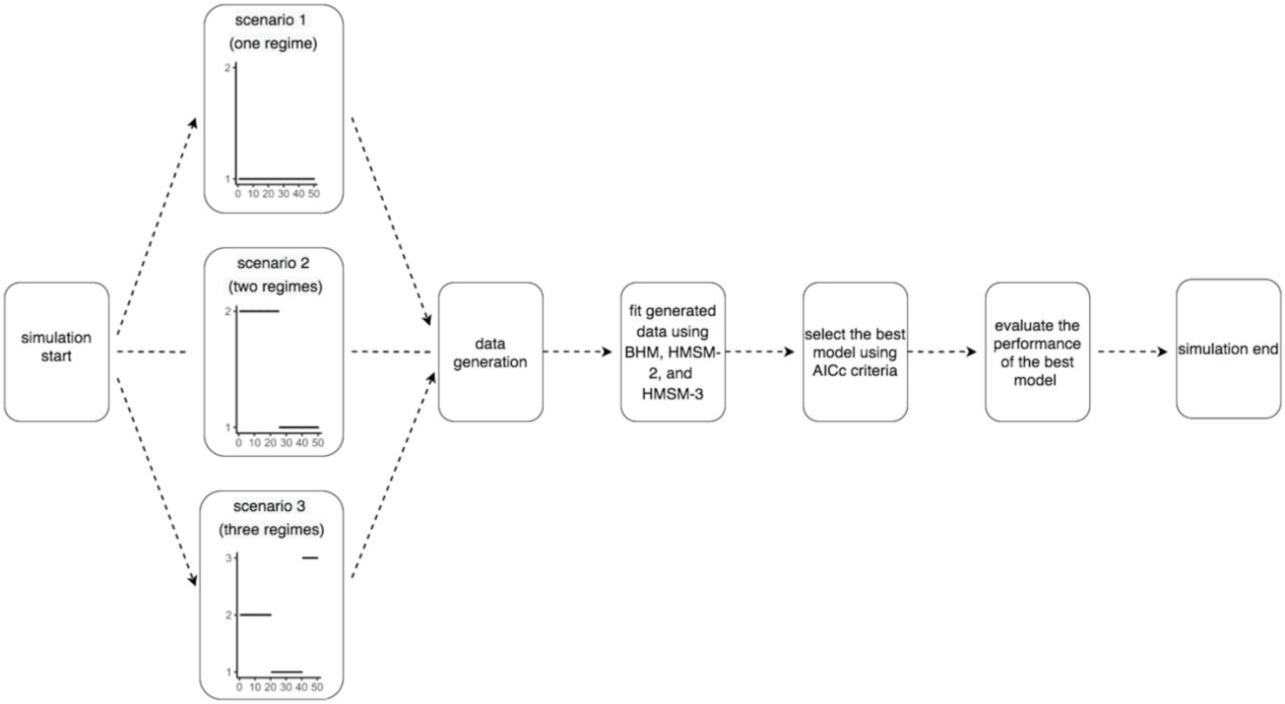

Figure 2.1 The simulation framework.

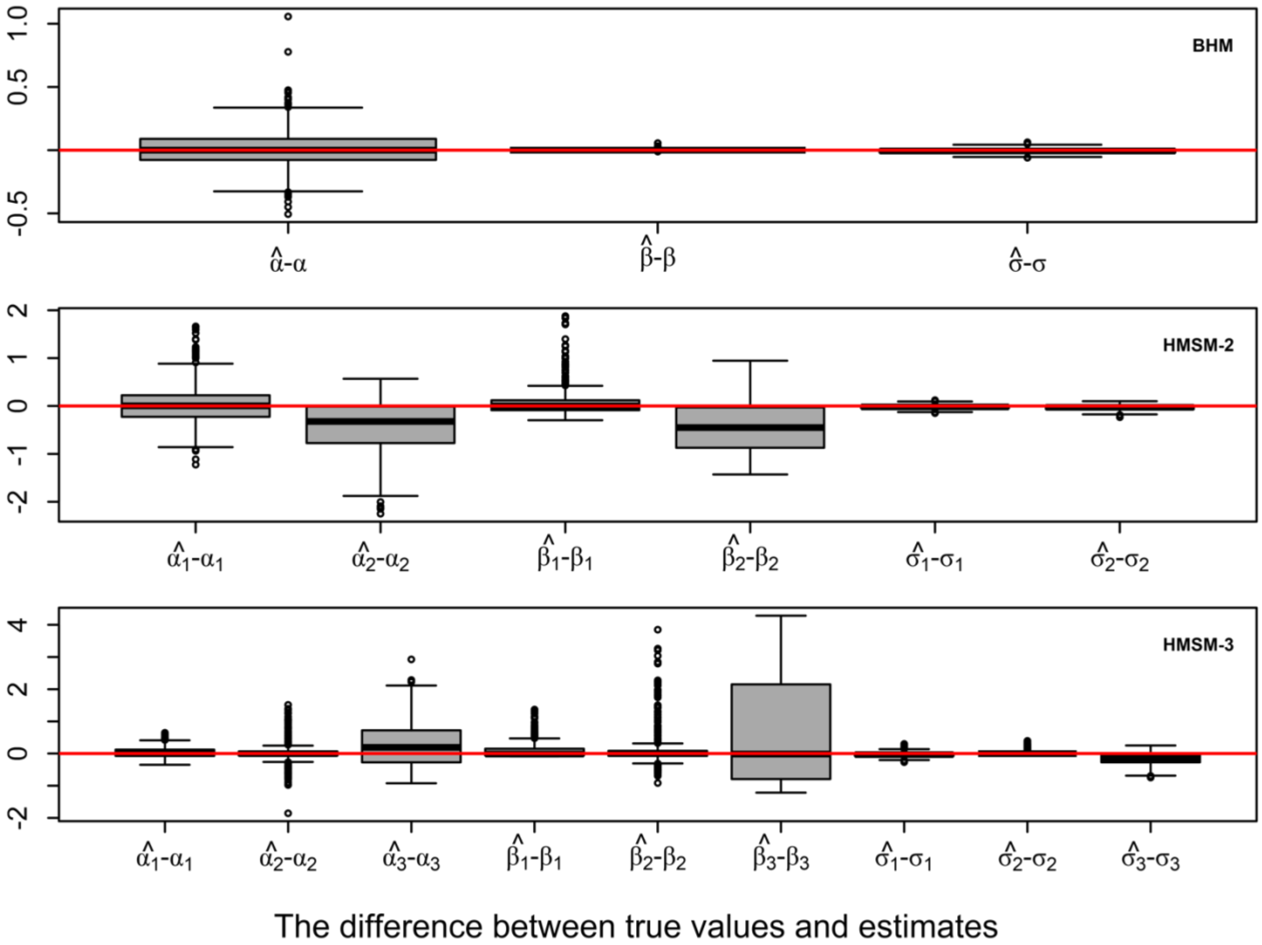

Figure 2.2 The bias of parameter estimates based on 1000 simulation trials with BHM, HMSM-2, and HMSM-3 for scenarios 1, 2 and 3, from top to bottom.

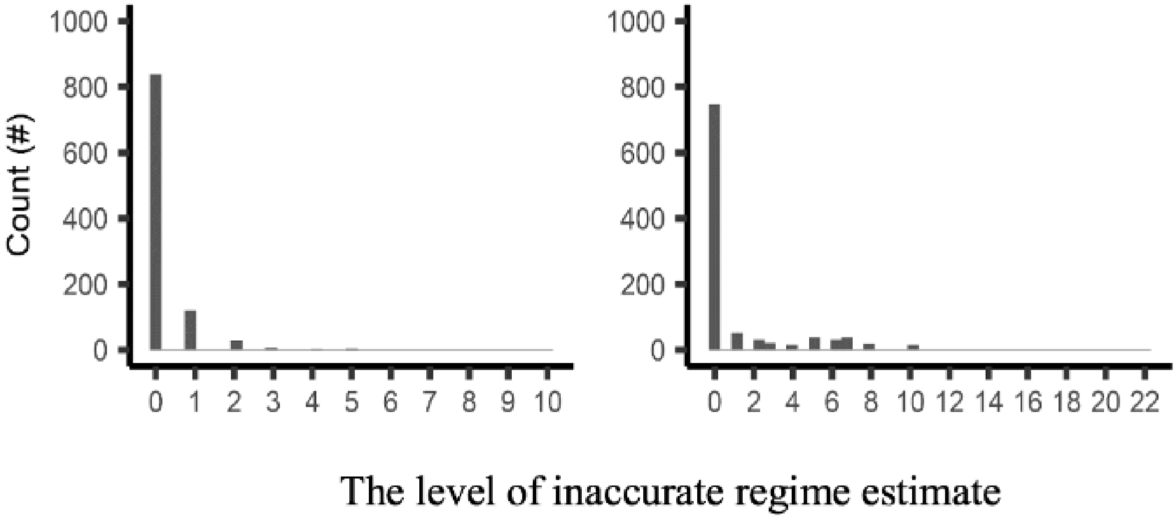

Figure 2.3 The regime detection accuracy of HMSM-2 (left column) and HMSM-3 (right column) simulations. Zero indicates that the predicted time series of regimes are exactly the same as the true dynamics, and 10 indicates that there are 10 years where the regime is mis-identified in one iteration, and so on. The vertical axis shows the count of each inaccurate estimate level across the 1000 trials.

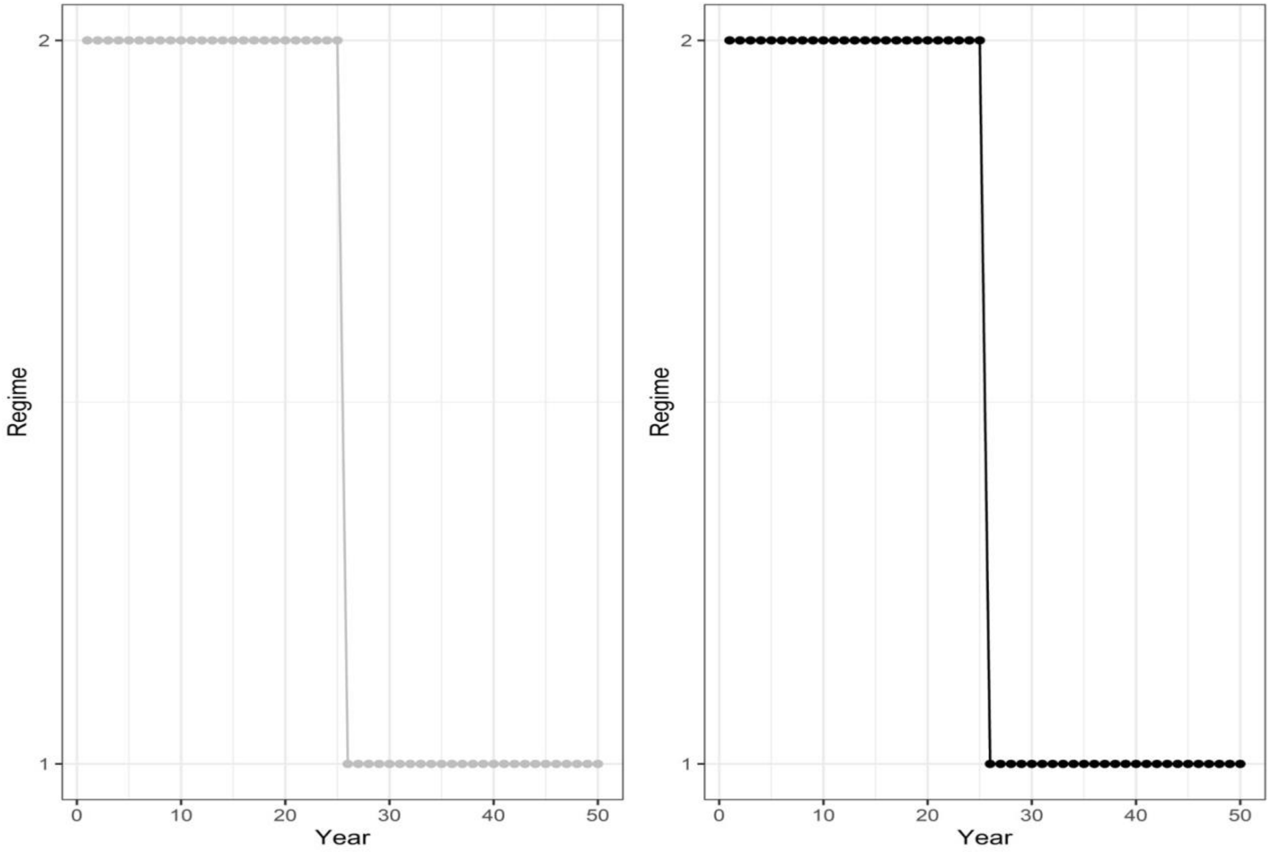

Figure 2.4 The regime state of each year for the true dynamics (left) and HMSM-2 predictions (right).

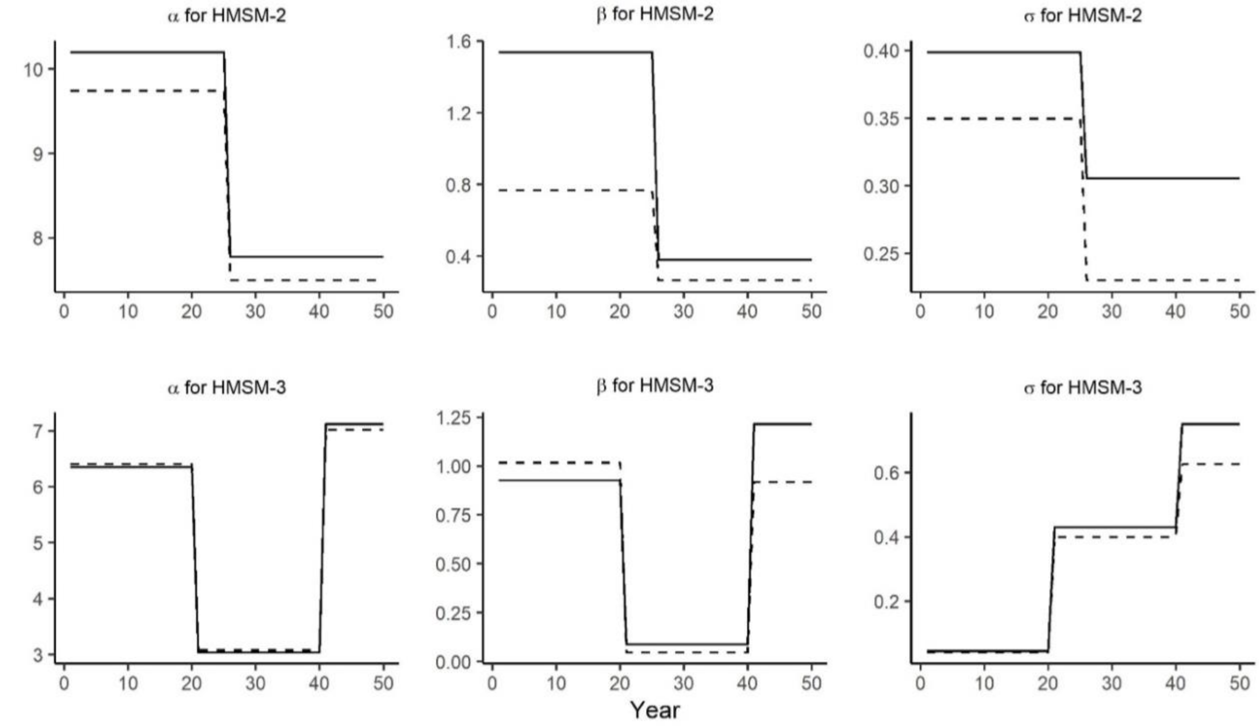

Figure 2.5 The estimated and true parameter time series for the selected model HMSM-2 and HMSM-3 under scenarios 2 and 3 from top to bottom. The solid lines denote true dynamics, and the dashed lines denote estimates.

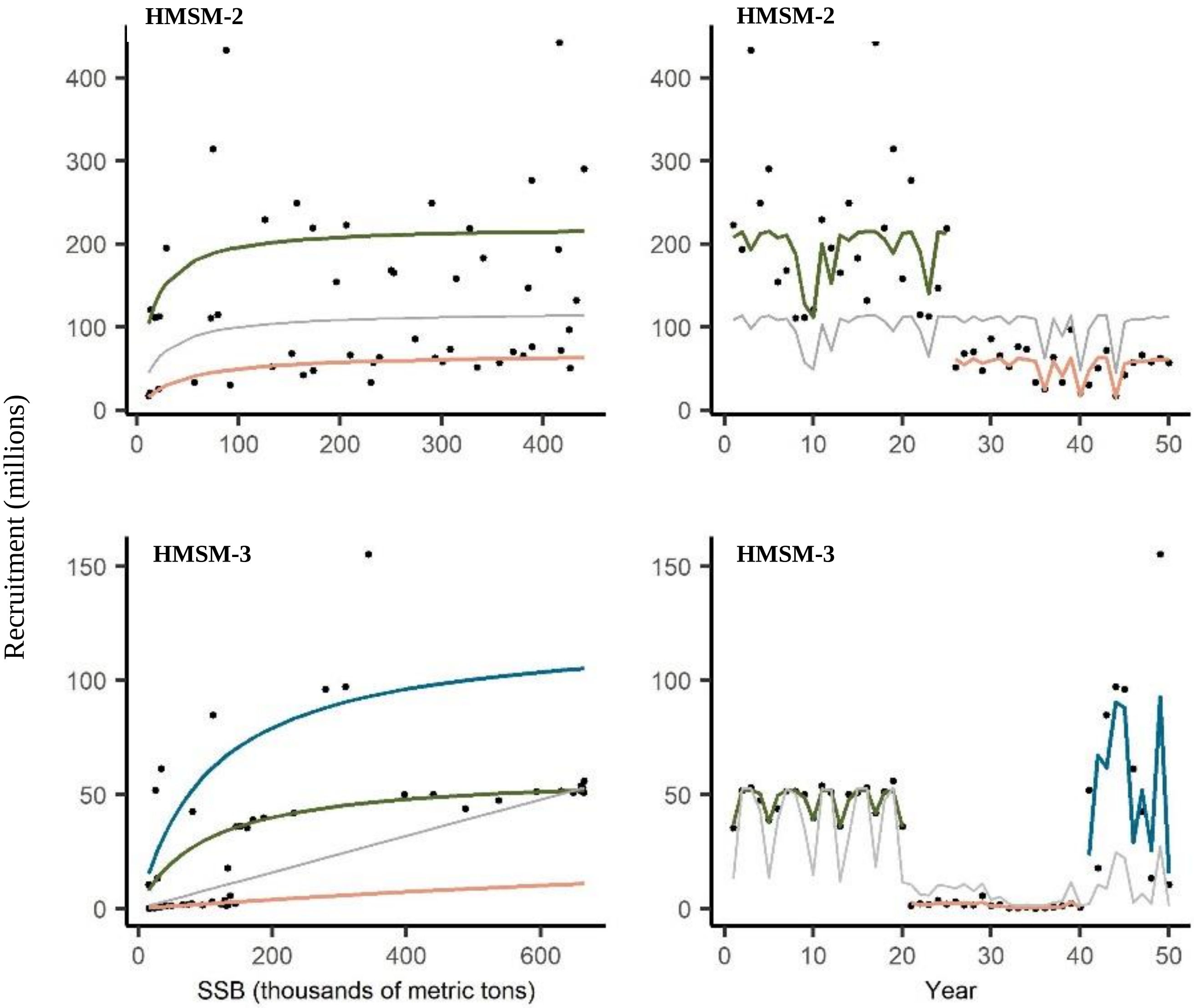

Figure 2.6 The fitted stock-recruitment curves (left column) and the predicted recruitment time series (right column) for HMSM-2 and HMSM-3 in one of the 1000 simulations. The solid dots in the left column denote the stock-recruitment observations, and the solid dots in the right column denote the observed recruitment time series. Regimes are denoted with different colors. The estimated BHM model are shown in gray lines.

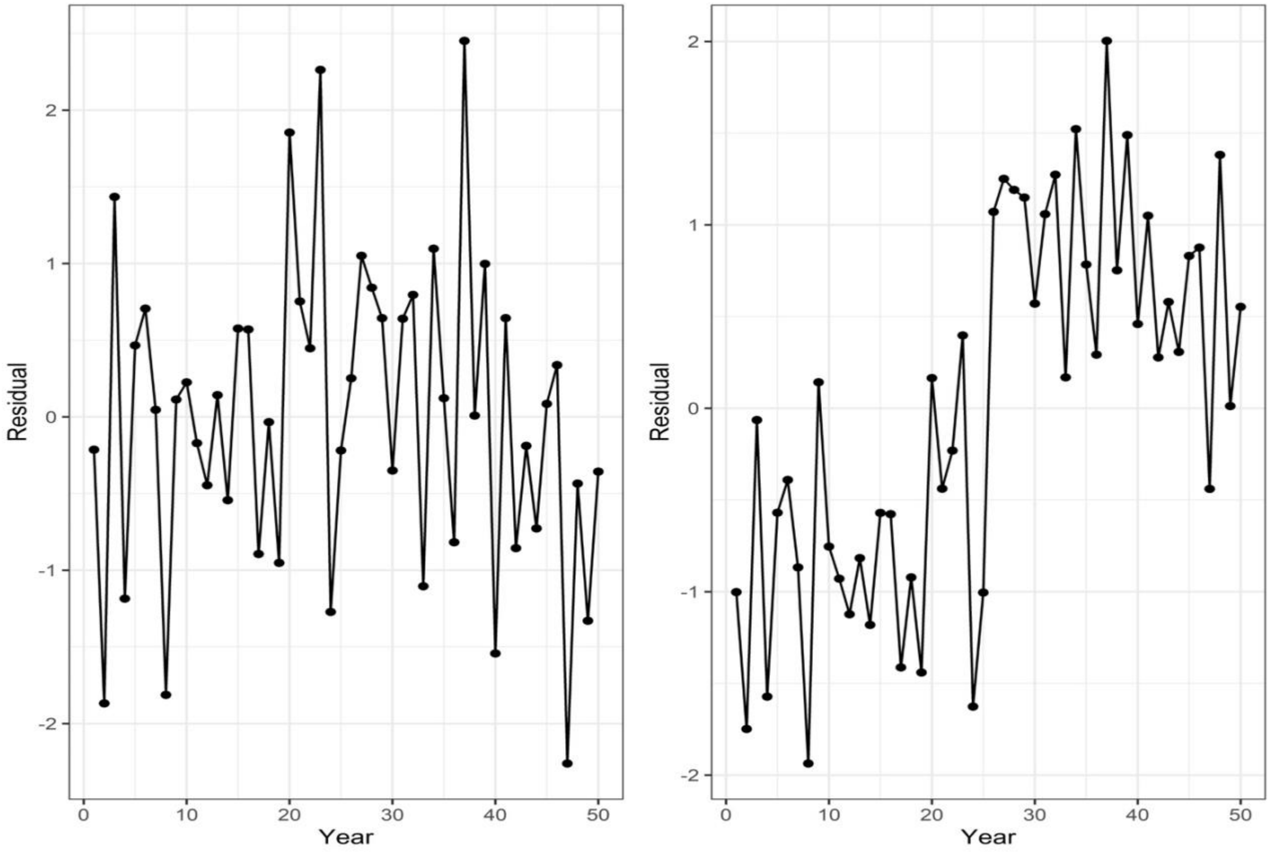

Figure 2.7 The standardized residuals versus year for HMSM-2 (left) and BHM (right).

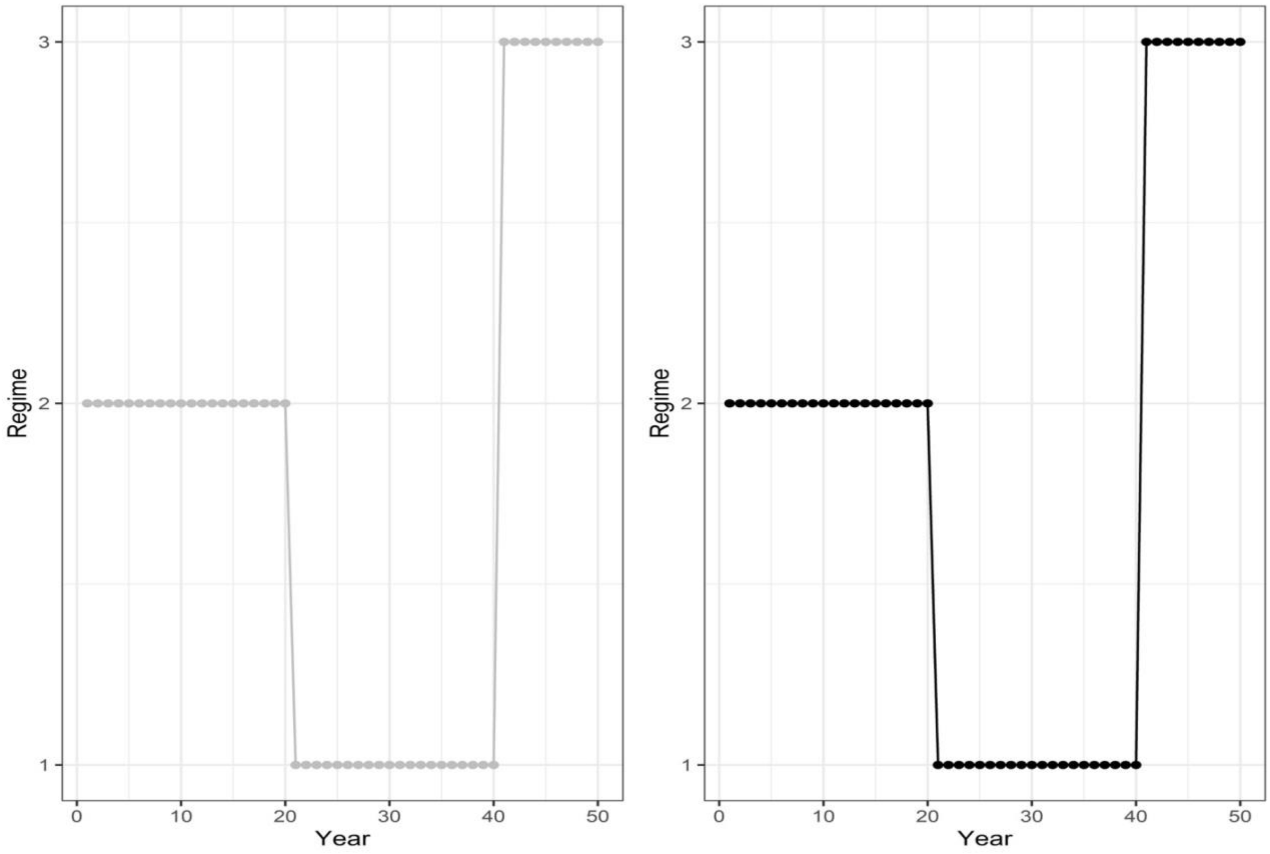

Figure 2.8 The regime state of each year for the true dynamics (left) and HMSM-3 predictions (right).

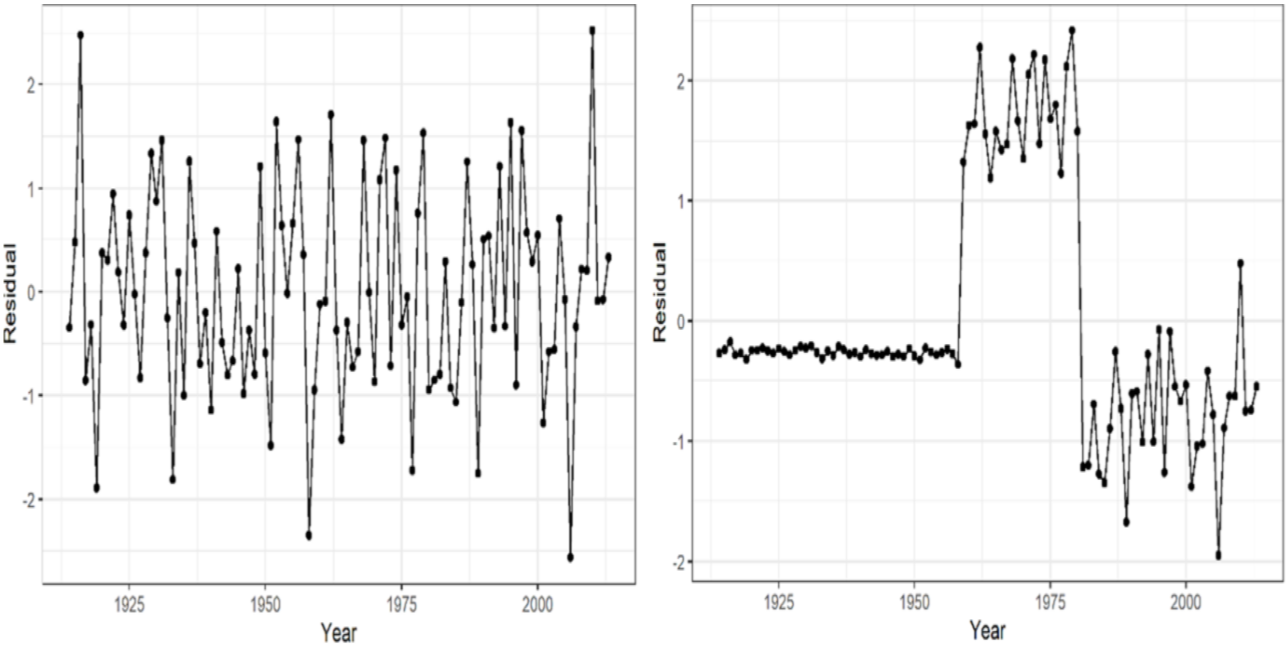

Figure 2.9 The standardized residuals versus year for HMSM-3 fitting (left) and BHM fitting (right).

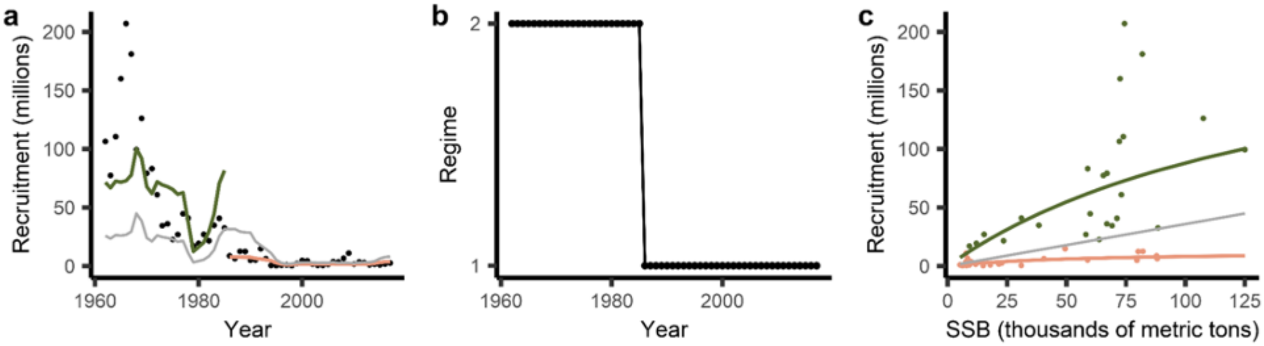

Figure 2.10 (a) The observed recruitment time series of 3NO cod (solid dots) and predicted recruitment for BHM (grey) and HMSM-2 (green and orange). The two coloured lines denote the HMSM-2 fit for the two regimes. (b) The predicted regime time series of HMSM-2 for 3NO cod. (c) Stock-recruitment relationships of 3NO cod (solid dots) and fitted stock-recruitment curves of BHM and HMSM-2.

Chapter 3

Hidden Markov Growth model (HMGM)

3.1 Introduction

Individual growth (i.e. somatic growth) is fundamentally important throughout the whole life history of fish species (Huang *et al.*, 2021). As a key factor regulating early life-stage survival, growth is highly related to natural mortality, recruitment, and fish productivity (Vert-pre *et al.*, 2013; Furuichi *et al.*, 2020), and is hence essential for fisheries stock assessment and management procedures (Shackell, 1997; Thorson and Minte-Vera, 2016; Frater *et al.*, 2019). There is an increasing number of studies supporting that fish somatic growth could also experience regime-like changes (Echave *et al.*, 2012; Perälä and Kuparinen, 2015). However, no previous works have ever attempted to model such abrupt changes in fish growth. The majority of the literature accounting for temporal variations in fish somatic growth either relate fish somatic growth to environmental variables using regression models (Dzul *et al.*, 2017; Mullowney *et al.*, 2019 Campana et al. 1995; Kimura 2008; Sigourney et al. 2012) or use the state-space models which assume continuous variables (e.g., Stawitz *et al.*, 2015). In this chapter, I am aimed to introduce a Hidden Markov Growth Model (HMGM) to account for abrupt changes in fish growth (i.e. relationship between body weight and age). The HMGM assumes discrete variables (i.e. environmental regimes) and may be better for describing the "discrepancies" between discrete regimes. The HMGM combines a hidden Markov model for unobserved environmental regimes and a von Bertalanffy growth model to describe the regime-specific growth curves. I applied the maximum likelihood (ML) method and used the efficient algorithm (see Appendix A) to calculate the marginal likelihood with Template Model Builder (TMB) (Kristensen *et al.*, 2020). In the following sections, I first describe the structure of the HMGM. I conduct simulation tests to evaluate whether the method can correctly identify the underlying regimes and provide precise estimates for long-term growth trends. Finally, I apply the method to the annual weight-at-age data of an Atlantic cod (*Gadus morhua*) stock on the southern Grand Bank off Newfoundland, Canada.

3.2 Model structure of HMGM

The HMGM incorporates a hidden Markov model (Scott, 2002) for the unobserved environmental regimes and a von Bertalanffy growth model (VBGM) for regime-specific growth (weight-at-age). I treat the unobserved regimes as latent random effects and assume that these environmental regimes evolve as a Markov chain; in each regime, fish growth follows a VBGM with regime-specific model parameters.

The total number and occurrences of regimes in the environment are all unknown. Let K denote the total number of regimes. Let $t \in \{1,2,\ldots,T\}$ denote the index of year, where T is the final year in which the time-series of weights-at-age were observed. The regime in year t is denoted by $r_t \in \{1,2,..K\}$. The regime in year t depends on the regime in year $t\text{-}1$ through q_{ij}, the probabilities of transitions into regime j from regime i; that is,

$$q_{ij} = p(r_t = j \mid r_{t-1} = i)\,.$$

I assume that q_{ij} are stationary; that is, they do not vary over time. The q_{ij} represent the Markov property of the model, namely, the probability distribution of future regimes conditional on both past and present regimes depends only upon the present regime. The notations of all the model parameters and variables are given in Table 3.1.

I applied the VBGM defining the relationship between weight (*w*) and age (*a*):

$$w_a = w_\infty \left\{ 1 - e^{-k(a-t_0)} \right\}^3 . \tag{3.1}$$

When $a = 0$,

$$w_0 = w_\infty \{ 1 - e^{kt_0} \}^3.$$

Hence,

$$e^{kt_0} = 1 - \left(\frac{w_0}{w_\infty}\right)^{\frac{1}{3}}, \tag{3.2}$$

and Equation (3.1) can also be written

$$w_a = w_\infty \left\{ 1 - \left[1 - \left(\frac{w_0}{w_\infty}\right)^{\frac{1}{3}} \right] e^{-ka} \right\}^3, \tag{3.3}$$

where w_∞ is asymptotic maximum weight, k is growth rate, and w_0 indicates the weight at age zero. Here, I use w_0 instead of t_0 for the following reasons. First of all, t_0, namely the age at weight 0, is an unrealistic parameter that cannot be measured, whereas w_0 has been well studied in the literature as the larvae weight. In this case I can fix w_0 based on the measurements of the weight of larvae. Secondly, in general t_0 is a hard parameter to estimate. In order to estimate t_0

well, sufficient weight data at age 1 and 2 are required. However, the sampling of fish at age 1 and age 2 may be poor in a survey due to the size selectivity of the fishing gear. Insufficient weight data at younger ages will lead to unrealistic estimations of t_0. Fixing w_0 is a good solution to this t_0-estimation issue. Finally, Equation (3.2) indicates that t_0 is highly correlated with *k*. If the growth rate k varies substantially for different regimes then t_0 should also have regime-specific parameters, and hence increasing the number of model parameters. In contrast, w_0 can be assumed identical for all the regime because w_0 is negligibly small relative to the weight of a mature fish, and variation in w_0 has little effect on model fitting. In Appendix J , I provided an example to demonstrate that different values of w_0 within a reasonable range have little effect on the model performance.

Given that the variation in weight for some fish populations tends to increase with weight (or equivalently age; i.e. Figure 3.1), I took the logarithm of Eq. (3.3) to stabilize the variability of data. Taking the logarithm of a response variables is a common method to achieve homogeneity of variance.

$$\mathrm{E}(\log(w_a)) = \mathrm{F}(a,\theta) = \log(\,w_\infty\,) + 3\,\log\left(1 - \left[1 - \left(\frac{w_0}{w_\infty}\right)^{\frac{1}{3}}\right]\,e^{-ka}\right), \tag{3.4}$$

Eq. (3.4) is the form of VBGM I use, and the parameters are $\theta = (w_\infty, k)$.

The data in year *t* is $y_t = (y_{t,a=3}, y_{t,a=4}, \dots, y_{t,a=12})'$, where $y_{t,a}$ is the logarithm of the average survey weight at age a. The regime-specific VBGM, conditional on regime $r_t = j$, is given by

$$y_{t,a} = \mathrm{F}(a,\theta_j) + \varepsilon_t,$$

where $\theta_j = \left(w_{\infty j}, k_j \right)$. Here the error term ε_t is modeled as an independent normal random variable with mean 0 and standard deviation σ_j. ε_t involves both process error (i.e. variations in environmental conditions) and the measurement error in data. Here the subscript j indexes the regime. Let $\theta = (\theta_1, \theta_2, \dots, \theta_K)'$, $Q = (q_{11}, \dots, q_{KK})'$, and $\sigma = (\sigma_1, \dots, \sigma_K)'$. Θ is further defined as a vector of all the elements of θ, Q and σ.

The joint likelihood function of $y_{1:T}$ and hidden regimes $r_{1:T}$ for HMGM is thus given by

$$p(\, y_{1:T}, r_{1:T} \mid \Theta \,) \;=\; \pi(r_1) \prod_{t=2}^{T} p(r_t \mid r_{t-1}) \prod_{t=1}^{T} p(y_t \mid r_t, \Theta), \tag{3.5}$$

I abbreviate $\{y_1, y_2, \dots, y_T\}$ and $\{r_1, r_2, \dots, r_T\}$ respectively as $y_{1:T}$ and $r_{1:T}$. The marginal likelihood is evaluated by summing out all the latent random effects $r_{1:T}$; that is,

$$p(y_{1:T} \mid \Theta) \;= \sum_{r_{1:T}} \pi(r_1) \prod_{t=2}^{T} p(r_t \mid r_{t-1}) \prod_{t=1}^{T} p(y_t \mid r_t, \Theta). \tag{3.6}$$

Recall from Chapter 2 that the modelling approach provides statistical inference about the unknown environmental regimes. The regime for each year is predicted by maximizing their conditional distributions given the data. That is,

$$p\,(r_t = j \mid \; y_{1:T}\,, \Theta\,) = \frac{p(r_t = j,\; y_{1:T} \mid \Theta\,)}{p(y_{1:T} \mid \Theta)},$$

where

$$p(r_t = j,\; y_{1:T} \mid \Theta\,) = \sum_{r_{1:(t-1)}, r_{(t+1):T}} p\big(r_{1:(t-1)}, r_t = j\,, r_{(t+1):T}\,,\; y_{1:T} \,\big|\, \Theta\,\big).$$

The fast evaluation of $p\ (r_t = j \mid\ y_{1:T}\ , \Theta\ )$ is presented in Appendix B.

3.3 Simulation

I validate the method by first simulating time series of weights-at-age with known patterns of regimes. I then test the ability of our method to 1) determine whether there is regime shift in fish growth, 2) identify the exact regime for each year, and 3) precisely estimate the regime-specific parameters.

I conducted simulation tests for two scenarios: 1) single regime (no regime shift), and 2) two regimes (regime shift; Figure 3.2). The time series of weight-at-age data were simulated for 60 years, and each scenario is repeated 1000 times.

I generated time-series of weights-at-age $y_{t,a}$ using the re-parametrized VBGM:

$$y_{t,a} = \log(\ w_{\infty_t}\ ) + 3\ \log\left(1 - \left[1 - \left(\frac{w_0}{w_{\infty_t}}\right)^{\frac{1}{3}}\right]\ e^{-k_t a}\right) + \varepsilon_t,$$

where age a ranged from 3 to 12 years old and w_0 was fixed at the larvae weight of Atlantic cod (*Gadus morhua*). To be more realistic, I used the weight of the larvae in the later stage where the larvae have absorbed all the yolk sac and are about to become juveniles. In this paper w_0 was fixed at the value of 0.27×10^{-3} g (Penglase *et al.*, 2013).

Under scenario 1 with a single regime (i.e. no regime shift), the parameters w_{∞_t} , k_t and σ_t are constant (Table 3.2). Under scenario 2 with two regimes, the generated $y_{t,a}$ are characterized by two underlying regimes with parameters $w_{\infty_t} \epsilon \{\ w_{\infty_1},\ w_{\infty_2}\}$, $k_t\ \epsilon \{\ k_1, k_2\ \}$, and $\sigma_t\ \epsilon \{\ \sigma_1, \sigma_2\ \}$

depending on the regime in year *t* (Table 3.2). The time series of the latent random effects (i.e. the temporal variation of regimes), $\{r_1, r_2, \ldots, r_T\}$, are specified to follow a step-wise change among two regimes (Figure 3.2).

I fitted two models to each of the generated data sets, i.e. a model without regime shift (VBGM), and a model with regime shift (HMGM). I compared model performance using the Akaike information criterion with a correction for small sample sizes (AICc).

Let *n* be the number of parameters in the model, and S be the sample size (i.e. the total number of data points observed). AICc is given by

$$AICc = 2n - 2\log(\hat{L}_{\Theta}) + (2n^2 + 2n)/(S - n - 1)$$

Finally, I evaluated the simulation parameter estimates of the selected model under each scenario by root-mean-squared error (RMSE), relative root-mean-squared error (RRMSE), and bias,

$$RMSE = \sqrt{\frac{\sum_{z=1}^{1000}\left(\hat{\theta}_z - \theta\right)^2}{1000}}$$

$$RRMSE = \frac{RMSE}{\theta}$$

$$bias = \frac{\sum_{z=1}^{1000}(\hat{\theta}_z - \theta)}{1000},$$

where hat denotes the parameter estimates, and θ denotes the true parameter values.

3.4 Case study

After verifying the ability of our modeling approach to accurately identify regime shifts in simulated data, I applied the two models (VBGM and HMGM) to identify potential abrupt shifts in growth based on empirical annual weight-at-age data for the Atlantic cod stock on the southern Grand Bank (Northwest Atlantic Fisheries Organization (NAFO) Divisions 3NO) (Rideout *et al.*, 2018). The beginning-of-year mean weights-at-age data during 1959-2018 and ages 3-12 were calculated from commercial catches of cod in Divs. 3NO (Figure 3.1). The overall trend of weights at age for the cod stock increased in the mid-1960s and remained high throughout the 1970s and 1980s, then dramatically decreased in the early 1990s, accompanied by the population collapse. The weights at age increased again in early 2000s but declined quickly in the late 2000s and remained low until the present (Rideout *et al.*, 2018). The interannual trend of mean weights-at-age is especially apparent for cod at age 8-12 (Figure 3.10). The stock declined dramatically during the mid-1980s and the 2018 estimate of spawner stock biomass is 18,537 t, which is still well below the B_{lim} (60,000 t) (Rideout *et al.*, 2018). This stock has been under a fishing moratorium since February 1994 and fishing mortality has been declining since 2006. However, the cod stock has shown little recovery despite severe restrictions on directed fishing.

I fitted the VBGM and HMGM to the mean weight-at-age data for the cod stock. The starting values of parameters for the VBGM were fixed at $w_\infty = 47.76$, $k = 0.065$, and $\sigma = 0.086$. For the HMGM, w_∞'s, k's, and $\sigma's$ were assigned the same initial values of 100, 0.1, and

0.5, respectively. The initial values of the VBGM and HMGM were set randomly. I fixed w_0 at the value of $0.27 \times 10^{-3}\ g$, which is the empirical weight of the Atlantic cod (*Gadus morhua*) larvae after 30 days post hatch (Penglase *et al.*, 2013). The initial 2 X 2 matrix of q_{ij} was assigned equal values summing to 1 on each row. The models were compared using AICc and the selected model was used to identify abrupt shifts in the growth for 3NO cod. I tried different initial values for the HMGM and found that the estimates for w_∞ and k are somewhat sensitive to starting values. However, the model means predicted by the HMGM were almost the same even with different initial values. The estimated parameters and model means for the HMGM with different starting values are provided in Appendix I.

3.5 Results

3.5.1 Simulation results

Results confirmed that fitting the HMGM to the weight-at-age time series data and comparing model performance using AICc is an effective and objective way of identifying abrupt shifts in weight-and-age relationships. For single regime scenarios (i.e. scenario 1), the VBGM outperformed HMGM across almost all 1000 trials, and for 2-regime scenarios (i.e. scenario 2) the HMGM outperformed VBGM in almost all the 1000 iterations (Table 3.3). The estimates of parameters w_∞, k, and σ for the selected VBGM and HMGM were close to the true parameter values that were used to simulate the data (Figure 3.3). The relatively poor estimate of $w_{\infty 2}$ could be attributed to insufficient weight data at older ages (the simulated age ranged from 3 to 12 years old). The precision of parameter estimates for each selected model across two scenarios was evaluated by root-mean-squared error (RMSE), relative root-mean-squared error (RRMSE), and bias. The RRMSEs and bias of parameters for VBGM were very close to zero, which indicated the high precision of parameter estimates. The parameter estimates for HMGM were also good with some exceptions (i.e. the RMSEs of $w_{\infty1}, w_{\infty2} > 1$), but the precision was acceptable (Table 3.4). Although the bias and RMSEs of the parameter estimates for $w_{\infty1}$ and $w_{\infty2}$ were a bit high, the HMGM can fit the model mean very well. For both regimes, the simulated model means fell between the first and third quartiles of the estimated model means across all ages, indicating the good performance of HMGM to predict the model mean (Figure 3.4). The HMGM was effective at correctly identifying the true regime for individual years. For the 2-regime scenario, 949 out of the 1000 trials accurately predicted the year-specific regime for all of the years in the time series (Figure 3.5).

3.5.2 One example of HMGM fit

Taking one of the 1000 trials as an example, the AICc values of HMGM and VBGM were -145.906 and -29.7973, respectively. The predicted r_t's of HMGM were the same as the true r_t's (Figure 3.6). The parameter estimates of HMGM were close to true parameter values (Figure 3.7). The HMGM fits the simulated weight-at-age data better than VBGM (Figure 3.8).

3.5.3 Case study results

Fitting the two models to empirical time-series of average weight-at-age data for cod in Divs. 3NO suggested the existence of two distinct growth regimes for this stock. The HMGM outperformed VBGM with better fit to data (Figure 3.9a) and lower AICc (Table 3.5). Four regime shifts taking place in 1967, 1993, 2001, and 2009 were identified for the cod stock, dividing the time series into a favorable regime (regime 2) and an unfavorable regime (regime 1) (Figure 3.9b). Compared to the favorable regime, the unfavorable regime was characterized with lower growth rate *k* and lower asymptotic weight w_∞ (Table 3.5). The two regimes had substantially different growth curves, which led to different levels of weight at the same age (Figure 3.9a). The estimated interdecadal trend in weights across all ages was consistent with the observed pattern, with weight in a higher level during the 1970s, 1980s, and 2000s, and in a lower level in the 1990s, 2010s, and before the mid-1960s (Figure 3.10). The standardized residuals for the HMGM by year, age, cohort, and predicted log mean weights did not show obvious patterns, and the means of these standardized residuals are quite close to zero (Figure 3.11). Furthermore, according to the estimated probability of transition from the low growth regime to the high growth regime ($q_{12} = 0.082$), I predicted that the cod stock was very likely to shift back to the high growth regime with a probability more than 0.5 within 9 years, and with a probability of 0.95 within 35 years (Table 3.6).

3.6 Discussion

3.6.1 Model somatic growth using HMGM

The growth of fish is highly variable and remarkably plastic (Jorgensen, 1992; King and Mcfarlane, 2006a; King *et al.*, 2015). Interannual variations in weight-at-age have been thoroughly documented (Krohn, 1997; King and Mcfarlane, 2006a; Mullowney *et al.*, 2019; Mion *et al.*, 2020). However, fish growth might change in a dramatic way, instead of changing slowly. I proposed an objective and effective way to account for abrupt shifts in fish growth under changing environmental regimes. The methodology I proposed was able to correctly identify abrupt shifts in fish growth, predict the year-specific regime for all of the years in the time series with high precision, and provide good estimates for VonB growth model and especially for the mean weights at ages in the data age range. Moreover, the method can be easily extended to multiple HMGM (i.e. three-regime HMGM, and four-regime HMGM) if three or even more different levels of weight-at-age in the time series were observed. One thing to be aware of when applying our method to empirical data is that the w_∞ and k parameters may not be estimated very well when weights at older ages are not available. For example, the weight-at-age data for the cod stock in Divs. 3NO is limited at age of 12. The absence of weights at older ages could lead to unreliable estimates for the maximum weight w_∞, and hence imprecise estimates for the growth rate k, because k is highly correlated with w_∞. However, simulation tests showed that even the biased estimates of w_∞ and k will not affect the model predicted mean weight-at-age, which indicated the capability of the method to provide scientific information for fisheries stock assessment and management. I describe this part of simulation in Appendix D .

3.6.2 Abrupt shifts in growth of 3NO cod

The weight-at-age of the cod stock on the southern Grand Bank was estimated to alternate between low and high levels in the time series of 1959 to 2018, with four abrupt shifts in growth taking place in 1967, 1993, 2001, and 2009. Variations in weights at age are generally attributed to changes in growth rate attributable to environmental variables (i.e. temperature), food availability, size-selective effects of fishing, and to their combinations (Sinclair *et al.*, 2002; Brander, 2007; Kuriyama *et al.*, 2016). Many studies suggested that annual variations in weight-at-age of North Atlantic cod (*Gadus morhua*) populations might be largely controlled by water temperature (Brander, 1995; Rätz *et al.*, 1999; Sinclair *et al.*, 2002). Our findings are consistent with these previous studies, and I conclude that the growth of the cod stock on the southern Grand bank is highly correlated with water temperature. The four growth shifts I identified throughout these decades coincided with changes in water temperature on the southern Grand Bank. The 1967 abrupt shift coincided with the arrival of the maximum temperature in the mid-to-late 1960s (Colbourne, 2004), the 1993 shift was concomitant with the extreme cold water temperature in the early 1990s, the 2001 shift was concurrent with the recovered warm water temperature in 2000, and the 2009 shift coincided with the decreased temperature after a notable 61-year high in 2006 (Templeman, 2010). There is apparently a positive relationship between the cod growth and water temperature on the southern Grand Bank. The cod growth seems to be very vulnerable to variations in water temperature and will react immediately once water temperature changes. Although there are other factors that are responsible for changes in the growth of 3NO cod, water temperature seems to be a key factor causing the observed temporal variation of growth pattern.

The cod stock was in the low growth regime before the mid-1960s, then suddenly shifted to the high growth regime in 1967, concomitant with the maximum water temperature in the mid-to-late 1960s (Colbourne, 2004). Throughout the 1970s and 1980s, the stock has remained in the high growth regime, with higher growth rate and higher weights at age. There was a dramatic decline in weights-at-age of the cod stock in 1993. This abrupt shift in cod growth was expected as it is well known that there was a large-scale regime shift in the marine ecosystem off Newfoundland during the late-1980s and early-1990s (Lilly *et al.*, 2000; Dempsey *et al.*, 2017; Buren *et al.*, 2019), with the marine ecosystem shifting to an environmental regime where conditions (i.e. temperature, and food availability) are unfavorable for fish populations. Fish growth is generally considered to be strongly dependent on temperature, and low temperatures could depress growth (Millar *et al.*, 1990; Brander, 1995; Dwyer *et al.*, 2003; Thorsen *et al.*, 2010). The ocean temperatures on the southern Grand Bank generally started to decline in 1984 and reached the minimum of record since 1950s at the end of 1980s (Templeman, 2010). In addition, capelin off Newfoundland (*Mallotus villosus*) suffered an order of magnitude decline in biomass in the early 1990s (Buren *et al.*, 2014; Buren *et al.*, 2019; Mullowney *et al.*, 2019). While cod diet was historically dominated by capelin (Rose and O'Driscoll, 2002), the unavailability of prey could directly result in the dramatic decline in cod growth. The marked decline in cod growth in 1993 could be the consequence of the joint effects of cold water temperature and absence of capelin.

After the 1993 growth shift, the cod stock has generally remained in the low growth regime, with only a brief respite from 2001 to 2008. The brief rebounding of cod growth could be attributed to a general warming in oceanographic conditions from 1995 to 2010 (Murphy, 2018). After the mid-1990s, a slight recovery of water temperatures commenced on the Grand Bank, and water temperatures had returned to warmer conditions and are closer to the long term average in 2000 (Dwyer *et al.*, 2003; Drinkwater, 2005). The ocean temperature in the Grand Bank region continues to increase, with a notable 61-year high in 2006 (Templeman, 2010). It is very likely that increased water temperature accelerated the growth rate of the cod stock, leading to higher weights at age during 2001 and 2008. However, water temperature on the southern Grand Bank showed a downward trend after 2006, when temperature cooled but remained above normal from 2007 to 2011 and decreased significantly in the following four years to below normal in 2015 (Colbourne *et al.*, 2016). The cooling water temperature after 2006 seems to be the only plausible explanation for the sharp decline in weights at age of the cod stock in 2009. The effect of fishing mortality on the growth of this stock was weak and not even in the same direction as the changes in weight at age. For example, although the cod stock in Divs. 3NO has been under a fishing moratorium since February 1994, fishing mortality has not declined until 2006 (PoIr *et al.*, 2010; Rideout *et al.*, 2018). The weight at age of 3NO cod increased in 2001 when fishing mortality was high and declined in 2009 while fishing mortality was reduced. Hence, I conclude that rather than fishing mortality, environmental forcing such as water temperature and food availability are important causes of the abrupt changes in the growth of the cod stock.

3.6.3 Is there an evolutionary impact of fishing mortality on fish growth?

Since the regime shift in 2009, despite imposition of severe catch restrictions (PoIr *et al.*, 2010; Rideout *et al.*, 2018), the cod stock in Divs. 3NO has remained in the low growth regime and showed no appreciable signs of recovery. The probable causes of this are mainly two, one is unfavorable environmental conditions, including cold water temperatures and poor feeding conditions, and another is the commonly assumed evolutionary impacts of size-selective fishing mortality. Interest in the impact of size-selective fishing on the evolution of growth rates is long standing (Hilborn and Minte-Vera, 2008). Numerous studies suggested that the cumulative size-selective mortality will result in long-term changes in population growth characteristics (e.g., growth potential w_∞) (Sinclair *et al.*, 2002; Hutchings 2005; Shelton *et al.*, 2006). For example, Swain *et al.* (2007) suggest that high size-selective fishing mortality has caused genetic changes in growth of the Atlantic cod stock in the southern Gulf of St Lawrence. Similarly, Sinclair *et al.* (2002) propose that the selective removal of large (or small) individuals would result in the surviving population having a lower (or higher) growth potential. On the contrary, others argue that environmental rather than evolutionary factors are far more likely to have affected growth of cod stocks (Brander, 2007; Hilborn and Minte-Vera, 2008). Here, in the case of 3NO cod, the rebound in the cod growth during 2001 and 2008 provided strong evidence that the cod stock in Divs. 3NO may not be strongly affected by evolutionary changes in growth despite the intensive size-selective fishing throughout the 1970s and 1980s. Moreover, our method predicted that the cod stock will return to the high growth regime in nine years with a probability of more than 0.5, and in 35 years with a probability of 0.95. Hence, I concluded that the lack of recovery of the cod stock somatic growth rates is more attributable to the adverse environmental conditions than to size-selective fishing mortality. Cold water temperature could be one impediment to the recovery of the cod growth. Capelin would be another key factor which delayed the cod growth recovery. Capelin off Newfoundland waters collapsed in the early-1990s and have showed no evidence for recovery over the subsequent three decades (Rose and O'Driscoll, 2002; Buren *et al.*, 2019; Zhang *et al.*, 2020a). More than a dozen studies have suggested that interannual variability in capelin abundance plays an important role in growth changes in individual cod stocks off Newfoundland and Labrador, and cod rebuilding requires capelin (Rose and O'Driscoll, 2002; Brander, 2007). The absence of capelin could be a big contributor to the prolonged slow growth for the cod stock. Overall, the changes in growth of this stock are more likely to be plastic variations rather than evolutionary changes. It is very likely that the cod stock will shift back to the high growth regime when the marine ecosystem shifts to a favorable environmental regime.

3.7 Tables

Table 3.1 Variables included in the model structure.

Variable	Denotation
t	The index of year, $t \in \{1, 2, \ldots, T\}$
T	The final year in which average weight-at-age data was observed
A	The maximum age
K	The number of possible regimes
r_t	The regime state in year t, $r_t \in \{1, 2, \ldots, K\}$
q_{ij}	The probabilities of transitions into regime j from regime i
w_a	The weight at age a
w_0	The weight at age zero
t_0	The age when the weight is zero
θ	$\theta = (w_\infty, k)$
θ_j	$\theta_j = \left(w_{\infty j}, k_j\right)$
$w_{\infty j}$	The asymptotic weight in regime j, j=1, 2, …K
k_j	The growth rate in regime j, j=1, 2, …K
ε_t	The process error and the measurement error of $y_{t,a}$
σ_j	The standard deviation of error term $\boldsymbol{\varepsilon_t}$ in regime j, j=1, 2, … K
y_t	The average weights-at-age in year t
$y_{t,a}$	The logarithm of average weight at age a, in year t

Table 3.2 The true values of the parameters w_{∞_t} , k_t, and σ_t used for data generation for the two scenarios.

	Scenario 1	Scenario 2	
w_{∞_t}	15	$w_{\infty 1} = 10$	$w_{\infty 2} = 15$
k_t	0.35	$k_1 = 0.45$	$k_2 = 0.4$
σ_t	0.08	$\sigma_1 = 0.06$	$\sigma_2 = 0.06$

Table 3.3 The counts of each model selected by AICc for the two simulation scenarios.

Scenario		VBGM	HMGM
1	#Best Model	999	1
2	#Best Model	0	998

Table 3.4 The bias, Root Mean Squared Error (RMSE) and Relative Root Mean Squared Error (RRMSE) of the parameter estimates for the selected model and two scenarios.

	Scenario 1			Scenario 2					
	VBGM			HMGM					
	w_∞	k	σ	$w_{\infty 1}$	$w_{\infty 2}$	k_1	k_2	σ_1	σ_2
True value	15	0.35	0.08	10	15	0.45	0.40	0.06	0.06
RMSE	0.16	0.004	0.007	1.91	1.90	0.11	0.14	0.0079	0.0081
RRMSE	0.011	0.013	0.09	0.19	0.13	0.26	0.36	0.132	0.135
Bias	-0.023	0.0008	-0.001	0.88	-0.80	-0.02	0.07	-0.0013	-0.0018

Table 3.5 The AICc and parameter estimates of the VBGM and HMGM for 3NO cod.

	VBGM	HMGM	
$AICc$	-39.68	-84.97	
w_∞	51.90	$w_{\infty 1} = 42.44$	$w_{\infty 2} = 53.07$
k	0.06	$k_1 = 0.06$	$k_2 = 0.07$
σ	0.17	$\sigma_1 = 0.08$	$\sigma_2 = 0.09$
q_{ij}	NA	$q_{11} = 0.92$	$q_{12} = 0.08$
		$q_{21} = 0.06$	$q_{22} = 0.94$

Table 3.6 The probability of transition from the low growth regime (regime 1) to the high growth regime (regime 2) within the following T years.

Year *T*	1	2	3	4	5	6	7	8
Probability	0.082	0.157	0.226	0.290	0.348	0.401	0.450	0.495
Year *T*	9	10	11	12	13	14	15	16
Probability	0.537	0.575	0.609	0.641	0.671	0.698	0.723	0.745
Year *T*	17	18	19	20	21	22	23	24
Probability	0.766	0.785	0.803	0.819	0.834	0.847	0.860	0.871
Year *T*	25	26	27	28	29	30	31	32
Probability	0.882	0.892	0.900	0.909	0.916	0.923	0.929	0.935
Year *T*	33	34	35	36	37	38	39	40
Probability	0.940	0.945	0.950	0.954	0.958	0.961	0.964	0.967

3.8 Figures

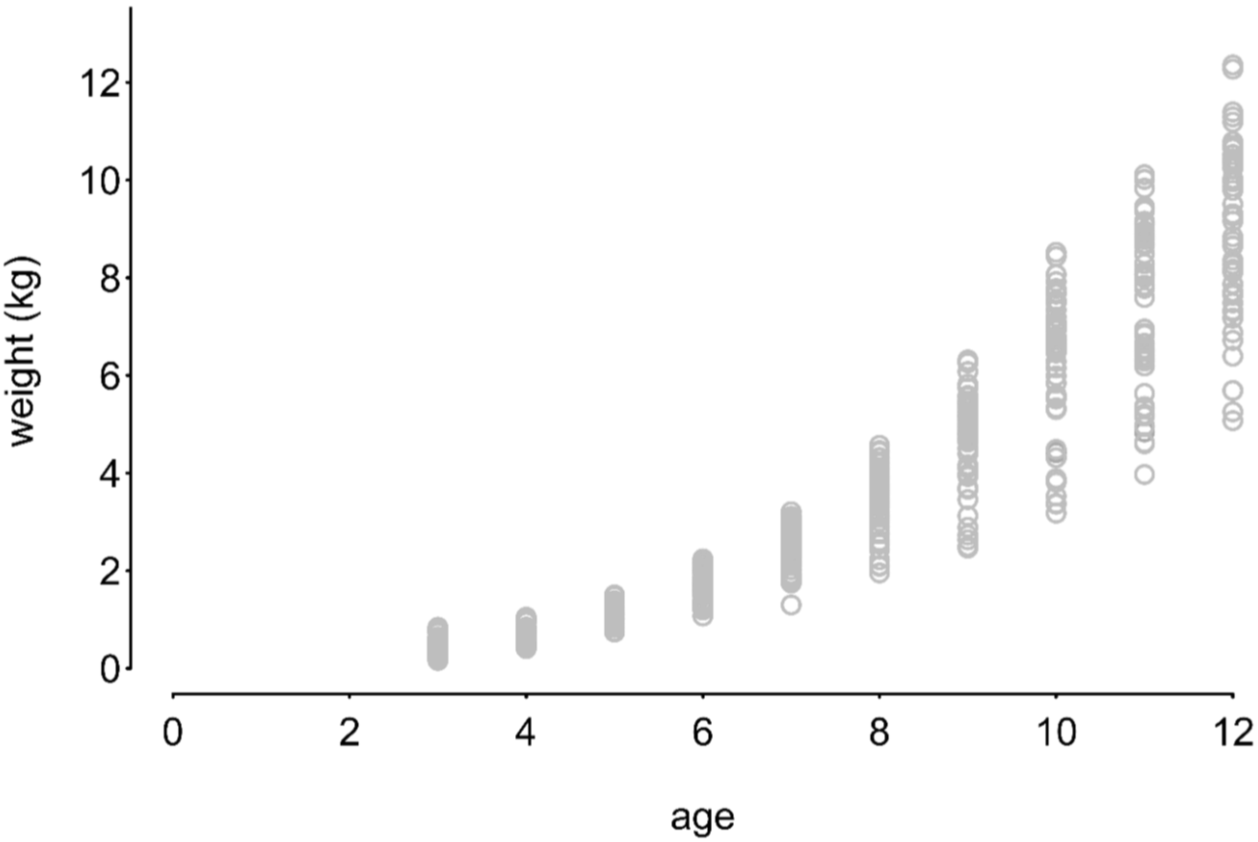

Figure 3.1 The annual weights-at-age of an Atlantic cod stock on the southern Grand Bank, Newfoundland.

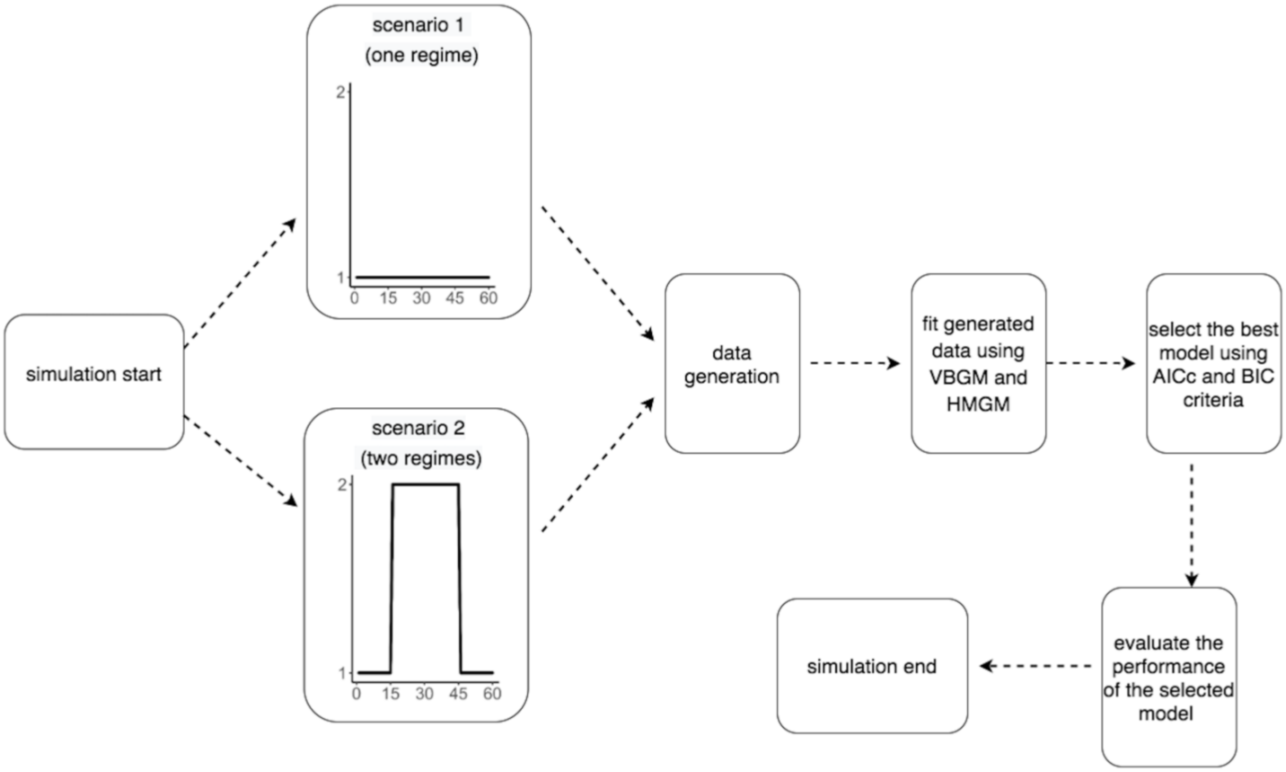

Figure 3.2 Simulation framework.

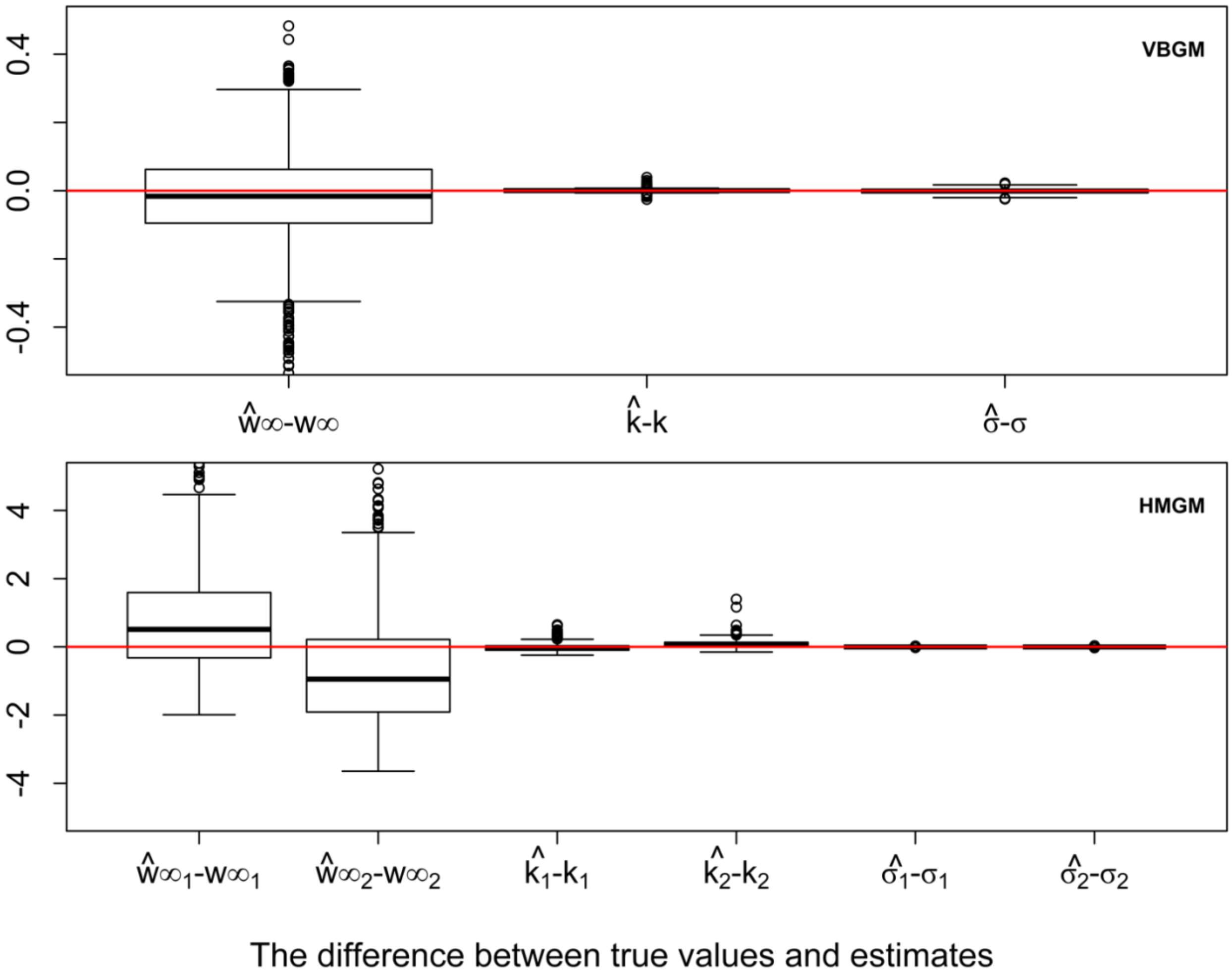

Figure 3.3 The bias of parameter estimates in all the 1000 simulation trials with the VBGM and HMGM for scenarios 1 and 2 from top to bottom.

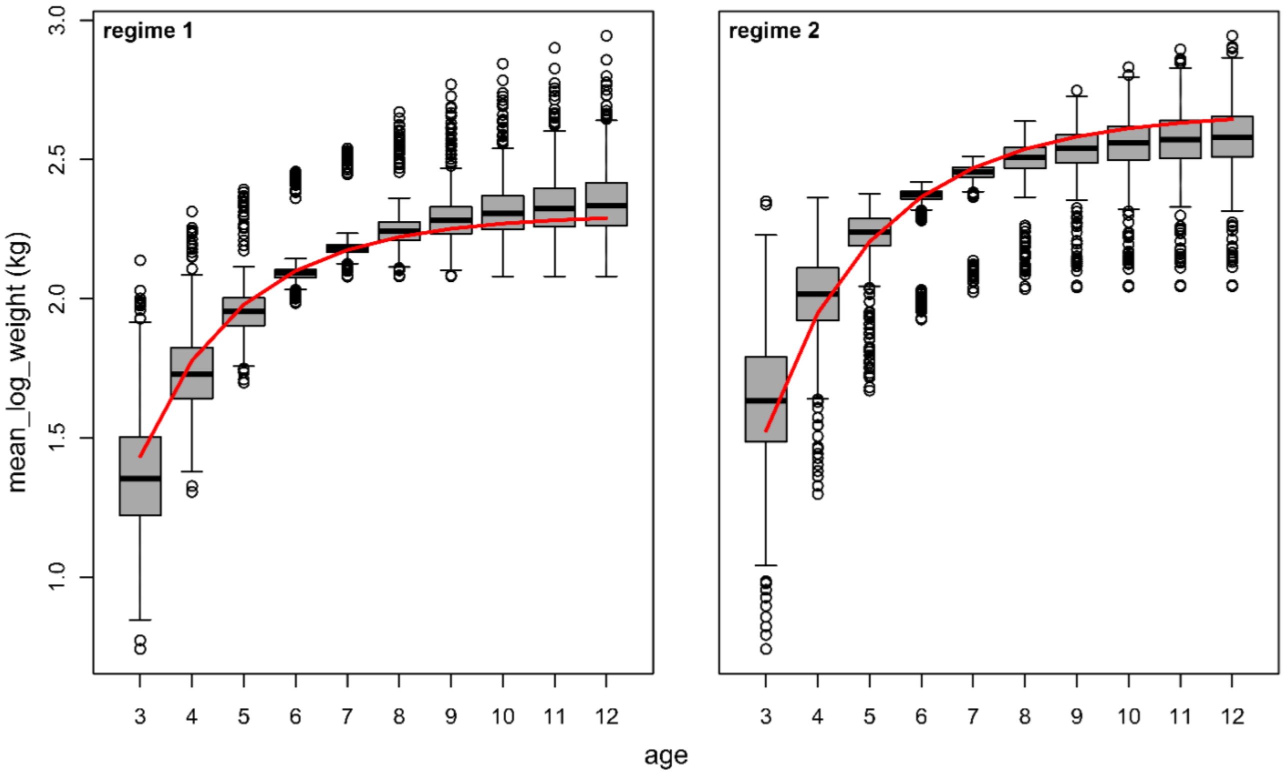

Figure 3.4 Boxplots are estimated model means versus age across 1000 repetitions, and the two red curves are simulated model means for the two regimes.

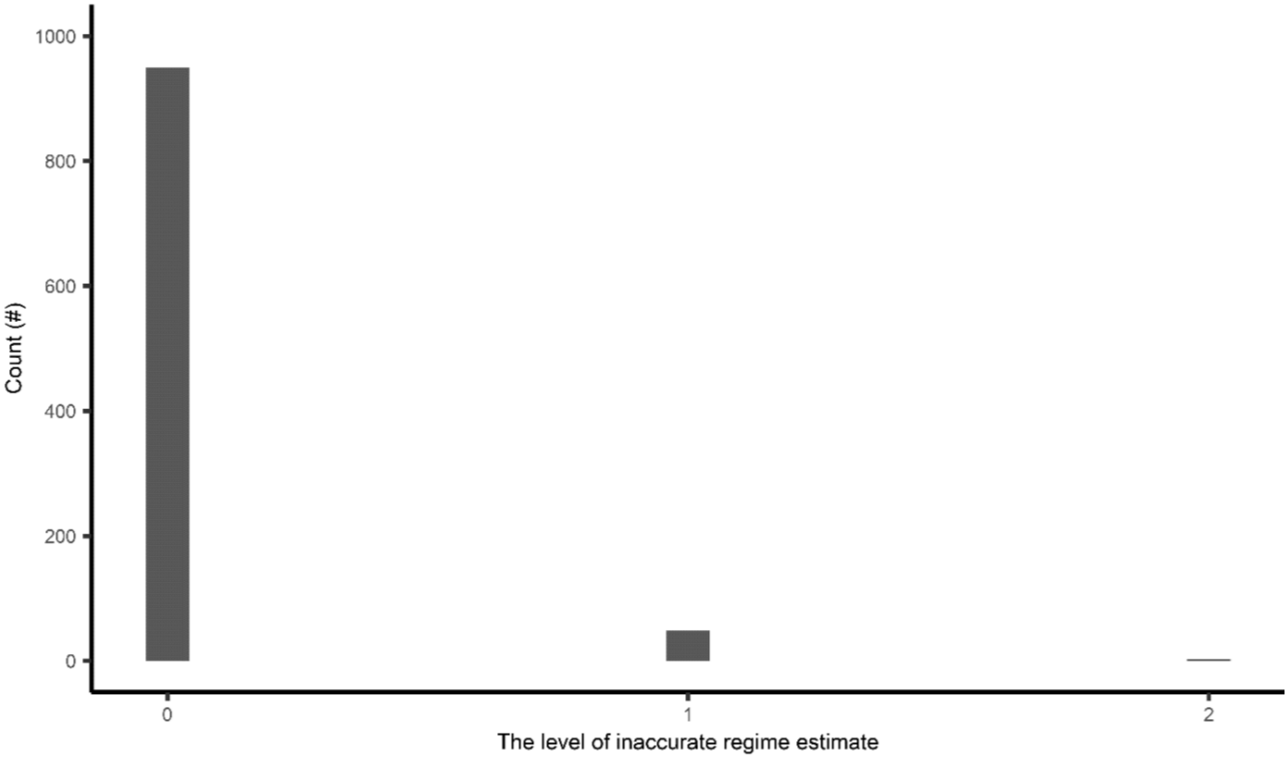

Figure 3.5 The regime detection accuracy of the HMGM-2 simulation. Zero indicates that the predicted time series of regimes are exactly the same as the true dynamics, and two indicates that there are two years where the regime is mis-identified in one iteration, and so on. The vertical axis shows the count of each estimate level across 1000 trials.

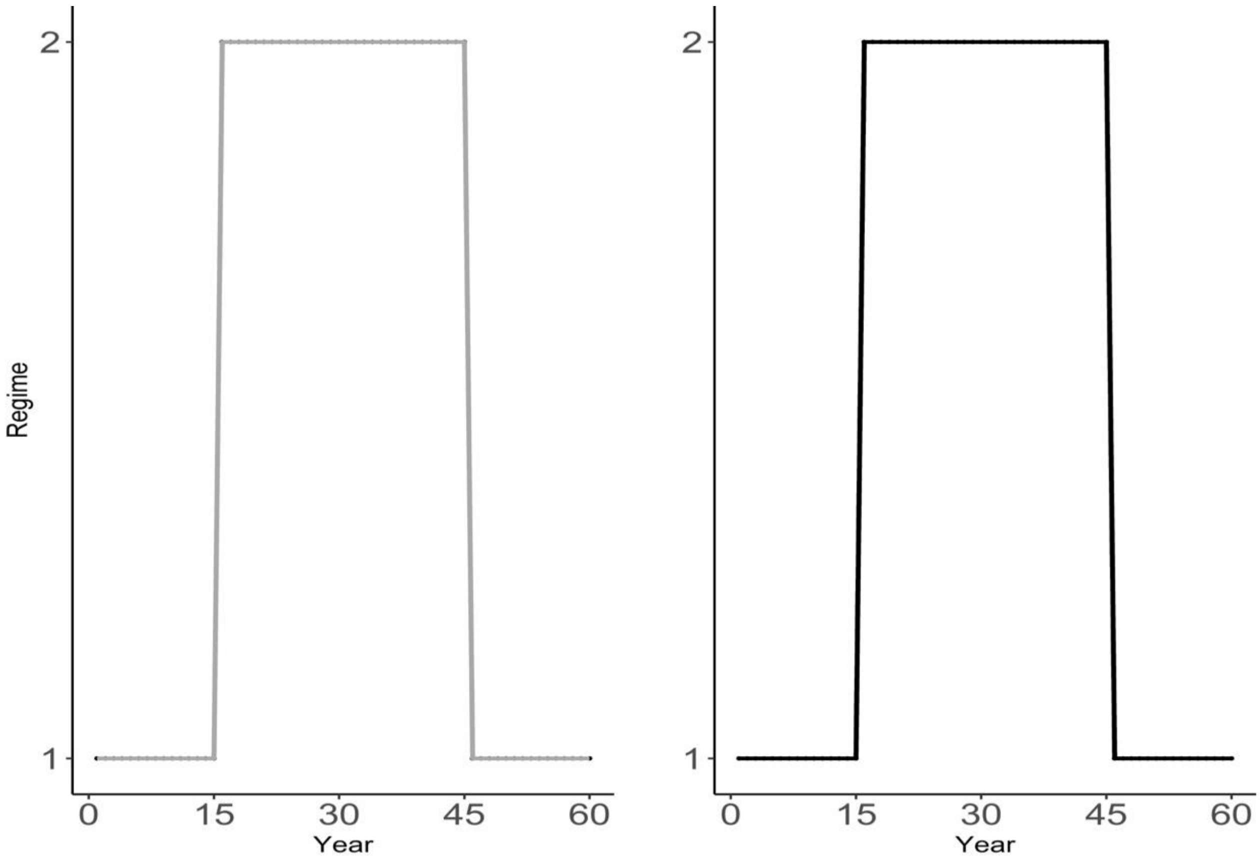

Figure 3.6 The regime state of each year for the true dynamics (left) and the HMGM predictions (right).

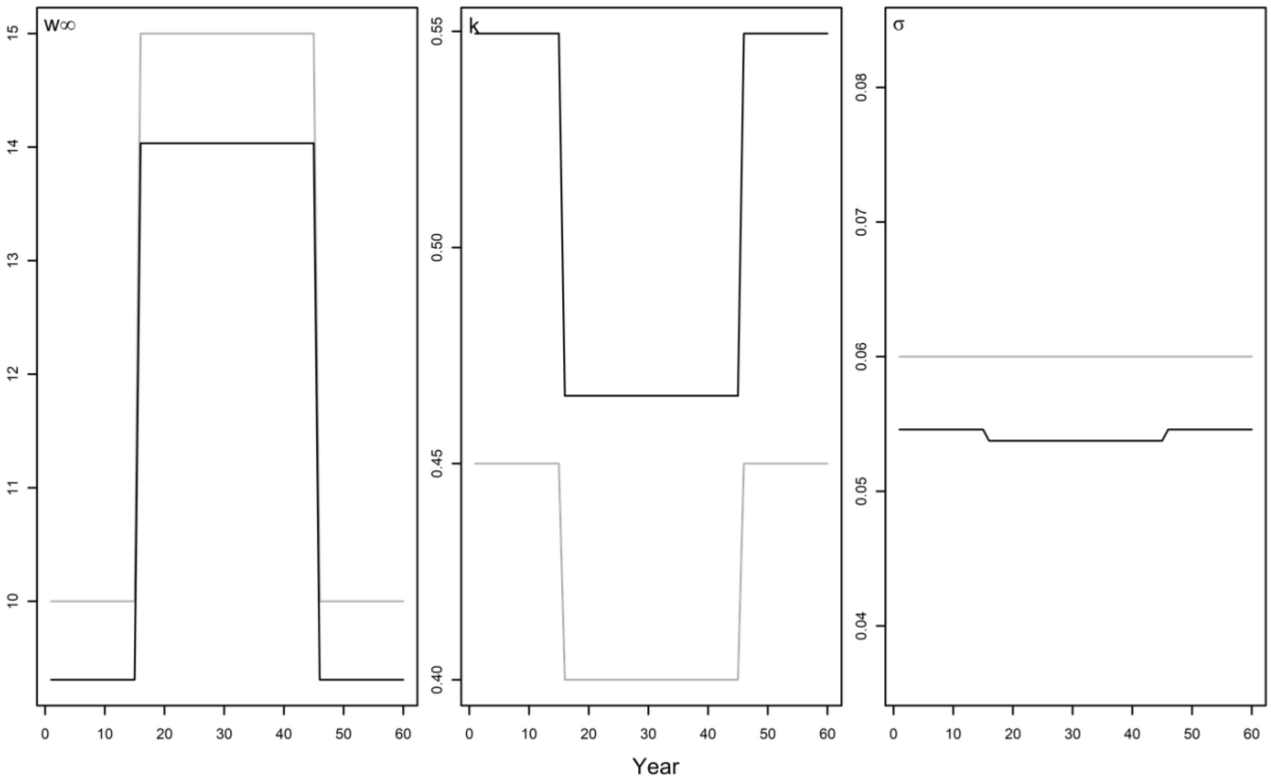

Figure 3.7 The time series of w_∞, k, and σ for the true dynamics (gray lines) and the HMGM (black lines). The true values of $w_{\infty 1}$ and $w_{\infty 2}$ were 10 and 15 respectively, and the estimated $\hat{w}_{\infty 1}$ and $\hat{w}_{\infty 2}$ were 9.31 and 14.03 respectively. The true values of k_1 and k_2 were 0.45 and 0.4 respectively, and the estimated $\hat{k}_1$ and $\hat{k}_2$ were 0.55 and 0.47 respectively. The true σ_1 and σ_2 were assigned the same value of 0.06, and the estimated $\hat{\sigma}_1$ and $\hat{\sigma}_2$ were 0.055 and 0.054 respectively.

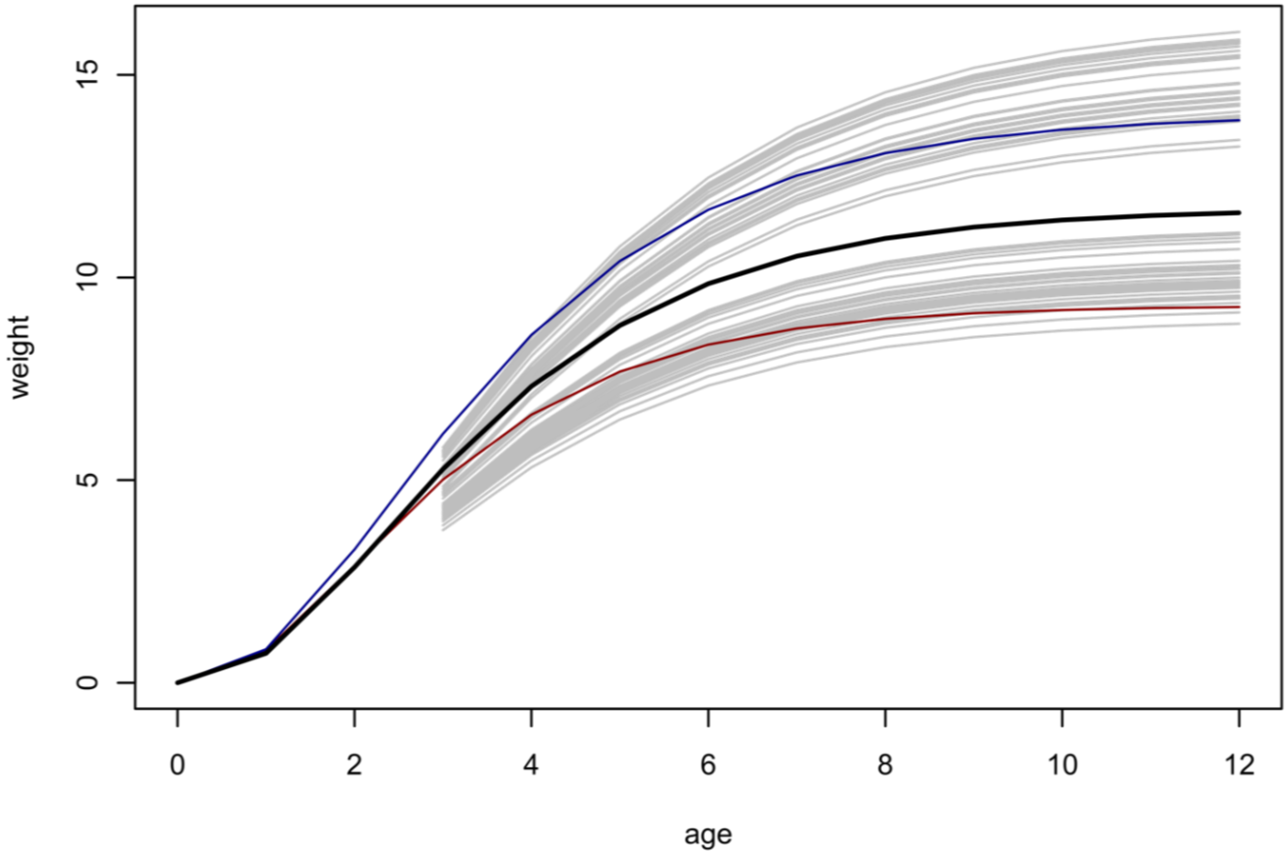

Figure 3.8 The fitted growth curves for the VBGM and HMGM. The gray lines are simulated annual weights-at-age. The VBGM fit is shown as a black line. The colored lines denote the HMGM fit in two regimes.

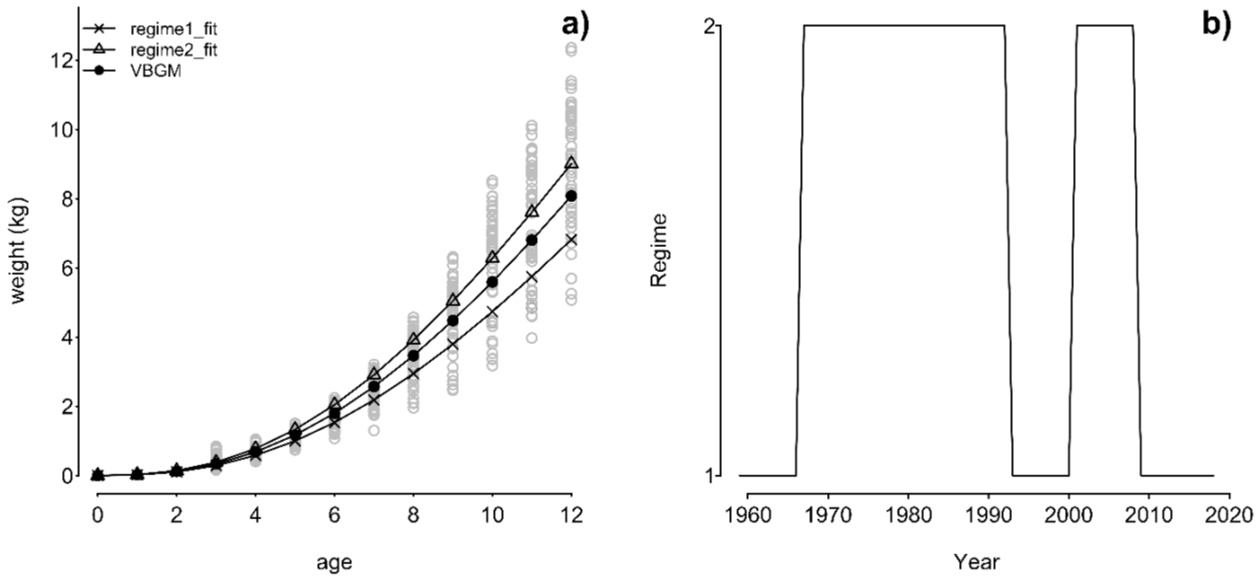

Figure 3.9 (a) The annual weight-at-age data of 3NO cod (gray dots) and fitted growth curves of the VBGM and HMGM. (b) The predicted regime time series of the HMGM for 3NO cod.

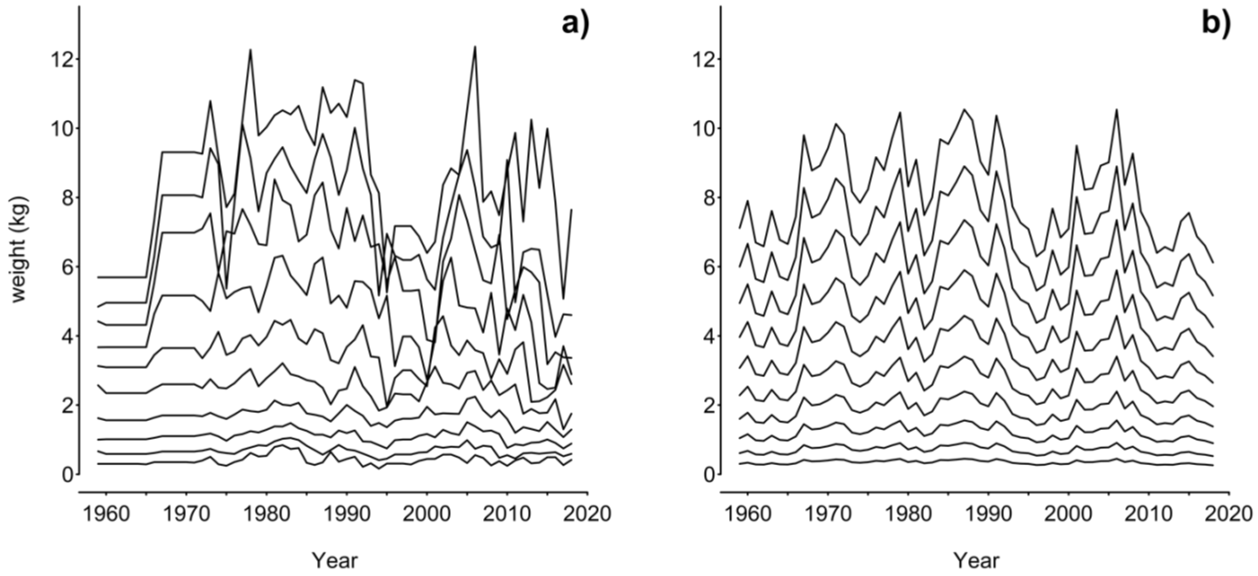

Figure 3.10 a) Empirical mean weight at ages 3 to 12 for southern Grand Bank cod (*Gadus morhua*; 1959–2018). b) weight at ages 3 to 12 estimated by the HMGM. The lines are for ages 3 to 12 are from bottom to top.

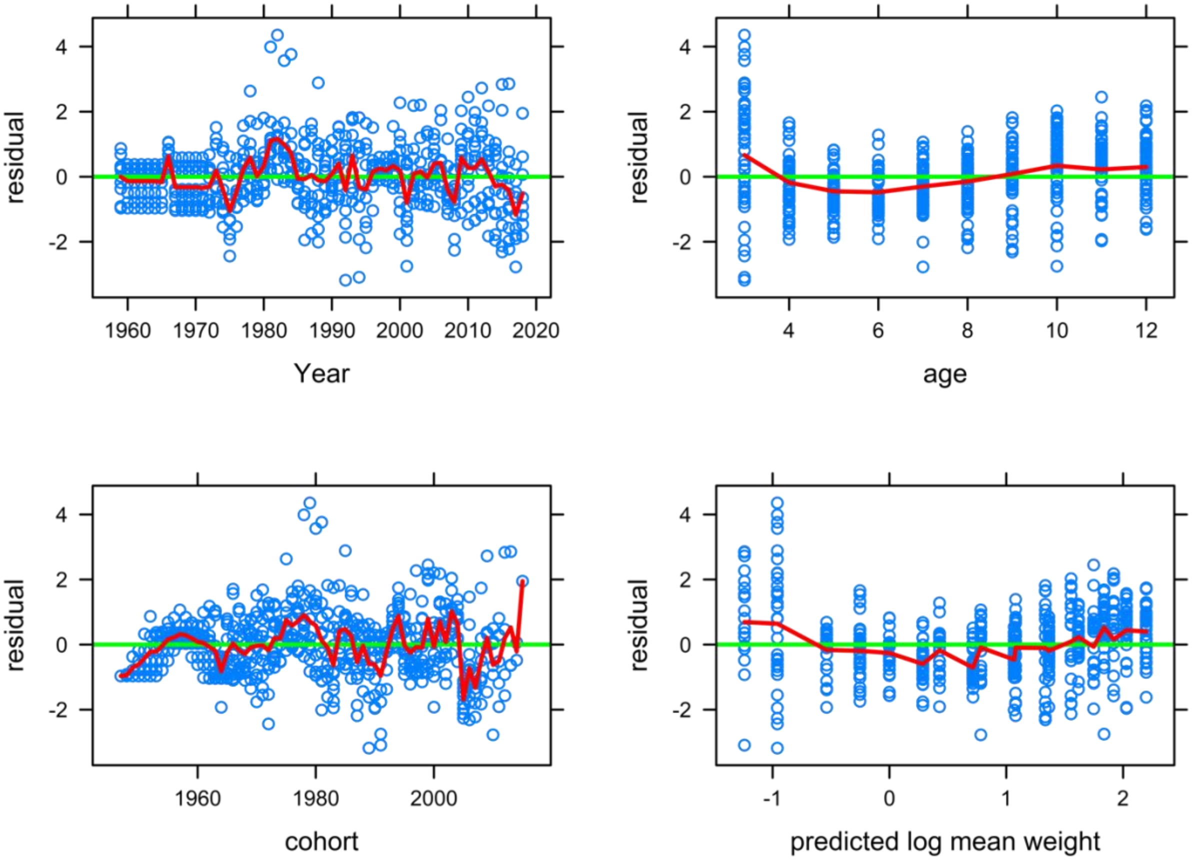

Figure 3.11 The standardized residuals of the HMGM for the 3NO cod.

Chapter 4

Manage abrupt shift in fish population dynamics

4.1 Management implications of abrupt shift in fish population dynamics

Biological reference points are important tools that facilitate assessing the status of fish stocks in relation to management objectives (Heino *et al.*, 2013). Reference points are most commonly derived from stock-recruitment relationships, yield-per-recruit relationships, or production models (Heino *et al.*, 2013), and hence depend on key population traits such as recruitment, growth, and mortality. Numerous studies suggest that changes in fish productivity caused by regime shifts, intensive fishing, or other environmental fluctuations could cause shifts in management reference points (Haltuch *et al.*, 2009; Köster *et al.*, 2009; Heino *et al.*, 2013; Morgan *et al.*, 2014; Zhang *et al.*, 2020b). Such shifts, if not accounted for, are likely to lead to reference points that lose their intended meaning and utility for fisheries management (Heino *et al.*, 2013).

The MSY (maximum sustainable yield) based reference points, such as B_{MSY} (biomass leading to maximum sustainable yield), F_{MSY} (the rate of fishing mortality leading to maximum sustainable yield), and limit reference points B_{lim} (the biomass threshold below which there is an increased probability of impaired recruitment) and F_{lim} (the fishing mortality leading to B_{lim}) are based on stock-recruitment relationships (Brunel *et al.*, 2010; Maunder, 2012; Zhang *et al.*, 2018). If recruitment changes drastically, these reference points that depend on recruitment may change accordingly, and unaccounted shifts will lead to management decisions that become either more or less precautious than originally intended. For example, if the management limit B_{MSY} is based on a higher recruitment regime, the risk of overfishing will increase when recruitment shifts to a lower productivity phase. Conversely, B_{MSY} based on a lower recruitment regime will lead to overly cautious harvest at the beginning of a higher recruitment regime, which is safe, but potentially costly (Vert-pre *et al.*, 2013).

Similar to these reference points that depend on a SRR, yield-per-recruit (YPR) reference points, including fishing mortality thresholds F_{MAX} (the rate of fishing mortality that maximizes yield per recruit) (Cooper, 2006) and $F_{0.1}$ (the fishing mortality rate corresponding to 10% of the slope of the yield-per-recruit curve at the origin) (Gabriel and Mace, 1999) could also change drastically for changing growth regimes. YPR reference points are determined by individual fish growth rate (Morgan *et al.*, 2014). While there is substantial evidence that fish somatic growth can experience abrupt shifts, the use of fishing mortality reference points that do not incorporate abrupt shifts in growth is likely to result in unexpected population decline or even collapse when productivity is low (Morgan *et al.*, 2014). Taking F_{MAX} as an example, the F_{MAX} estimated from YPR analysis based on rapid growth rate could be much higher than the F_{MAX} based on slow growth rate. If the fish stock suddenly shifts to a slow-growth regime while the fishing mortality rate remains unchanged, it is very likely that the fishing mortality will exceed the "true" F_{MAX} of the slow-growth regime, which may lead to growth overfishing (Cooper, 2006). Moreover, Morgan *et al.* (2014) reported that the level of F_{MAX} during low productivity was actually much greater than F_{MSY}. They found that when productivity was low, F_{MSY} was zero for 2J3KL and near zero for 3NO cod, whereas F_{MAX} was 0.54 and 0.27, respectively. Fishing at F_{MAX} under this condition would lead to unsustainable harvest levels. Given the dramatic impacts that regime shifts have on fish productivity, traditional approaches of calculating reference points that assume constant population traits cannot maintain sustainable fisheries when productivity is greatly reduced. Sustainable management of fisheries resources calls for adjusted reference points that take regime shifts in fish productivity into account.

4.2 Regime-specific management strategies and challenges

The population productivity may have changed systematically and may remain at this level for a long time after a regime shift has occurred (Yatsu *et al.*, 2005). In such cases, the stock may be better managed at its new level of productivity using corresponding biological reference points (Polovina, 2005; Karp *et al.*, 2019). Several recent studies suggest regime-based Harvest Control Rules (HCRs) for marine fish stocks that undergo marine ecosystem regime shifts (Freon, 2005; King and Mcfarlane, 2006b; Mohn and Chouinard, 2007; Szuwalski and HolloId, 2016), and various adaptive management practices have been examined. For example, the application of regime-specific harvest rates is one possible approach, in which fisheries managers apply a higher exploitation rate during the high productivity regime and a lower exploitation rate during the low productivity regime (Rothschild and Shannon, 2004; deYoung *et al.*, 2008).

Applying regime-based HCRs in regime-based systems could be an effective management strategy to incorporate the inferred productivity changes (Szuwalski and Punt, 2013). However, despite the considerable attention of regime-based management strategies, the implementation has languished. A major impediment to implementing regime-specific HCRs is the difficulty in determining whether the population dynamics are truly regime-based. Population processes such as recruitment and growth are highly variable, and the underlying mechanisms behind their fluctuations are extremely complicated. It is difficult to determine whether the changes in fish productivity is caused by marine ecosystem regime shifts or such changes are just temporal variations induced by fishing. Punt *et al.* (2014) suggest that the regime-based HCRs may be useful only when fish population dynamics are truly regime-based and could actually lead to greater risk when there are no regime shifts in fish productivity. Szuwalski and Punt (2013) conducted a management strategy evaluation for the snow crab (*Chionoecetes opilio*) fishery in the eastern Bering Sea, an ecosystem influenced by regime shifts. They found that the regime-based HCR did increase yield in regime-based systems, but slightly decrease yield and actually increase the probability of overfishing in non-regime-based systems. A'mar *et al.* (2009) also reported that overfishing of walleye pollock in the Gulf of Alaska actually increased under regime-based HCRs. They attributed this to the incorrect detection of regime shifts, which was believed to be caused by a high amount of variance in their recruitment data. Consequently, determining whether changes in fish productivity are definitely driven by regime shifts rather than temporal fish-induced variations is an essential step before the implementation of regime-based HCRs (Szuwalski and Punt, 2013; Szuwalski and HolloId, 2016).

The methodology I proposed in this work could be a useful tool to determine whether the population dynamics are truly regime-based because our method can accurately identify the environmental regime for each individual year in time series, and hence may improve the performance of regime-based HCRs. Another hurdle in implementing regime-based HCRs could be the challenge of calculating biological reference points under changing environmental regimes because the stock must be projected into the future (Szuwalski and HolloId, 2016). As a reliable tool to account for regime shifts in fish productivity, our method has the capability of informing short-to-medium term stock dynamics in the future. Our method can estimate the transition probabilities among different productivity regimes, which allows us to project future stock dynamics. It should be noted that the transition probability estimated by our method is non-mechanistic and based purely on historical data, and mechanistic modelling with ecological forecast may provide better prediction of future stock dynamics. However, when such mechanistic knowledge and ecological data are unavailable or unreliable, our method could be a useful tool to inform fisheries managers about potential future stock dynamics. Meanwhile, with the transition probability, I will know whether the fish productivity will revert to the previous high or low state soon, or the fish productivity will remain at the present state for an extended period of time. This may benefit the calculation of appropriate reference points for fisheries management (Szuwalski and HolloId, 2016).

4.3 Future research

As suggested by King and Mcfarlane (2006b), regime-specific management strategies can be useful for ecosystem-based fisheries management, only if the regime shifts can be detected soon after they occur. Our method might be useful for identifying abrupt shifts in population dynamics and projecting future stock dynamics. However, I need to admit that our method may not be able to detect regime shifts immediately after they occur. Regime shifts will not be recognized until several years after these regime changes have taken place. The lag between the occurrence and detection of regime shifts makes it unrealistic to immediately adjust the management strategy to match the new level of stock status, and thus could be a big challenge to the notion of regime-specific management strategies.

Given the fact that regime shifts are not detectable in the year they occurred, it might be useful to know how long it will take for regime shifts to be detectable. In future research, I will apply retrospective analysis to determine how long after a regime shift that the shift can be detected. If our method is able to detect such changes close to the real-year regime shifts occurred, it would make management actions more effective by providing a quantitative way to determine whether and when regime-specific strategies may be adopted (Rothschild and Shannon, 2004; King and Mcfarlane, 2006b; King *et al.*, 2015). Additionally, in future research, I will apply our methodology to other collapsed fish stocks (i.e. Canadian cod stocks) to explore potential regime-like growth or recruitment patterns, and to predict the probability of recovery of these fish stocks according to the estimated transition probability, because the probability of recovery is a key parameter of interest to fisheries management (Lindegren *et al.*, 2010; Costello *et al.*, 2016; Britten *et al.*, 2017), and may help to inform short-to-medium term stock dynamics in the future and affect the corresponding fisheries anticipations and management strategies. Moreover, I am also interested in applying our methodology to multi-species to explore large-scale regime shift patterns in fish populations.

A limitation of our methodology is that it does not take account of the uncertainties associated with the parameters in each regime. I assume that the regime-specific model parameters are constant over time. However, it might not be realistic in reality. In future research, I will try to include a hierarchical structure on regime-specific parameters to allow for uncertainties in these model parameters. For example, I will allow the regime-specific parameters involve as random walk processes or auto-correlated (e.g. AR1) processes.

4.4 summary

The objective of our work was to introduce a novel methodology for modeling fish population dynamics under changing environmental regimes. I used simulations to demonstrate the ability of our method to model regime-like changes of SRRs and somatic growth, and then applied the method to the cod stock on the southern Grand Bank off Newfoundland, Canada. Although our study focusses on abrupt shifts in recruitment and growth, the proposed approach can also be applied to detect abrupt shifts in other population dynamics, such as shifts in recruit-per-spawner time series (Perälä and Kuparinen, 2015), carrying capacity, and natural mortality, or any other key population parameters that may experience regime-like changes. Systematic changes of any population traits and ecological conditions could be indicative of abrupt changes in fish population dynamics, which if not accounted for, can lead to inaccurate perceptions and predictions regarding stock status and ultimately ineffective management decisions (Benson and Trites, 2002; Yatsu *et al.*, 2005; Perretti *et al.*, 2017). There is now growing evidence for regime shifts in marine ecosystems (Beaugrand, 2004; Wooster and Zhang, 2004; Alheit *et al.*, 2005), calling for development of more flexible and adaptive management practices (Hughes *et al.*, 2005; deYoung *et al.*, 2008). Meanwhile, more effective analytic tools (e.g., the HMSM), which are useful in enhancing our ability to detect, predict and manage regime shifts, are needed to explore the utility and effectiveness of potential regime-specific management measures.

Bibliography

Alheit, J., Möllmann, C., Dutz, J., Kornilovs, G., Loewe, P., Mohrholz, V., and Wasmund, N. 2005. Synchronous ecological regime shifts in the central Baltic and the North Sea in the late 1980s. ICES Journal of Marine Science, 62: 1205–1215.

A'mar, Z. T., Punt, A. E., and Dorn, M. W. 2009. The impact of regime shifts on the performance of management strategies for the Gulf of Alaska walleye pollock (Theragra chalcogramma) fishery. Canadian Journal of Fisheries and Aquatic Sciences, 66: 2222–2242.

Beaugrand, G. 2004. The North Sea regime shift: Evidence, causes, mechanisms and consequences. Progress in Oceanography, 60: 245–262.

Benson, A. J., and Trites, A. W. 2002. Ecological effects of regime shifts in the Bering Sea and eastern North Pacific Ocean. Fish and Fisheries, 3: 95–113.

Brander, K. 1995. The effect of temperature on growth of Atlantic cod (Gadus morhua L.). ICES Journal of Marine Science, 52: 1–10.

Brander, K. 2005. Spawning and life history information for North Atlantic cod stocks. ICES Cooperative Research Report. 122 pp.

Brander, K. M. 2007. The role of growth changes in the decline and recovery of North Atlantic cod stocks since 1970. ICES Journal of Marine Science, 64: 211–217.

Britten, G. L., Dowd, M., and Worm, B. 2016. Changing recruitment capacity in global fish stocks. Proceedings of the National Academy of Sciences, 113 (1): 134–139.

Britten, G. L., Dowd, M., Kanary, L., and Worm, B. 2017. Extended fisheries recovery timelines in a changing environment. Nature Communications, 8: 15325.

Brunel, T., Piet, G. J., van Hal, R., and Röckmann, C. 2010. Performance of harvest control rules in a variable environment. ICES Journal of Marine Science, 67: 1051–1062.

Bundy, A., Heymans, J. J., Morissette, L., and Savenkoff, C. 2009. Seals, cod and forage fish: A comparative exploration of variations in the theme of stock collapse and ecosystem change in four Northwest Atlantic ecosystems. Progress in Oceanography, 81: 188–206.

Buren, A., Murphy, H., Adamack, A., Davoren, G., Koen-Alonso, M., Montevecchi, W., Mowbray, F., *et al.* 2019. The collapse and continued low productivity of a keystone forage fish species. Marine Ecology Progress Series, 616: 155–170.

Buren, A. D., Koen-Alonso, M., Pepin, P., Mowbray, F., Nakashima, B., Stenson, G., Ollerhead, N., *et al.* 2014. Bottom-Up Regulation of Capelin, a Keystone Forage Species. PLoS ONE, 9: e87589.

Chib, S. 1996. Calculating posterior distributions and modal estimates in Markov mixture models. Journal of Econometrics, 75: 79–97.

Clark, W. G., Hare, S. R., Parma, A. M., Sullivan, P. J., and Trumble, R. J. 1999. Decadal changes in growth and recruitment of Pacific halibut (Hippoglossus stenolepis), 56: 11.

Colbourne, E. 2004. Decadal Changes in the Ocean Climate in Newfoundland and Labrador Waters from the 1950s to the 1990s. Journal of Northwest Atlantic Fishery Science, 34: 43–61.

Colbourne, E., Holden, J., Senciall, D., Bailey, W., Snook, S., and Higdon, J. 2016. Physical Oceanographic Conditions on the Newfoundland and Labrador Shelf during 2015. Canadian Science Advisory Secretariat (CSAS).

Cooper, A. B. 2006. A Guide to Fisheries Stock Assessment from data to recommendations. University of New Hampshire, Sea Grant College Program: 47.

Costello, C., Ovando, D., Clavelle, T., Strauss, C. K., Hilborn, R., Melnychuk, M. C., Branch, T. A., *et al.* 2016. Global fishery prospects under contrasting management regimes. Proceedings of the National Academy of Sciences of the United States of America, 113: 5125–5129. National Academy of Sciences.

Crépin, A.-S., Biggs, R., Polasky, S., Troell, M., and de Zeeuw, A. 2012. Regime shifts and management. Ecological Economics, 84: 15–22.

Daskalov, G. 2002. Overfishing drives a trophic cascade in the Black Sea. Marine Ecology Progress Series, 225: 53–63.

Dempsey, D. P., Koen-Alonso, M., Gentleman, W. C., and Pepin, P. 2017. Compilation and discussion of driver, pressure, and state indicators for the Grand Bank ecosystem, Northwest Atlantic. Ecological Indicators, 75: 331–339.

Deriso, R. B. 1987. Optimal F0.1 Criteria and Their Relationship to Maximum Sustainable Yield. Canadian Journal of Fisheries and Aquatic Sciences, 44: s339–s348.

deYoung, B., Barange, M., Beaugrand, G., Harris, R., Perry, R. I., Scheffer, M., and Werner, F. 2008. Regime shifts in marine ecosystems: detection, prediction and management. Trends in Ecology & Evolution, 23(7): 402–409.

Dortel, E., Sardenne, F., Bousquet, N., Rivot, E., Million, J., Le Croizier, G., and Chassot, E. 2015. An integrated Bayesian modeling approach for the growth of Indian Ocean yellowfin tuna. Fisheries Research, 163: 69–84.

Drinkwater, K. F. 2005. The response of Atlantic cod (Gadus morhua) to future climate change. ICES Journal of Marine Science, 62: 1327–1337.

Dwyer, K. S., Walsh, S. J., and Campana, S. E. 2003. Age determination, validation and growth of Grand Bank yellowtail flounder (Limanda ferruginea). ICES Journal of Marine Science, 60: 1123–1138.

Dzul, M. C., Yackulic, C. B., Korman, J., Yard, M. D., and Muehlbauer, J. D. 2017. Incorporating temporal heterogeneity in environmental conditions into a somatic growth model. Canadian Journal of Fisheries and Aquatic Sciences, 74: 316–326.

Echave, K. B., Hanselman, D. H., Adkison, M. D., and Sigler, M. F. 2012. Interdecadal change in growth of sablefish (Anoplopoma fimbria) in the northeast Pacific Ocean. Fishery Bulletin, 110(3): 361–374.

Folke, C., Carpenter, S., Walker, B., Scheffer, M., Elmqvist, T., Gunderson, L., and Holling, C. S. 2004. Regime Shifts, Resilience, and Biodiversity in Ecosystem Management. Annual Review of Ecology, Evolution, and Systematics, 35: 557–581.

Frank, K. T., Petrie, B., Leggett, W. C., and Boyce, D. G. 2016. Large scale, synchronous variability of marine fish populations driven by commercial exploitation. Proceedings of the National Academy of Sciences of the United States of America, 113: 8248–8253. National Academy of Sciences.

Frater, P. N., Hrafnkelsson, B., Elvarsson, B. T., and Stefansson, G. 2019. Drivers of growth for Atlantic cod (Gadus morhua L.) in Icelandic waters – A Bayesian approach to determine spatiotemporal variation and its causes. Journal of Fish Biology, 95: 401–410.

Freon, P. 2005. Sustainable Exploitation of Small Pelagic Fish Stocks Challenged by Environmental and Ecosystem Changes: A Review. BULLETIN OF MARINE SCIENCE, 76: 78.

Furuichi, S., Niino, Y., Kamimura, Y., and Yukami, R. 2020. Time-varying relationships between early growth rate and recruitment in Japanese sardine. Fisheries Research, 232: 105723.

Gabriel, W. L., and Mace, P. M. 1999. A Review of Biological Reference Points in the Context of the Precautionary Approach. Proceedings of the fifth national NMFS stock assessment workshop: providing scientific advice to implement the precautionary approach under the Magnuson-Stevens fishery conservation and management act. NOAA Tech Memo NMFS-F/SPO-40, pp. 34-45: 12.

Gay, D. M. 1990. Usage Summary for Selected Optimization Routines. Computing Science Technical Report 153, AT&T Bell Laboratories, Murray Hill.

Gilbert, D. J. 1997. Towards a new recruitment paradigm for fish stocks. Canadian Journal of Fisheries and Aquatic Sciences, 54: 969–977.

Graham, R. L., Knuth, D. E., and Patashnik, O. 1990. Concrete Mathematics 7th printing, Chapter 1. https://1library.net/document/yj70egmy-graham-ronald-concrete-mathematics-pdf.html.

Haltuch, M. A., Punt, A. E., and Dorn, M. W. 2009. Evaluating the estimation of fishery management reference points in a variable environment. Fisheries Research, 100: 42–56.

Hare, S. R., and Mantua, N. J. 2000. Empirical evidence for North Pacific regime shifts in 1977 and 1989. Progress in Oceanography, 47: 103–145.

Harvey, C. J., Cox, S. P., Essington, T. E., Hansson, S., and Kitchell, J. F. 2003. An ecosystem model of food web and fisheries interactions in the Baltic Sea. ICES Journal of Marine Science, 60: 939–950.

Heino, M., Baulier, L., Boukal, D. S., Ernande, B., Johnston, F. D., Mollet, F. M., Pardoe, H., *et al.* 2013. Can fisheries-induced evolution shift reference points for fisheries management? ICES Journal of Marine Science, 70: 707–721.

Hilborn, R., and Minte-Vera, C. V. 2008. Fisheries-Induced Changes in Growth Rates in Marine Fisheries: Are they Significant? BULLETIN OF MARINE SCIENCE, 83: 11.

Huang, M., Ding, L., Wang, J., Ding, C., and Tao, J. 2021. The impacts of climate change on fish growth: A summary of conducted studies and current knowledge. Ecological Indicators, 121: 106976.

Hughes, T., Bellwood, D., Folke, C., Steneck, R., and Wilson, J. 2005. New paradigms for supporting the resilience of marine ecosystems. Trends in Ecology & Evolution, 20: 380–386.

Hutchings, J. A., and Myers, R. A. 1994. What can be learned from the collapse of a renewable resource? Atlantic cod, Gadus morhua, of Newfoundland and Labrador. Canadian Journal of Fisheries and Aquatic Sciences, 51: 2126–2146.

Jackson, J. B. C. 2001. Historical Overfishing and the Recent Collapse of Coastal Ecosystems. Science, 293: 629–637.

Jiao, Y. 2009. Regime shift in marine ecosystems and implications for fisheries management, a review. Reviews in Fish Biology and Fisheries, 19: 177–191.

Jiao, Y., Rogers-Bennett, L., Taniguchi, I., Butler, J., and Crone, P. 2010. Incorporating temporal variation in the growth of red abalone (Haliotis rufescens) using hierarchical Bayesian growth models, 67: 13.

Jorgensen, T. 1992. Long-term changes in growth of North-east Arctic cod (Gadus morhua) and some environmental influences. ICES Journal of Marine Science, 49: 263–278.

Karp, M. A., Peterson, J. O., Lynch, P. D., Griffis, R. B., Adams, C. F., Arnold, W. S., Barnett, L. A. K., *et al.* 2019. Accounting for shifting distributions and changing productivity in the development of scientific advice for fishery management. ICES Journal of Marine Science, 76: 1305–1315.

King, J. R., and Mcfarlane, G. A. 2006a. Shift in size-at-age of the Strait of Georgia population of Pacific hake (Merluccius productus). California Cooperative Oceanic Fisheries Investigations Report, 47: 9.

King, J. R., and Mcfarlane, G. A. 2006b. A framework for incorporating climate regime shifts into the management of marine resources. Fisheries Management and Ecology, 13: 93–102.

King, J. R., McFarlane, G. A., and Punt, A. E. 2015. Shifts in fisheries management: adapting to regime shifts. Philosophical Transactions of the Royal Society B: Biological Sciences, 370: 20130277.

Klaer, N. L., O'Boyle, R. N., Deroba, J. J., Wayte, S. E., Little, L. R., Alade, L. A., and Rago, P. J. 2015. How much evidence is required for acceptance of productivity regime shifts in fish stock assessments: Are we letting managers off the hook? Fisheries Research, 168: 49–55.

Köster, F., Vinther, M., Mackenzie, B., Eero, M., and Plikshs, M. 2009. Environmental Effects on Recruitment and Implications for Biological Reference Points of Eastern Baltic Cod (Gadus morhua). J. Northw. Atl. Fish. Sci, 41: 205–220.

Kristensen, K., Bell, B., and Skaug, H. 2020. Template Model Builder: A General Random Effect Tool Inspired by 'ADMB'.

Krohn, M. 1997. Declining Weight-at-age in Northern Cod and the Potential Importance of the Early Years and Size-selective Fishing Mortality. Northwest Atl. Fish. Org. Sci. Council Stud: 43–50.

Kuriyama, P. T., Ono, K., Hurtado-Ferro, F., Hicks, A. C., Taylor, I. G., Licandeo, R. R., Johnson, K. F., *et al.* 2016. An empirical weight-at-age approach reduces estimation bias compared to modeling parametric growth in integrated, statistical stock assessment models when growth is time varying. Fisheries Research, 180: 119–127.

Levin, P. S., and Möllmann, C. 2015. Marine ecosystem regime shifts: challenges and opportunities for ecosystem-based management. Philosophical Transactions of the Royal Society B: Biological Sciences, 370: 20130275.

Lilly, G. R., Parsons, D. G., and Kulka, D. W. 2000. Was the Increase in Shrimp Biomass on the Northeast Newfoundland Shelf a Consequence of a Release in Predation Pressure from Cod? Journal of Northwest Atlantic Fishery Science, 27: 45–61.

Lindegren, M., Diekmann, R., and Möllmann, C. 2010. Regime shifts, resilience and recovery of a cod stock. Marine Ecology Progress Series, 402: 239–253. Inter-Research Science Center.

Mangel, M., MacCall, A. D., Brodziak, J., Dick, E. J., Forrest, R. E., Pourzand, R., and Ralston, S. 2013. A perspective on steepness, reference points, and stock assessment. Canadian Journal of Fisheries and Aquatic Sciences, 70 (6): 930–940.

Maunder, M. N. 2012. Evaluating the stock–recruitment relationship and management reference points: Application to summer flounder (Paralichthys dentatus) in the U.S. mid-Atlantic. Fisheries Research, 125–126: 20–26.

Millar, R. B., Fahrig, L., and Shelton, P. A. 1990. Effect of capelin biomass on cod growth. International Council for the Exploration of the Sea, Committee Meeting, 1990: 25.

Minobe, S. 2000. Spatio-temporal structure of the pentadecadal variability over the North Pacific. Progress in Oceanography, 47: 381–408.

Mion, M., Haase, S., Hemmer-Hansen, J., Hilvarsson, A., Hüssy, K., Krüger-Johnsen, M., Krumme, U., *et al.* 2020. Multidecadal changes in fish growth rates estimated from tagging data: A case study from the Eastern Baltic cod (Gadus morhua, Gadidae). Fish and

Fisheries, n/a. http://onlinelibrary.wiley.com/doi/abs/10.1111/faf.12527 (Accessed 25 February 2021).

Mohn, R. K., and Chouinard, G. A. 2007. Harvest control rules for stocks displaying dynamic production regimes. ICES Journal of Marine Science, 64: 693–697.

Möllmann, C., Folke, C., Edwards, M., and Conversi, A. 2015. Marine regime shifts around the globe: theory, drivers and impacts. Philosophical Transactions of the Royal Society B: Biological Sciences, 370: 20130260.

Morgan, M. J., Shelton, P. A., and Rideout, R. M. 2014. An evaluation of fishing mortality reference points under varying levels of population productivity in three Atlantic cod (Gadus morhua) stocks. ICES Journal of Marine Science, 71: 1407–1416.

Morrongiello, J. R., Horn, P. L., Ó Maolagáin, C., and Sutton, P. J. H. 2021. Synergistic effects of harvest and climate drive synchronous somatic growth within key New Zealand fisheries. Global Change Biology, 27: 1470–1484.

Mueter, F. J., Boldt, J. L., Megrey, B. A., and Peterman, R. M. 2007. Recruitment and survival of Northeast Pacific Ocean fish stocks: temporal trends, covariation, and regime shifts. Canadian Journal of Fisheries and Aquatic Sciences, 64: 911–927.

Mullowney, D. R. J., Rose, G. A., Dawe, E. G., Rowe, S., Maillet, G. L., and Pedersen, E. J. 2019. Temperature influences on growth of unfished juvenile Northern cod (Gadus morhua) during stock collapse. Fisheries Oceanography, 28: 612–627. Wiley-Blackwell.

Munch, S. B., and Kottas, A. 2009a. A Bayesian modeling approach for determining productivity regimes and their characteristics. Ecological Applications: A Publication of the Ecological Society of America, 19: 527–537.

Munch, S. B., and Kottas, A. 2009b. A Bayesian modeling approach for determining productivity regimes and their characteristics. Ecological Applications, 19: 527–537.

Murphy, H. M. 2018. Re-visiting the drivers of capelin recruitment in Newfoundland since 1991. Fisheries Research: 10.

Myers, R. A., Hutchings, J. A., and Barrowman, N. J. 1997. Why Do Fish Stocks Collapse? The Example of Cod in Atlantic Canada. Ecological Applications, 7: 91–106.

Nisbet, R. M., and Bence, J. R. 1989. Alternative Dynamic Regimes for Canopy-Forming Kelp: A Variant on Density-Vague Population Regulation. The American Naturalist, 134: 377–408.

Nogueira, A., Paz, X., and González, D. 2013. Persistence and Variation on the Groundfish Assemblages on the Southern Grand Banks (NAFO Divisions 3NO): 2002–2011. Journal of Northwest Atlantic Fishery Science, 45: 19–41.

Overland, J., Rodionov, S., Minobe, S., and Bond, N. 2008. North Pacific regime shifts: Definitions, issues and recent transitions. Progress in Oceanography, 77: 92–102.

Pedersen, E. J., Thompson, P. L., Ball, R. A., Fortin, M.-J., Gouhier, T. C., Link, H., Moritz, C., *et al.* 2017. Signatures of the collapse and incipient recovery of an overexploited marine ecosystem. Royal Society Open Science, 4: 170215.

Penglase, S., Harboe, T., Sæle, Ø., Helland, S., Nordgreen, A., and Hamre, K. 2013. Iodine nutrition and toxicity in Atlantic cod (*Gadus morhua*) larvae. PeerJ, 1: e20.

Perälä, T., and Kuparinen, A. 2015. Detecting regime shifts in fish stock dynamics. Canadian Journal of Fisheries and Aquatic Sciences, 72: 1619–1628.

Perälä, T. A., Swain, D. P., and Kuparinen, A. 2017. Examining nonstationarity in the recruitment dynamics of fishes using Bayesian change point analysis. Canadian Journal of Fisheries and Aquatic Sciences, 74: 751–765.

Perretti, C., Fogarty, M., Friedland, K., Hare, J., Lucey, S., McBride, R., Miller, T., *et al.* 2017. Regime shifts in fish recruitment on the Northeast US Continental Shelf. Marine Ecology Progress Series, 574: 1–11.

Peterson, W. T., and Schwing, F. B. 2003. A new climate regime in northeast pacific ecosystems. Geophysical Research Letters, 30. https://agupubs.onlinelibrary.wiley.com/doi/abs/10.1029/2003GL017528 (Accessed 13 April 2020).

Plagányi, É. E., Haywood, M. D. E., Gorton, R. J., Siple, M. C., and Deng, R. A. 2019. Management implications of modelling fisheries recruitment. Fisheries Research, 217: 169–184.

Polovina, J. J. 2005. Climate Variation, Regime Shifts, and Implications for Sustainable Fisheries. BULLETIN OF MARINE SCIENCE, 76: 12.

Power, D., Morgan, J., Murphy, E. F., Brattey, J., and Healey, B. 2010. An Assessment of the Cod Stock in NAFO Divisions 3NO: 52.

Punt, A. E., A'mar, T., Bond, N. A., Butterworth, D. S., de Moor, C. L., De Oliveira, J. A. A., Haltuch, M. A., *et al.* 2014. Fisheries management under climate and environmental uncertainty: control rules and performance simulation. ICES Journal of Marine Science, 71: 2208–2220.

RAM Legacy Stock Assessment Database. 2018, December 22. RAM Legacy Stock Assessment Database v4.44. Zenodo. https://zenodo.org/record/2542919#.X8aYMKpKg1I.

Rätz, H., Stein, M., and Lloret, J. 1999. Variation in Growth and Recruitment of Atlantic Cod (Gadus morhua) off Greenland During the Second Half of the Twentieth Century. Journal of Northwest Atlantic Fishery Science, 25.

Reid, P. 2000. Impacts of fisheries on plankton community structure. ICES Journal of Marine Science, 57: 495–502.

Rice, J. 2011. Managing fisheries well: delivering the promises of an ecosystem approach. Fish and Fisheries, 12: 209–231.

Ricker, W. E. 1954. Stock and Recruitment. Journal of the Fisheries Research Board of Canada, 11: 559–623.

Rideout, R. M., B. Rogers, and D.W. Ings. 2018a. An Assessment of the Cod Stock in NAFO Divisions 3NO. NAFO SCR Doc., 18/028.

Rideout, R. M., Rogers, B., and Ings, D. W. 2018b. An Assessment of the Cod Stock in NAFO Divisions 3NO. NAFO SCR Doc.: 52.

Rocha, J., Yletyinen, J., Biggs, R., Blenckner, T., and Peterson, G. 2015. Marine regime shifts: drivers and impacts on ecosystems services. Philosophical Transactions of the Royal Society B: Biological Sciences, 370: 20130273.

Rose, G. A., and O'Driscoll, R. L. 2002. Capelin are good for cod: can the northern stock rebuild without them? ICES Journal of Marine Science, 59: 1018–1026.

Rothschild, B. J., and Shannon, L. J. 2004. Regime shifts and fishery management. Progress in Oceanography, 60: 397–402.

Scheffer, M., Carpenter, S., Foley, J. A., Folke, C., and Walker, B. 2001. Catastrophic shifts in ecosystems. Nature, 413: 591–596.

Scott, S. L. 2002. Bayesian Methods for Hidden Markov Models: Recursive Computing in the 21st Century. Journal of the American Statistical Association, 97: 337–351.

Shackell, N. 1997. Growth of cod (Gadus morhua) estimated from mark-recapture programs on the Scotian Shelf and adjacent areas. Ices Journal of Marine Science - ICES J MAR SCI, 54: 383–398.

Sinclair, A. F., Swain, D. P., and Hanson, J. M. 2002a. Disentangling the effects of size-selective mortality, density, and temperature on length-at-age. Canadian Journal of Fisheries and Aquatic Sciences, 59: 372–382.

Sinclair, A. F., Swain, D. P., and Hanson, J. M. 2002b. Disentangling the effects of size-selective mortality, density, and temperature on length-at-age. Canadian Journal of Fisheries and Aquatic Sciences, 59: 372–382.

Slatkin, M. 1978. The Dynamics of a Population in a Markovian Environment. Ecology, 59: 249–256. Ecological Society of America.

Stawitz, C. C., Essington, T. E., Branch, T. A., Haltuch, M. A., Hollowed, A. B., and Spencer, P. D. 2015. A state-space approach for detecting growth variation and application to North Pacific groundfish. Canadian Journal of Fisheries and Aquatic Sciences, 72: 1316–1328.

Steele, J. H. 1996. Regime shifts in fisheries management. Fisheries Research, 25: 19–23.

Swain, D. P., Sinclair, A. F., and Mark Hanson, J. 2007. Evolutionary response to size-selective mortality in an exploited fish population. Proceedings of the Royal Society B: Biological Sciences, 274: 1015–1022.

Szuwalski, C. S., and Punt, A. E. 2013. Fisheries management for regime-based ecosystems: a management strategy evaluation for the snow crab fishery in the eastern Bering Sea. ICES Journal of Marine Science, 70: 955–967.

Szuwalski, C. S., and Hollowed, A. B. 2016. Climate change and non-stationary population processes in fisheries management. ICES Journal of Marine Science, 73: 1297–1305.

Szuwalski, C. S., Britten, G. L., Licandeo, R., Amoroso, R. O., Hilborn, R., and Walters, C. 2019. Global forage fish recruitment dynamics: A comparison of methods, time-variation, and reverse causality. Fisheries Research, 214: 56–64.

Templeman, N. D. 2010. Ecosystem Status and Trends Report for the Newfoundland and Labrador Shelf. Canadian Science Advisory Secretaria: 78.

Thorsen, A., Witthames, P. R., Marteinsdóttir, G., Nash, R. D. M., and Kjesbu, O. S. 2010. Fecundity and growth of Atlantic cod (Gadus morhua L.) along a latitudinal gradient. Fisheries Research, 104: 45–55.

Thorson, J. T., Hicks, A. C., and Methot, R. D. 2015. Random effect estimation of time-varying factors in Stock Synthesis. ICES Journal of Marine Science, 72: 178–185.

Thorson, J. T., and Minte-Vera, C. V. 2016. Relative magnitude of cohort, age, and year effects on size at age of exploited marine fishes. Fisheries Research, 180: 45–53.

Vert-pre, K. A., Amoroso, R. O., Jensen, O. P., and Hilborn, R. 2013. Frequency and intensity of productivity regime shifts in marine fish stocks. Proceedings of the National Academy of Sciences, 110: 1779–1784.

Wada, T., and Jacobson, L. D. 1998. Regimes and stock-recruitment relationships in Japanese sardine (Sardinops melanostictus), 1951–1995. Canadian Journal of Fisheries and Aquatic Sciences, 55: 2455–2463.

Wooster, W. S., and Zhang, C. I. 2004. Regime shifts in the North Pacific: early indications of the 1976–1977 event. Progress in Oceanography, 60: 183–200.

Yatsu, A., Watanabe, T., Ishida, M., Sugisaki, H., and Jacobson, L. D. 2005. Environmental effects on recruitment and productivity of Japanese sardine Sardinops melanostictus and chub mackerel Scomber japonicus with recommendations for management. Fisheries Oceanography, 14: 263–278.

Zhang, F., Reid, K. B., and Nudds, T. D. 2018. Ecosystem change and decadal variation in stock–recruitment relationships of Lake Erie yellow perch (Perca flavescens). ICES Journal of Marine Science, 75: 531–540.

Zhang, F., Rideout, R. M., and Cadigan, N. G. 2020a. Spatiotemporal variations in juvenile mortality and cohort strength of Atlantic cod (*Gadus morhua*) off Newfoundland and Labrador. Canadian Journal of Fisheries and Aquatic Sciences, 77: 625–635.

Zhang, F. 2020. Early warning signals of population productivity regime shifts in global fisheries. Ecological Indicators, 115: 106371.

Zhang, F., Regular, P. M., Wheeland, L., Rideout, R. M., and Morgan, M. J. 2020b. Accounting for non-stationary stock–recruitment relationships in the development of MSY-based reference points. ICES Journal of Marine Science: fsaa176.

Appendices

Appendix A An efficient method for evaluating marginal likelihood

In this efficient method, I conducted the summations in eq. 2.2) year by year as follows. The likelihood function is given by summing out all the random effects $r_{1:T}$,

$$p(y_{1:T} \mid \Theta) = \sum_{r_{1:T}} \pi(r_1) \prod_{t=2}^{T} p(r_t \mid r_{t-1}) \prod_{t=1}^{T} p(y_t \mid r_t, \Theta)$$

$$= \sum_{r_{2:T}} \sum_{r_1} \pi(r_1) p(y_1 \mid r_1, \Theta) \prod_{t=2}^{T} p(r_t \mid r_{t-1})\ p(y_t \mid r_t, \Theta).$$

Let Sr1= $\pi(r_1)p(y_1 \mid r_1, \Theta)$. I now make the summation over r_1. The Markov property allows us to rearrange the terms involving r_1 as

$$p(y_{1:T} \mid \Theta) = \sum_{r_{2:T}} \sum_{r_1} Sr_1 \prod_{t=2}^{T} p(r_t \mid r_{t-1})\ p(y_t \mid r_t, \Theta)$$

$$= \sum_{r_{2:T}} \{ \sum_{r_1} Sr_1\, p(r_2 \mid r_1) \}\, p(y_2 \mid r_2, \Theta) \prod_{t=3}^{T} p(r_t \mid r_{t-1})\ p(y_t \mid r_t, \Theta).$$

In this step, the summation in the curly bracket $\sum_{r_1} Sr_1\, p(r_2 \mid r_1)$ finishes the summation over r_1. Defining $Sr_2 = \{\sum_{r_1} Sr_1\, p(r_2 \mid r_1)\} p(y_2 \mid r_2, \Theta)$ and using Markov property again, I can rearrange the terms involving r_2 as

$$p(y_{1:T} \mid \Theta) = \sum_{r_{3:T}} \{ \sum_{r_2} Sr_2\, p(r_3 \mid r_2) \}\, p(y_3 \mid r_3, \Theta) \prod_{t=4}^{T} p(r_t \mid r_{t-1})\ p(y_t \mid r_t, \Theta).$$

The summation in the curly bracket $\sum_{r_2} Sr_2\, p(r_3 \mid r_2)$ finishes the summation over r_2. Based on Sr2 , I define Sr3 = $\{ \sum_{r_2} Sr_2\ p(r_3 \mid r_2)\}\, p(y_3 \mid r_3, \Theta)$, and

$$p(y_{1:T} \mid \Theta) \quad = \sum_{r_{4:T}} \{ \sum_{r_3} Sr_3\, p(r_4 \mid r_3) \}\, p(y_4 \mid r_4, \Theta) \prod_{t=5}^{T} p(r_t \mid r_{t-1})\ p(y_t \mid r_t, \Theta),$$

where the summation in the curly bracket finishes the summation over r_3. This procedure continues until summing out all the *T* random effects.

Appendix B Efficient prediction of the regime probabilities

For the conditional distribution of $r_t = j$ given the data,

$$p\ (r_t = j \mid\ y_{1:T}\ ,\Theta\ ) = \frac{p(r_t = j,\ y_{1:T} \mid \Theta\ )}{p(y_{1:T} \mid \Theta)}.$$

The denominator is just the marginal likelihood, which I have evaluated efficiently in Appendix A. Therefore, here I just discuss the calculation of the numerator.

$$p\big(r_{1:(t-1)}, r_t = j\ , r_{(t+1):T}\ ,\ y_{1:T} \,\big|\, \Theta\ \big) = \pi(r_1)p(y_1 \mid r_1, \Theta) \times\ p(r_2 \mid r_1)p(y_2 \mid r_2, \Theta) \times$$

$$\ldots p(r_{t-1} \mid r_{t-2})p(y_{t-1} \mid r_{t-1}, \Theta) \times p(r_t = j \mid r_{t-1})p(y_t \mid r_t, \Theta) \times$$

$$p(r_{t+1} \mid r_t = j\ )p(y_{t+1} \mid r_{t+1}\ , \Theta) \times \ldots \times p(r_T \mid r_{T-1})p(y_T \mid r_T\ , \Theta)$$

$$= p\big(\ r_{1:(t-1)}, y_{1:(t-1)}, r_t = \mathrm{j} \,\big|\, \Theta\big) \times p(y_t \mid r_t, \Theta) \times p\big(r_t = \mathrm{j}, r_{(t+1):T},$$

$$y_{(t+1):T}, \big| \Theta\big),$$

where

$$p\big(\ \ r_{1:(t-1)}, y_{1:(t-1)}, r_t = \mathrm{j} \big| \Theta\big) =\ \pi(r_1)p(y_1 \mid r_1, \Theta) \times\ p(r_2 \mid r_1)p(y_2 \mid r_2, \Theta) \times$$

$$\ldots p(r_{t-1} \mid r_{t-2})p(y_{t-1} \mid r_{t-1}, \Theta) \times p(r_t = j \mid r_{t-1})$$

and

$$p\big(r_t = \mathrm{j}, r_{(t+1):T}, y_{(t+1):T}, \big| \Theta\big) =\ p(r_{t+1} \mid r_t = j\ )p(y_{t+1} \mid r_{t+1}\ , \Theta) \times \quad \ldots \quad \times$$

$$p(r_T \mid r_{T-1})p(y_T \mid r_T\ , \Theta).$$

$$p(r_t = j,\ y_{1:T} \mid \Theta\ ) =\ \textstyle\sum_{r_{1:(t-1)}, r_{(t+1):T}}\ p\big(r_{1:(t-1)}, r_t = j\ , r_{(t+1):T}\ ,\ y_{1:T} \,\big|\, \Theta\ \big)$$

$$= \{\textstyle\sum_{r_{1:(t-1)}} p\big(\ r_{1:(t-1)}, y_{1:(t-1)}, r_t = \mathrm{j} \,\big|\, \Theta\big)\} \times p(y_t \mid r_t, \Theta) \times \{\textstyle\sum_{r_{(t+1):T}} p\big(r_t =$$

$$\mathrm{j}, r_{(t+1):T}, y_{(t+1):T}, \big| \Theta\big)\}$$

The two summations in the curly brackets can be evaluated efficiently with the same methods presented in Appendix A.

Appendix C The method of setting true regime-specific parameters $\{\boldsymbol{\alpha}, \boldsymbol{\beta}, \boldsymbol{\sigma}\}$for HMSM simulation tests

Under scenario 2 with two regimes, the regime-specific parameters $\{\alpha_1, \alpha_2\}$, $\{\beta_1, \beta_2\}$, and $\{\sigma_1, \sigma_2\}$ were derived from the empirical SRR data of the golden redfish stock from ICES (International Council for the Exploration of the Sea) subareas V, VI, XII, and XIV (Iceland and Faroes grounds, west of Scotland, North of Azores, East of Greenland). The SR data of the golden redfish stock were fitted to BHM, HMSM-2, and HMSM-3, and then I compared their model performance using AICc. The results indicated that the HMSM-2 had the lowest AICc, outperforming the other two models (Table 1). I applied the estimated regime-specific parameters of HMSM-2 to the data generation under the simulation scenario 2.

Table 1. The AICc values and estimated parameters of BHM, HMSM-2, and HMSM-3 for the golden redfish stock.

	BHM	**HMSM-2**		**HMSM-3**		
AICc	97.61	94.57		127.43		
$\boldsymbol{\alpha}$	$\alpha = 7.39$	$\alpha_1 = 7.78$	$\alpha_2 = 10.20$	$\alpha_1 = 5.16$	$\alpha_2 = 7.78$	$\alpha_3 = 10.20$
$\boldsymbol{\beta}$	$\beta = 0.12$	$\beta_1 = 0.38$	$\beta_2 = 1.54$	$\beta_1 = 0.53$	$\beta_2 = 0.38$	$\beta_3 = 1.54$
$\boldsymbol{\sigma}$	$\sigma = 0.65$	$\sigma_1 = 0.31$	$\sigma_2 = 0.40$	$\sigma_1 = 0.41$	$\sigma_2 = 0.31$	$\sigma_3 = 0.40$

Under scenario 3 with three regimes, the regime-specific parameters $\{\alpha_1, \alpha_2, \alpha_3\}$, $\{\beta_1, \beta_2, \beta_3\}$, and $\{\sigma_1, \sigma_2, \sigma_3\}$ were derived from the empirical data of Acadian redfish from Gulf of Maine / Georges Bank in USA. Similar to the steps in scenario 2, I applied BHM, HMSM-2, and HMSM-3 to the SR data of the Acadian redfish from Gulf of Maine / Georges Bank, and compared AICc values.

According to the results, the HMSM-3 outperformed BHM and HMSM-2 (Table 2). Thus, the estimated regime-specific parameters for HMSM-3 were used for the data generation under scenario 3.

Table 2. The AICcs value and estimated parameters of BHM, HMSM-2, and HMSM-3 for the Acadian redfish from Gulf of Maine/Georges Bank.

	BHM	**HMSM-2**		**HMSM-3**		
AICc	323.94	219.22		43.96		
$\boldsymbol{\alpha}$	$\alpha = 6.57$	$\alpha_1 = 3.04$	$\alpha_2 = 7.44$	$\alpha_1 = 3.04$	$\alpha_2 = 6.35$	$\alpha_3 = 7.12$
$\boldsymbol{\beta}$	$\beta = 1.49$	$\beta_1 = 0.09$	$\beta_2 = 2.84$	$\beta_1 = 0.09$	$\beta_2 = 0.93$	$\beta_3 = 1.21$
$\boldsymbol{\sigma}$	$\sigma = 1.185$	$\sigma_1 = 0.43$	$\sigma_2 = 0.55$	$\sigma_1 = 0.43$	$\sigma_2 = 0.04$	$\sigma_3 = 0.75$

Appendix D Simulation tests in the absence of weights at older ages

I first fitted the annual weight-at-age data of the cod stock in Divs. 3NO using HMGM assuming two regimes. Then I used the estimated transition probabilities and regime-specific parameters $\{w_{\infty 1}, w_{\infty 2}\}$, $\{k_1, k_2\}$, and $\{\sigma_1, \sigma_2\}$ for HMGM to simulate weight-at-age dynamics for simulation tests. I conducted simulation tests under two scenarios, i.e. single regime (no regime shift), and two regimes (regime shift). The parameters used for data generation are listed in Table 3. The time series of weight-at-age data were simulated for 60 years, and each scenario is repeated 1000 times.

I generated the time-series of weights-at-age $y_{t,a}$ using the re-parametrized VBGM:

$$y_{t,a} = \log\left(w_{\infty_t} \right) + 3\log\left(1 - \left[1 - \left(\frac{w_0}{w_{\infty_t}}\right)^{\frac{1}{3}}\right] e^{-k_t a}\right) + \varepsilon_t,$$

where age a was simulated from 3 to 12 years old. w_0 was fixed at the larvae weight of Atlantic cod (*Gadus morhua*). To be more realistic, I used the weight of the larvae in the later stage where the larvae have absorbed all the yolk sac and are about to become juveniles. In this paper w_0 was fixed at the value of 0.27×10^{-3} kg (Penglase *et al.*, 2013).

Under two regimes, the generated $y_{t,a}$ were characterized by two underlying regimes with parameters $w_{\infty_t} \epsilon \{ w_{\infty_1}, w_{\infty_2}\}$, $k_t \epsilon \{ k_1, k_2 \}$, and $\sigma_t \epsilon \{ \sigma_1, \sigma_2 \}$ depending on the regime in year *t* (Table 3). The time series of the latent random effects (i.e. the temporal variation of regimes), $\{r_1, r_2, \dots, r_T\}$, are specified to follow a step-wise change among two regimes (Figure 1). I fitted two models to each of the generated data sets, i.e. model without regime shift (VBGM), and model with regime shift (HMGM). I compared model performance using AICc.

The simulated weight-at-age data is limited at the age of 12 (Figure 2). The absence of larger weights could lead to unreliable estimates for the maximum weight w_{∞}, and growth rate k. According to simulation results, the estimates of parameters w_{∞} were biased (Figure 3), and thus the estimates for k were unreliable either. However, despite the biased parameter estimates for $w_{\infty 1}$ and $w_{\infty 2}$, HMGM can correctly identify regime shifts, accurately predict the year-specific regime, and fit the model mean very well. Under 2-regime scenario, the HMGM outperformed VBGM in 998 out of 1000 iterations. The HMGM was effective at correctly identifying the true regime for individual years; 721 out of the 1000 trials accurately predicted the year-specific regime for all of the years in the time series (Figure 4). For both regimes, the simulated model means fell between the first and third quartiles of the estimated model means across all ages, indicating the good performance of HMGM to predict the model mean (Figure 5).

Table 3. The values of the parameters used for data generation under the two scenarios.

	Scenario 1	Scenario 2	
w_{∞_t}	15	$w_{\infty 1} = 42.44$	$w_{\infty 2} = 53.07$
k_t	0.35	$k_1 = 0.06$	$k_2 = 0.07$
σ_t	0.08	$\sigma_1 = 0.08$	$\sigma_2 = 0.09$
q_{ij}	NA	$q_{11} = 0.92$	$q_{12} = 0.08$
		$q_{21} = 0.06$	$q_{22} = 0.94$

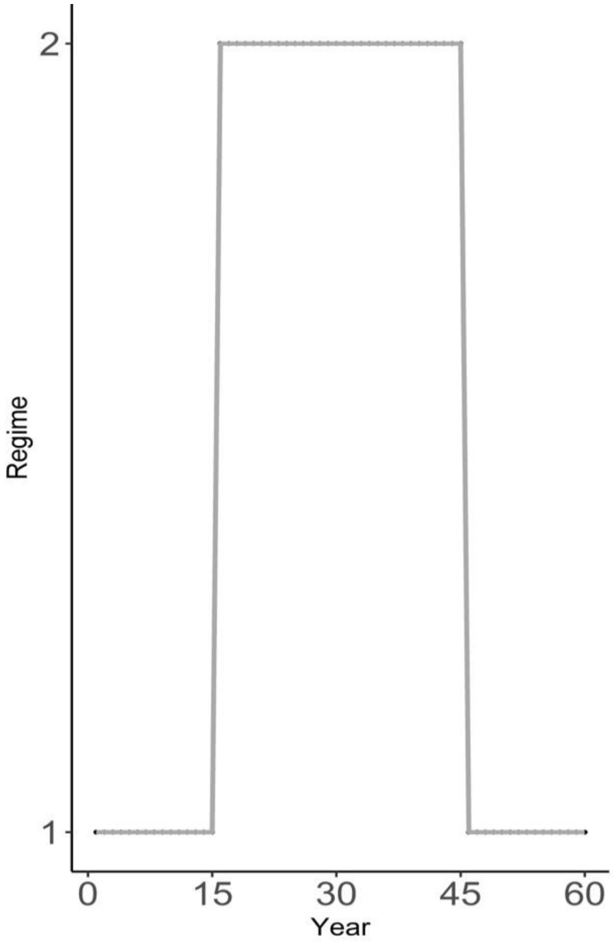

Figure 1. The simulated regime for each year.

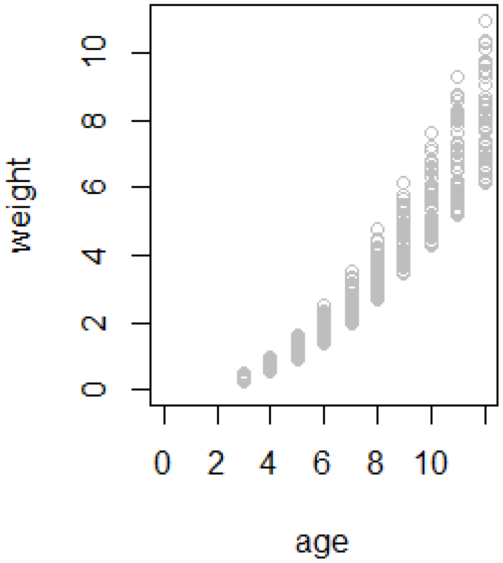

Figure 2. One example of simulated weight-at-age data.

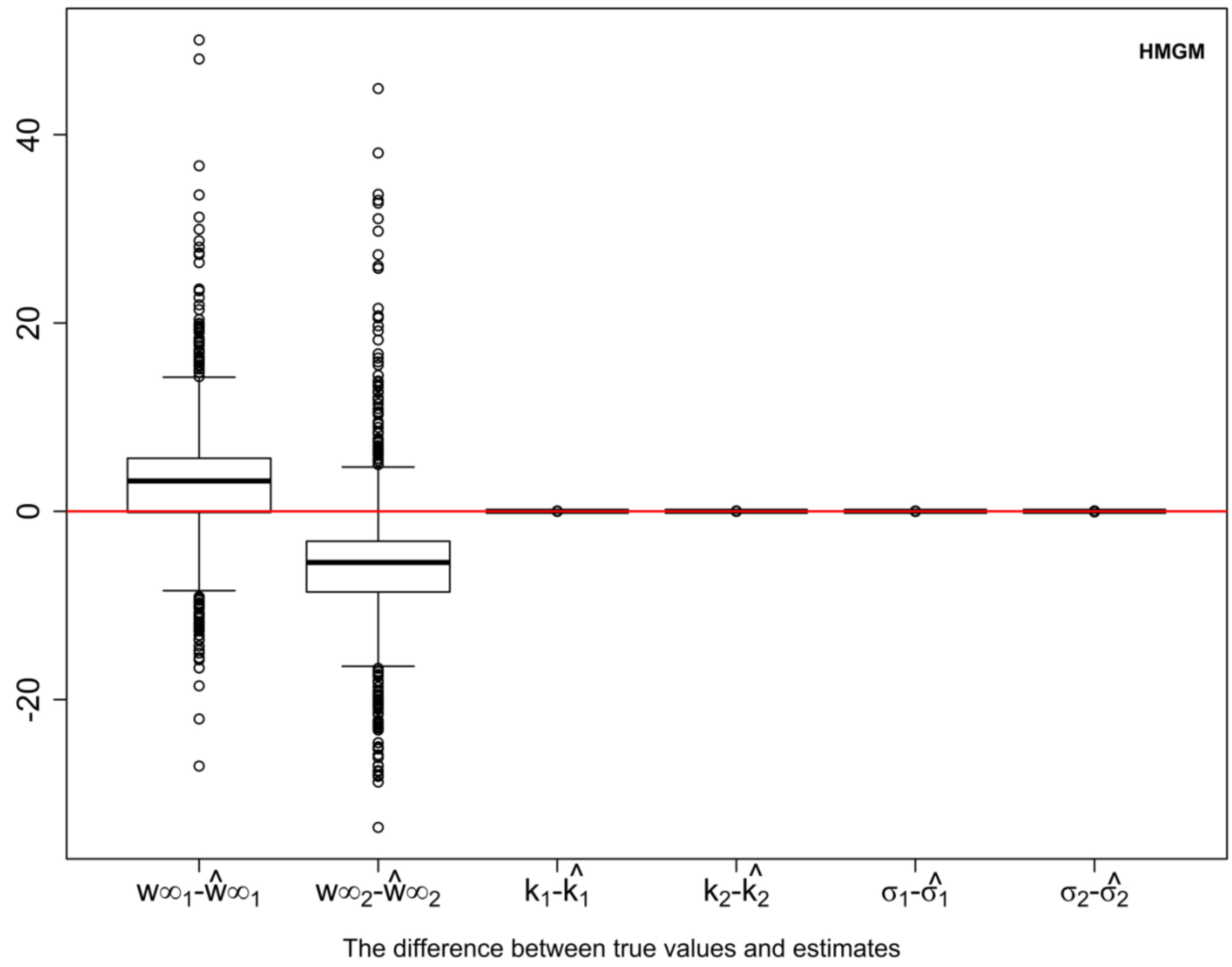

Figure 3. The bias of parameter estimates in all the 1000 simulation trials for HMGM.

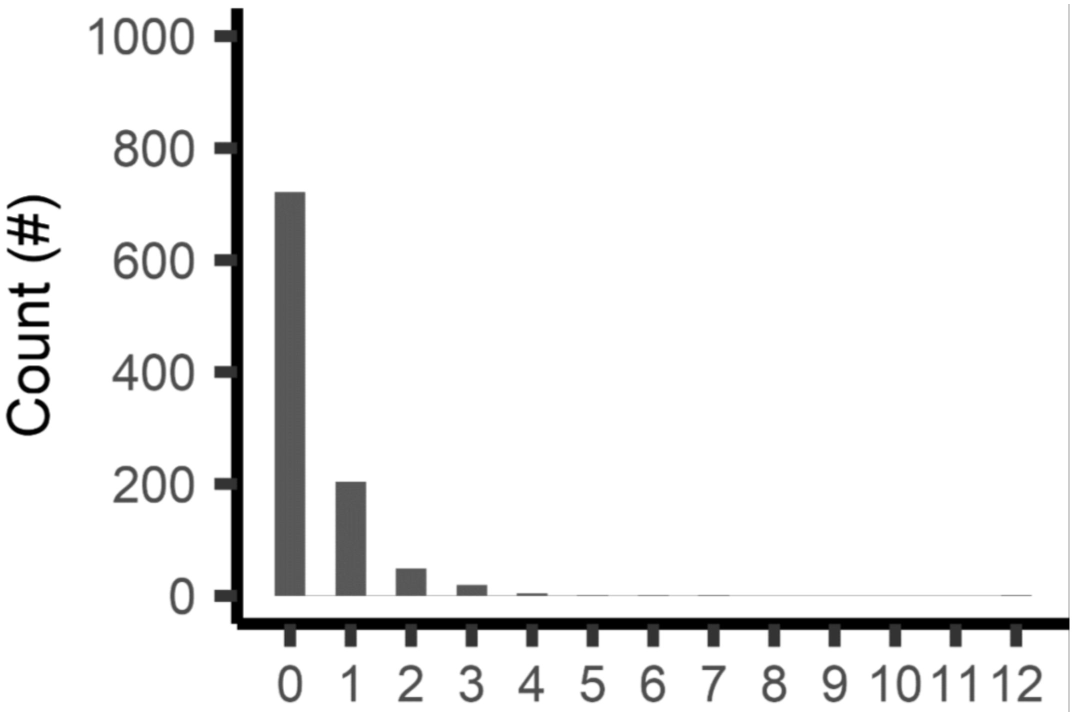

Figure 4. The display of the regime detection accuracy of HMGM simulation. The level zero indicates that the predicted time series of regimes are exactly the same as the true dynamics, and the level two indicates that there are two regime estimates that are different from the true regime time series in one iteration, and so on. The vertical axis shows the count of each inaccurate estimate level across 1000 trials.

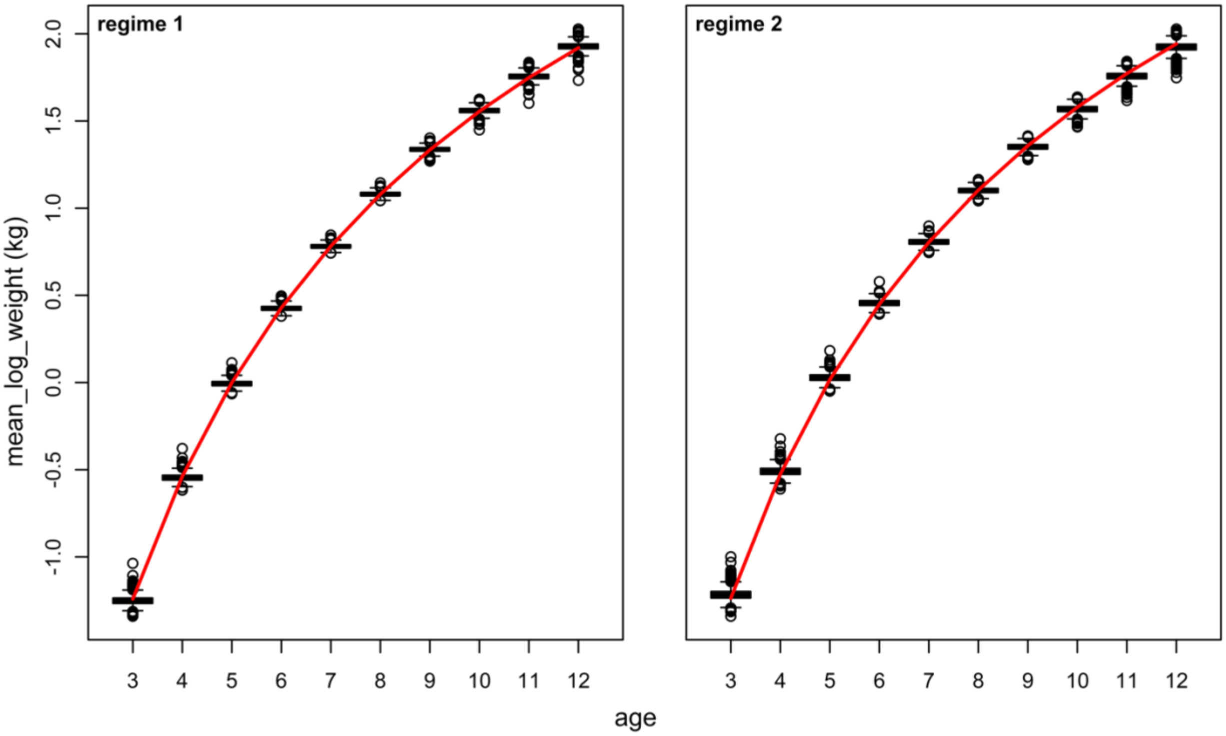

Figure 5. Boxplots are estimated model means via ages across 1000 repetitions, and the two red curves are simulated model means for two regimes.

Appendix E The comparison of brute-force method and the efficient algorithm

Coding:

```
library(distr)
library(TMB)
library(FSA)
sample_size<-6
compile("hidden_Markov.cpp")
dyn.load( "hidden_Markov" )
compile("hidden_Markov_brutal_force.cpp")
dyn.load( "hidden_Markov_brutal_force" )
set.seed(888)
sigma = c(1,sqrt(2),sqrt(3),2)
alpha = 1:4
beta = c(1,4,7,10)
pi1 = rep(1/4,4)
qij = matrix(c(0.7,0.3,0.15,0.1,0.2,0.4,0.15,0.2,0.1,0.1,0.2,0.2,0,0.2,0.5,0.5), nrow=4,ncol=4)
yt = rep(0,sample_size)
rt_save = rep(0,sample_size)
st = runif(sample_size, min = 0, max = 30)
rt = rmultinom(1, 1, pi1)
rt = which(rt==1)
f_now = alpha[rt] - beta[rt]*st[1]
yt[1] = rnorm(1,f_now,sigma[rt])
rt_save[1] = rt
for(i in 2:sample_size){
rt = rmultinom(1, 1, qij[rt,])
rt = which(rt==1)
f_now = alpha[rt] - beta[rt]*st[i]
yt[i] = rnorm(1,f_now,sigma[rt])
rt_save[i] = rt
}
plot(st,yt)

    k_regime = 4

     tmb.data = list(
       yt = yt,
       st = st
      )
```

```
        parameters <- list(
          alpha = c(0.5,0.8,1,2),
          lbeta = c(1,1,1,1),
          lsigma = rep(log(1),k_regime),
          pi1_tran = rep(0,k_regime-1),
          qij_tran = matrix(0,nrow=k_regime,ncol=k_regime-1)
        )
error_r<-try((obj<
MakeADFun(tmb.data,parameters,DLL="hidden_Markov",inner.control=list(maxit=50000,trace
=F)) ),silent=TRUE )

obj$env$tracemgc <- FALSE

 obj$fn(obj$par)

 error_r<-try((obj_brutal<-
MakeADFun(tmb.data,parameters,DLL="hidden_Markov_brutal_force",inner.control=list(maxit
=50000,trace=F)) ),silent=TRUE )

obj_brutal$env$tracemgc <- FALSE

 obj_brutal$fn(obj_brutal$par)
```

results:

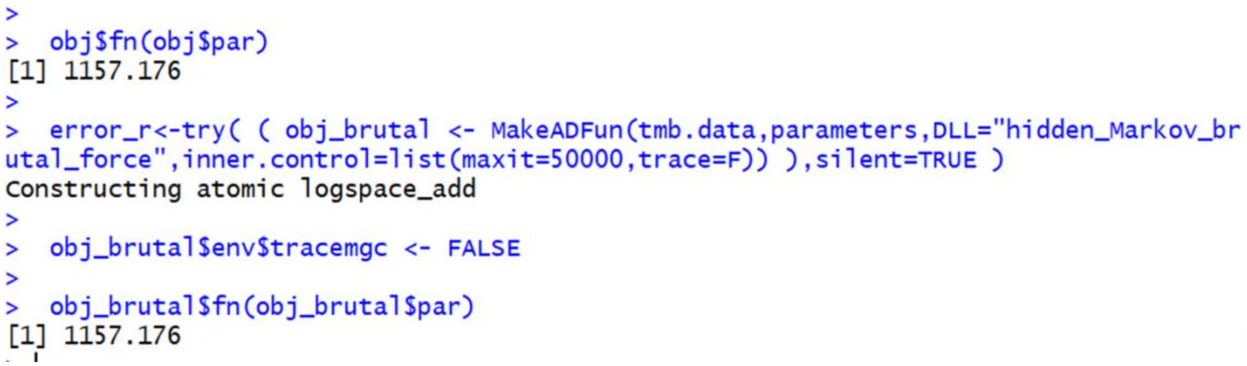

```
>
>  obj$fn(obj$par)
[1] 1157.176
>
>  error_r<-try( ( obj_brutal <- MakeADFun(tmb.data,parameters,DLL="hidden_Markov_br
utal_force",inner.control=list(maxit=50000,trace=F)) ),silent=TRUE )
Constructing atomic logspace_add
>
>  obj_brutal$env$tracemgc <- FALSE
>
>  obj_brutal$fn(obj_brutal$par)
[1] 1157.176
```

The brute-force method and the efficient algorithm gave exactly the same marginal likelihood evaluations, which was 1157.176.

Appendix F Template Model Builder (TMB) code for hidden-Markov Stock-recruit Model (HMSM)

```
#include <TMB.hpp>
#include <iostream>

template<class Type>
vector<Type>  segment_1(vector<Type>  yt,  vector<Type>  st,  matrix<Type>  qij,vector<Type>
pi1,vector<Type> alpha,vector<Type> beta,vector<Type> sigma,int t){
  int k_regime = beta.size();
  Type small = pow(10,-300);

      vector<Type> sr = log(pi1 + small);
  for(int j = 0;j < k_regime;++j){
     Type f_now = alpha(j) - beta(j)*st(0);
     sr(j) += dnorm(yt(0), f_now, sigma(j),true);
  }

  for(int i = 1;i <= t;++i){

     vector<Type> sr_new = sr;
     for(int j = 0;j < k_regime;++j){
         sr_new(j) = sr(0) +qij(0,j);
         for(int jj = 1;jj < k_regime;++jj){
            Type temp = sr(jj) +qij(jj,j);
            sr_new(j) =  logspace_add(sr_new(j),temp);
         }
     }

     sr = sr_new;

     for(int j = 0;j < k_regime;++j){
        Type f_now = alpha(j) - beta(j)*st(i);
        sr(j) += dnorm(yt(i), f_now, sigma(j),true);
     }

  }

  return sr;
}

template<class Type>
```

```
Type segment_2(vector<Type> yt, vector<Type> st, matrix<Type> qij,vector<Type>
pi1,vector<Type> alpha,vector<Type> beta,vector<Type> sigma,int rt,int t){
  int k_regime = beta.size();
  int n = yt.size();

  vector<Type> sr = qij.row(rt);
  for(int j = 0;j < k_regime;++j){
     Type f_now = alpha(j) - beta(j)*st(t+1);
     sr(j) += dnorm(yt(t+1), f_now, sigma(j),true);
  }

  for(int i = t+2;i < n;++i){

     vector<Type> sr_new = sr;
     for(int j = 0;j < k_regime;++j){
         sr_new(j) = sr(0) +qij(0,j);
         for(int jj = 1;jj < k_regime;++jj){
            Type temp = sr(jj) +qij(jj,j);
            sr_new(j) =  logspace_add(sr_new(j),temp);
         }
     }

     sr = sr_new;

     for(int j = 0;j < k_regime;++j){
        Type f_now = alpha(j) - beta(j)*st(i);
        sr(j) += dnorm(yt(i), f_now, sigma(j),true);
     }

  }

  Type seg2 = sr(0);
  for(int j = 1;j < k_regime;++j){
     seg2 = logspace_add(seg2,sr(j));
  }

  return seg2;
}

//main ////////////////////////////////////////////

template<class Type>
  Type objective_function<Type>::operator() ()
{

  DATA_VECTOR(yt);
```

```
  DATA_VECTOR(st);
  DATA_SCALAR(alpha_u);
  DATA_SCALAR(alpha_l);
  DATA_SCALAR(beta_u);
  DATA_SCALAR(sigma_u);

  PARAMETER_VECTOR(lalpha);
  PARAMETER_VECTOR(lbeta);
  PARAMETER_VECTOR(lsigma);
  PARAMETER_VECTOR(pi1_tran);
  PARAMETER_MATRIX(qij_tran);


  int k_regime = lbeta.size();

//  vector<Type> alpha = alpha_tr;
//  for(int i = 1;i < k_regime;++i){
//   alpha(i) = alpha(i-1) + exp(alpha_tr(i));
//  }

  vector<Type> beta = beta_u/(1+exp(-lbeta));// when lbeta is negative infinity, beta=0; when lbeta
is positive infinity, beta=beta_u

  vector<Type> alpha(k_regime);
  alpha(0) = (alpha_u-alpha_l)/(1+exp(-lalpha(0)))+alpha_l;
  for(int i = 1;i < k_regime;++i){
    alpha(i) = alpha(i-1) + (alpha_u-alpha(i-1))/(1+exp(-lalpha(i)));
  } // alpha(1) from alpha(0) to alpha_u

  vector<Type> sigma = sigma_u/(1+exp(-lsigma));

  vector<Type> pi1(k_regime);

  for(int i = 0;i < k_regime-1;++i){
    pi1(i) = exp(pi1_tran(i));
  }
  pi1(k_regime-1) = 1;
  pi1 = pi1/(pi1.sum());

  Type small = pow(10,-300);

  matrix<Type> qij(k_regime,k_regime);
  for(int i = 0;i < k_regime;++i){
    for(int j = 0;j < k_regime-1;++j){
      qij(i,j) = exp(qij_tran(i,j));
    }
```

```
    qij(i,k_regime-1) = 1;
    vector<Type> qij_row = qij.row(i);
    Type row_sum = qij_row.sum();
    for(int j = 0;j < k_regime;++j){
      qij(i,j) = qij(i,j)/row_sum;

      qij(i,j) = log(qij(i,j)+small);

    }

  }

 int n = yt.size();

vector<Type> sr = segment_1(yt, st, qij,pi1,alpha,beta,sigma,n-1);

  Type nll = sr(0);

  for(int j = 1;j < k_regime;++j){

     nll = logspace_add(nll,sr(j));

  }

  nll = -nll;

// predict r_t //////////////////////////////////



  matrix<Type> r_pred(k_regime,n);



  for(int i = 0;i < n-1;++i){

     sr = segment_1(yt, st, qij,pi1,alpha,beta,sigma,i);

     for(int j = 0;j < k_regime;++j){

         Type tempt = sr(j) + segment_2(yt, st, qij,pi1,alpha,beta,sigma,j,i) + nll;

         r_pred(j,i) = exp(tempt);

     }
```

```
}


sr = segment_1(yt, st, qij,pi1,alpha,beta,sigma,n-1);

for(int j = 0;j < k_regime;++j){

    Type tempt = sr(j) + nll;

    r_pred(j,n-1) = exp(tempt);

}

qij = exp(qij.array());

REPORT(beta);

REPORT(alpha);

REPORT(sigma);

REPORT(pi1);

REPORT(qij);

REPORT(r_pred);


ADREPORT(alpha);

ADREPORT(beta);

ADREPORT(sigma);

ADREPORT(pi1);

ADREPORT(qij);


return nll;

}
```

Appendix G Template Model Builder (TMB) code for hidden-Markov Growth Model (HMGM)

```
#include <TMB.hpp>
#include <iostream>

template<class Type>
vector<Type> segment_1(matrix<Type> yt,int n, vector<Type> st, matrix<Type>
qij,vector<Type> pi1,vector<Type> alpha,Type w0, vector<Type> beta,vector<Type> sigma,int
t){
  int k_regime = beta.size();
  Type small = pow(10,-300);

      vector<Type> sr = log(pi1 + small);
  for(int j = 0;j < k_regime;++j){
     vector<Type> f_now = log(alpha(j)) + 3*log(1 - ( 1-pow(w0/alpha(j),Type(1)/Type(3)) )*exp(-
beta(j)*st) );
//    f_now = exp(f_now);
     vector<Type> yt_now = yt.row(0);
     yt_now = yt_now - f_now;
     sr(j) += dnorm(yt_now.mean(), Type(0), sigma(j),true);
  }

  for(int i = 1;i <= t;++i){

     vector<Type> sr_new = sr;
     for(int j = 0;j < k_regime;++j){
         sr_new(j) = sr(0) +qij(0,j);
         for(int jj = 1;jj < k_regime;++jj){
            Type temp = sr(jj) +qij(jj,j);
            sr_new(j) =  logspace_add(sr_new(j),temp);
         }
     }

     sr = sr_new;

     for(int j = 0;j < k_regime;++j){
        vector<Type> f_now = log(alpha(j)) +3*log(1-(1-pow(w0/alpha(j),Type(1)/Type(3)) )*exp(-
beta(j)*st) );
//       f_now = exp(f_now);
        vector<Type> yt_now = yt.row(i);
        yt_now = yt_now - f_now;
        sr(j) += dnorm(yt_now.mean(), Type(0), sigma(j),true);
     }
```

```
  }

  return sr;
}

template<class Type>
Type segment_2(matrix<Type> yt,int n, vector<Type> st, matrix<Type> qij,vector<Type>
pi1,vector<Type> alpha,Type w0, vector<Type> beta,vector<Type> sigma,int rt,int t){
  int k_regime = beta.size();
//  int n = yt.array().rows();

  vector<Type> sr = qij.row(rt);
  for(int j = 0;j < k_regime;++j){
     vector<Type> f_now = log(alpha(j)) + 3*log(1 - ( 1-pow(w0/alpha(j),Type(1)/Type(3)) )*exp(-
beta(j)*st) );
//     f_now = exp(f_now);
     vector<Type> yt_now = yt.row(t+1);
     yt_now = yt_now - f_now;
     sr(j) += dnorm(yt_now.mean(), Type(0), sigma(j),true);
  }

  for(int i = t+2;i < n;++i){

     vector<Type> sr_new = sr;
     for(int j = 0;j < k_regime;++j){
         sr_new(j) = sr(0) +qij(0,j);
         for(int jj = 1;jj < k_regime;++jj){
            Type temp = sr(jj) +qij(jj,j);
            sr_new(j) =  logspace_add(sr_new(j),temp);
         }
     }

     sr = sr_new;

     for(int j = 0;j < k_regime;++j){
        vector<Type> f_now = log(alpha(j))+3*log(1-( 1-pow(w0/alpha(j),Type(1)/Type(3)) )*exp(-
beta(j)*st) );
//        f_now = exp(f_now);
        vector<Type> yt_now = yt.row(i);
        yt_now = yt_now - f_now;
        sr(j) += dnorm(yt_now.mean(), Type(0), sigma(j),true);
     }

  }
```

```
  Type seg2 = sr(0);
  for(int j = 1;j < k_regime;++j){
    seg2 = logspace_add(seg2,sr(j));
  }

  return seg2;
}

//main //////////////////////////////////////////////

template<class Type>
  Type objective_function<Type>::operator() ()
{

  DATA_MATRIX(yt);
  DATA_INTEGER(nobs);
  DATA_VECTOR(st);
  DATA_SCALAR(alpha_u);
  DATA_SCALAR(alpha_l);
  DATA_SCALAR(beta_u);
  DATA_SCALAR(sigma_u);
  DATA_SCALAR(w0);
  DATA_VECTOR(pi1);

  PARAMETER_VECTOR(lalpha);
//  PARAMETER(log_w0);
  PARAMETER_VECTOR(lbeta);
  PARAMETER_VECTOR(lsigma);
//  PARAMETER_VECTOR(pi1_tran);
  PARAMETER_MATRIX(qij_tran);


  int k_regime = lbeta.size();

  vector<Type> alpha = exp(lalpha);
//  alpha(0) = exp(lalpha(0));
//  for(int i = 1;i < k_regime;++i){
//    alpha(i) = alpha(i-1) + exp(lalpha(i));
//  }

//  Type w0 = exp(log_w0);

  vector<Type> beta = exp(lbeta);   // beta_u/(1+exp(-lbeta));// when lbeta is negative infinity, beta=0; when lbeta is positive infinity, beta=beta_u

//  vector<Type> alpha(k_regime);
```

```
//  alpha(0) = (alpha_u-alpha_l)/(1+exp(-lalpha(0)))+alpha_l;
//  for(int i = 1;i < k_regime;++i){
//    alpha(i) = alpha(i-1) + (alpha_u-alpha(i-1))/(1+exp(-lalpha(i)));
//  } // alpha(1) from alpha(0) to alpha_u

  vector<Type> sigma = exp(lsigma);  //sigma_u/(1+exp(-lsigma));

//  vector<Type> pi1(k_regime);

//  for(int i = 0;i < k_regime-1;++i){
//    pi1(i) = exp(pi1_tran(i));
//  }
//  pi1(k_regime-1) = 1;
//  pi1 = pi1/(pi1.sum());

  Type small = pow(10,-300);

  matrix<Type> qij(k_regime,k_regime);
  for(int i = 0;i < k_regime;++i){
    for(int j = 0;j < k_regime-1;++j){
      qij(i,j) = exp(qij_tran(i,j));
    }
    qij(i,k_regime-1) = 1;
    vector<Type> qij_row = qij.row(i);
    Type row_sum = qij_row.sum();
    for(int j = 0;j < k_regime;++j){
      qij(i,j) = qij(i,j)/row_sum;
      qij(i,j) = log(qij(i,j)+small);
    }
  }

  int n = nobs;

  vector<Type> sr = segment_1(yt,n, st, qij,pi1,alpha,w0,beta,sigma,n-1);

  Type nll = sr(0);
  for(int j = 1;j < k_regime;++j){
     nll = logspace_add(nll,sr(j));
  }

  nll = -nll;

// predict r_t /////////////////////////////////

  matrix<Type> r_pred(k_regime,n);
```

```
for(int i = 0;i < n-1;++i){
  sr = segment_1(yt,n, st, qij,pi1,alpha,w0,beta,sigma,i);
  for(int j = 0;j < k_regime;++j){
     Type tempt = sr(j) + segment_2(yt,n, st, qij,pi1,alpha,w0,beta,sigma,j,i) + nll;
     r_pred(j,i) = exp(tempt);
  }
}

sr = segment_1(yt,n, st, qij,pi1,alpha,w0,beta,sigma,n-1);
for(int j = 0;j < k_regime;++j){
   Type tempt = sr(j) + nll;
   r_pred(j,n-1) = exp(tempt);
}

qij = exp(qij.array());

REPORT(beta);
REPORT(alpha);
REPORT(w0);
REPORT(sigma);
REPORT(pi1);
REPORT(qij);
REPORT(r_pred);

ADREPORT(alpha);
ADREPORT(w0);
ADREPORT(beta);
ADREPORT(sigma);
ADREPORT(pi1);
ADREPORT(qij);

return nll;
}
```

Appendix H Different initial values and their corresponding parameter estimates for the HMSM-2

I conducted several trials of fitting the SR data of 3NO cod using the BHM, HMSM-2, and HMSM-3. In each trial, BHM, HMSM-2, and HMSM-3 were assigned different initial values. Results showed that HMSM-2 outperformed BHM and HMSM-3 in all the trials, with the lowest AICc (Table 1), and the parameter estimates for HMSM-2 were not sensitive to starting values (Table 2).

Table 1. The AICc values of the three models in four trials.

Trial		HMSM-2	HMSM-3	BHM
1	AICc	150.64	159.43	186.51
2	AICc	150.64	159.43	186.51
3	AICc	150.64	159.43	186.51
4	AICc	150.64	159.43	186.51

Table 2. The starting values and parameter estimates for the HMSM-2 in four trials.

Trial	Parameters	Starting values	Estimates
	α_1	1	-1.44
	α_2	1.5	0.38
Trial #1	β_1	0.6	0.19
	β_2	0.6	0.07
	σ_1	0.5	0.88
	σ_2	0.5	0.55
	q_{11}	0.5	1
	q_{12}	0.5	1.74×10^{-10}
	q_{21}	0.5	0.04
	q_{22}	0.5	0.96
Trial #2	α_1	0.1	-1.44
	α_2	0.8	0.38
	β_1	1	0.19
	β_2	1	0.07
	σ_1	1	0.88
	σ_2	1	0.55
	q_{11}	0.5	1
	q_{12}	0.5	1.38×10^{-10}
	q_{21}	0.5	0.04
	q_{22}	0.5	0.96
Trial #3	α_1	-3	-1.44
	α_2	3	0.38
	β_1	1.4	0.19
	β_2	1.4	0.07
	σ_1	1	0.88
	σ_2	1	0.55
	q_{11}	0.5	1
	q_{12}	0.5	1.34×10^{-10}
	q_{21}	0.5	0.04
	q_{22}	0.5	0.96
Trial #4	α_1	-2.5	-1.44
	α_2	0.4	0.38
	β_1	0.05	0.19
	β_2	0.05	0.07
	σ_1	0.6	0.88
	σ_2	0.6	0.55
	q_{11}	0.5	1
	q_{12}	0.5	7.75×10^{-12}
	q_{21}	0.5	0.04
	q_{22}	0.5	0.96

Appendix I Fit the SR data of 3NO cod using the HMGM with different starting values

I fit the SR data of 3NO cod using VBGM and HMGM. The VBGM and HMGM were assigned different initial values in each trial. The HMGM outperformed the VBGM in all trials with lower AICc (Table 1). The parameter estimates for the HMGM changed according to different starting values (Table 2). However, changing starting values did not significantly affect the predicted model mean for the HMGM (Fig. 1).

Table 1. The AICc values of the two models in four trials.

Trial		HMGM	VBGM
1	AICc	-84.97	-39.68
2	AICc	-84.97	-39.68
3	AICc	-84.97	-39.68
4	AICc	-84.97	-39.68

Table 2. The starting values and parameter estimates for the HMGM in four trials.

Trial	Parameters	Starting values	Estimates
	$w_{\infty 1}$	47.76	44.21
	$w_{\infty 2}$	47.76	46.16
Trial #1	k_1	0.07	0.06
	k_2	0.07	0.07
	σ_1	0.09	0.08
	σ_2	0.09	0.09
	q_{11}	0.5	0.92
	q_{12}	0.5	0.08
	q_{21}	0.5	0.06
	q_{22}	0.5	0.94
Trial #2	$w_{\infty 1}$	40	25.46
	$w_{\infty 2}$	40	23.14
	k_1	0.15	0.08
	k_2	0.15	0.10
	σ_1	0.4	0.08
	σ_2	0.4	0.09
	q_{11}	0.5	0.92
	q_{12}	0.5	0.08
	q_{21}	0.5	0.06
	q_{22}	0.5	0.94
Trial #3	$w_{\infty 1}$	42	38.43
	$w_{\infty 2}$	42	41.57
	k_1	0.05	0.07
	k_2	0.05	0.07
	σ_1	0.2	0.08
	σ_2	0.2	0.09
	q_{11}	0.5	0.92
	q_{12}	0.5	0.08
	q_{21}	0.5	0.06
	q_{22}	0.5	0.94
Trial #4	$w_{\infty 1}$	45	33.87
	$w_{\infty 2}$	45	50.24
	k_1	0.05	0.07
	k_2	0.05	0.07
	σ_1	0.2	0.08
	σ_2	0.2	0.09
	q_{11}	0.5	0.92
	q_{12}	0.5	0.08
	q_{21}	0.5	0.06
	q_{22}	0.5	0.94

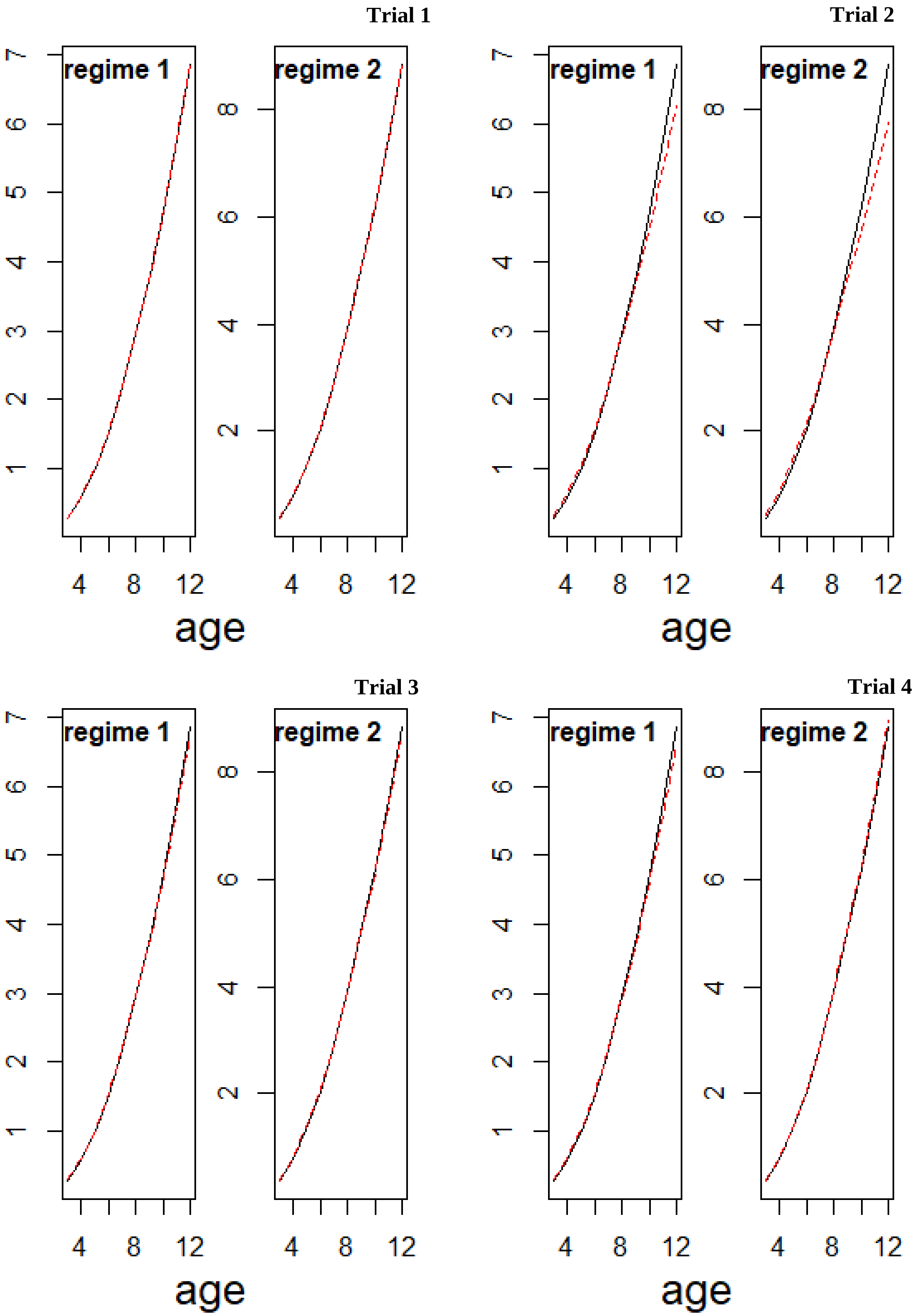

Fig. 1. In each trial, the back lines denote the regime-specific model mean predicted by the HMGM with the original starting values ($w_{\infty 1} = w_{\infty 1} = 100, k_1 = k_2 = 0.1, \sigma_1 = \sigma_2 = 0.5$). The red dashed lines denote the regime-specific model mean predicted by the HMGM with new starting values.

Appendix J Fit the SR data of 3NO cod using the HMGM with different values of w_0

The weight of the Atlantic cod (*Gadus morhua*) larvae after 30 days post hatch is estimated at $(0.27 \pm 0.07) \times 10^{-3}\ g$ (Penglase *et al.*, 2013). I tried two different values for w_0 at 2 standard errors from the estimate 0.27 mg, which were $(0.27 + 0.14) \times 10^{-3}\ g$ and $(0.27 - 0.14) \times 10^{-3}\ g$. Results showed that the estimates for w_∞ and *k* varied according to different w_0. However, I cannot draw a conclusion that the parameter estimates for the HMGM are sensitive to w_0 because the weight-at-age data for this stock is limited at the age of 12, and the absence of weights at older ages could lead to unreliable estimates for w_∞ and *k*. To determine whether w_0 variations will affect the model performance of the HMGM, I compared the predicted mean weights at age at different values of w_0. Results indicated that different values of w_0 within 2 standard errors of the estimated value do not significantly affect the estimated mean weights at age within the data age range (Figure 1). Thus, I concluded that different but reasonable values for w_0 will not significantly affect the model performance.

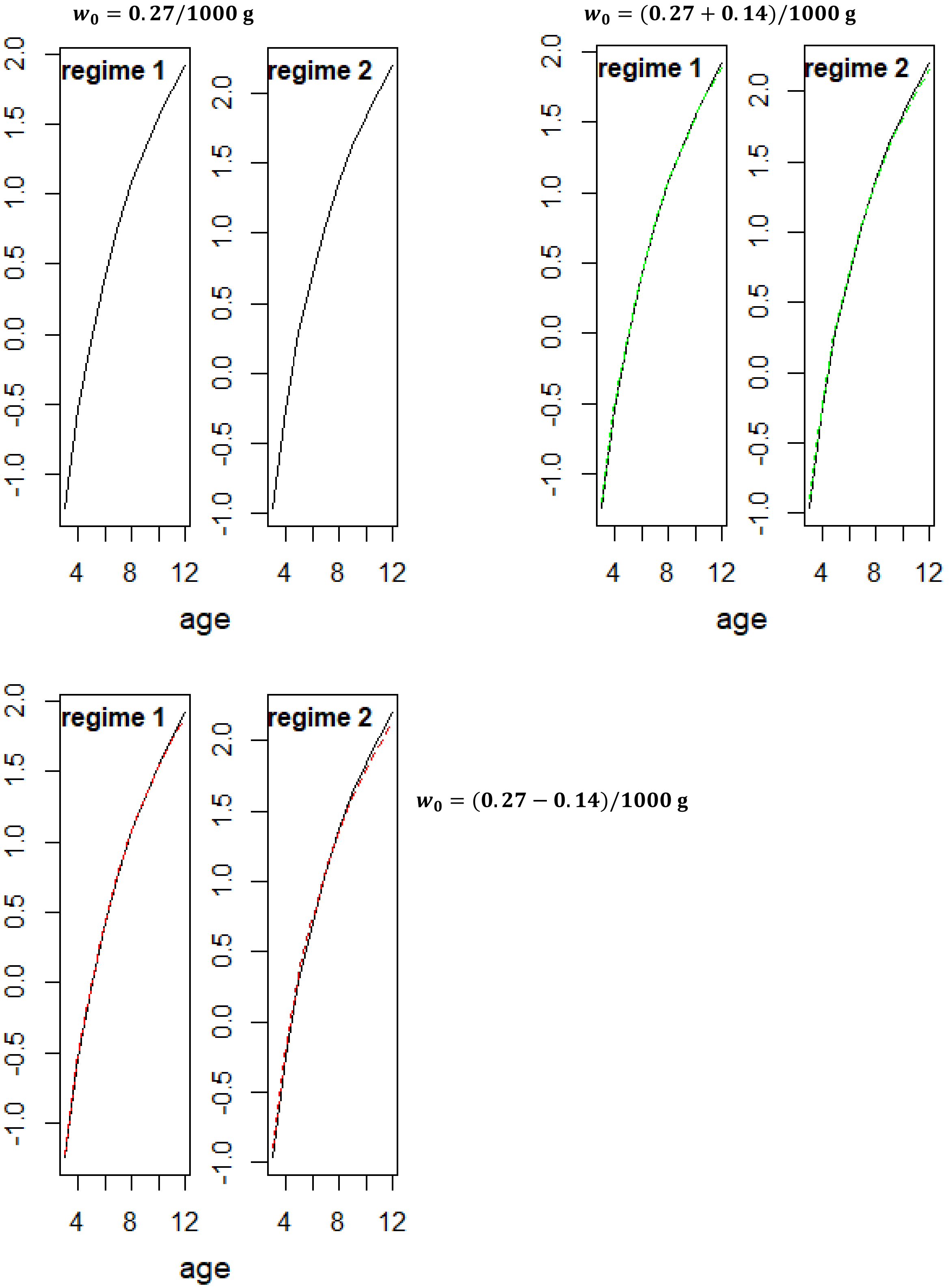

$w_0 = 0.27/1000$ g

$w_0 = (0.27 + 0.14)/1000$ g

$w_0 = (0.27 - 0.14)/1000$ g

Fig.1 Black, green, and red lines denote the predicted mean weights at age for the original w_0, $w_0 + 0.14$, and $w_0 - 0.14$, respectively.